ENGINE MODELLING FOR VIRTUAL MAPPING

Development of a physics based cycle-by-cycle virtual engine that can be used for cyclic engine mapping applications, engine flow modelling, ECU calibration, real-time engine control or vehicle simulation studies.

Antonios Pezouvanis

Submitted for the degree of

Doctor of Philosophy

School of Engineering, Design and Technology

University of Bradford

2009

Abstract

After undergoing a study about current engine modelling and mapping approaches as well as the engine modelling requirements for different applications, a major problem found to be present is the extensive and time consuming mapping procedure that every engine has to go through so that all control parameters can be derived from experimental data. To improve this, a cycle-by-cycle modelling approach has been chosen to mathematically represent reciprocating engines starting by a complete dynamics crankshaft mechanism model which forms the base of the complete engine model. This system is modelled taking into account the possibility of a piston pin offset on the mechanism. The derived Valvetrain model is capable of representing a variable valve lift and phasing Valvetrain which can be used while modelling most modern engines. A butterfly type throttle area model is derived as well as its rate of change which is believed to be a key variable for transient engine control. In addition, an approximation throttle model is formulated aiming at real-time applications. Furthermore, the engine inertia is presented as a mathematical model able to be used for any engine. A spark ignition engine simulation (SIES) framework was developed in MATLAB SIMULINK to form the base of a complete high fidelity cycle-by-cycle simulation model with its major target to provide an environment for virtual engine mapping procedures. Some experimental measurements from an actual engine are still required to parameterise the model, which is the reason an engine mapping (EngMap) framework has been developed in LabVIEW, It is shown that all the moving engine components can be represented by a single cyclic variable which can be used for flow model development.

Keywords: IC Engine, control, calibration, mathematical model

Acknowledgments

The completion of this thesis is the biggest challenge I have faced till this day and would not have been possible without the support of friends and people around me.

I am grateful to my supervisors, Professor K. M. Ebrahimi and Dr P. Olley, for their great guidance, invaluable assistance and support, as well as the EPSRC and Ford Motor Company UK for supporting this work.

I am grateful to my family and parents, who managed to create my learning character ever since I was a child, for their intensive love and support, and their huge patience and encouragement.

Table of contents

List of figures

List of tables

Nomenclature

CHAPTER 2: Literature review on engine modelling

$\dot{m}_{cyl}$	Mass air flow into the cylinders	(kg/sec)
$\dot{m}_{thr}$	Mass air flow through the throttle	(kg/sec)
A_{thr}	Throttle effective flow area	(m^2)
P_m	Intake manifold pressure	(kPa)
P_{thr}	Pressure before the throttle plate	(kPa)
T_m	Intake manifold temperature	(°K)
T_{thr}	Temperature before the throttle plate	(°K)
V_d	Engine displacement volume	(m^3)
V_m	Intake manifold volume	(m^3)
f_b	Mass fraction of fuel burnt	
m_f	Mass of fuel entering the cylinder	(kg)
m_{ff}	Mass of fuel film	(kg)
m_{fi}	Mass of fuel injected	(kg)
m_{fv}	Mass of fuel injected reaching the valves	(kg)
$\boldsymbol{C_D}$	Multidimensional discharge coefficient maps	
$\boldsymbol{X_f}$	Multidimensional fuel deposition proportion maps	(degrees)
θ_S	Crankshaft angle of combustion start	(degrees)
θ_c	Crankshaft angle of calculation	(degrees)
θ_d	Combustion duration in crankshaft rotation angle	
$\boldsymbol{\eta_V}$	Multidimensional volumetric efficiency maps	
$\boldsymbol{\tau_f}$	Multidimensional time constant for fuel vaporisation maps	
$\propto$	Wiebe function curve shape coefficient	
N	Engine speed	(RPM)
R	Gas constant of air	(kJ/kg K)
n	Wiebe function curve shape coefficient	
γ	Gas specific heat ratio	

CHAPTER 4: Crankshaft mechanism

h_{TDC}	Effective cylinder height of TDC volume	(m)
h_t	Total cylinder height	(m)
A_{cyl}	Cylinder area	(m^2)

FO_N	Cylinder-N firing order number	
F_p	Piston force	(N)
L_C	Connecting rod centre of mass position	(m)
O_c	Crankshaft offset	(m)
O_p	Piston pin offset	(m)
O_t	Total crankshaft mechanism offset	(m)
P_{case}	Crankcase pressure	(Pa)
P_{cyl}	Cylinder pressure	(Pa)
V_{BDC}	BDC cylinder volume	(m^3)
V_{TDC}	TDC cylinder volume	(m^3)
V_c	Crankcase volume	(m^3)
V_{cyl}	Cylinder volume	(m^3)
V_{swept}	Cylinder swept volume	(m^3)
a_{cyl}	Piston acceleration	(m/sec^2)
a_{pin}	Piston pin acceleration	(m/sec^2)
n_{cyl}	Number of cylinders	
v_G^x	Connecting rod centre of mass X axis velocity	(m/sec)
v_G^y	Connecting rod centre of mass Y axis velocity	(m/sec)
v_{Tcyl}	Sum of individual piston speeds	(m/sec)
v_{cyl}	Piston speed	(m/sec)
v_{pin}	Piston pin speed	(m/sec)
x_G	Connecting rod centre of mass X axis position	(m)
x_{Tcyl}	Sum of individual piston positions	(m)
x_{cyl}	Piston distance from TDC	(m)
x_{pin}	Piston pin position	(m)
y_G	Connecting rod centre of mass Y axis position	(m)
$\Phi_{BDC-TDC}$	BDC to TDC stroke duration in crankshaft rotation angle	(rad)
$\Phi_{TDC-BDC}$	TDC to BDC stroke duration in crankshaft rotation angle	(rad)
α_G^x	Connecting rod centre of mass X axis acceleration	(m/sec^2)
α_G^y	Connecting rod centre of mass Y axis acceleration	(m/sec^2)
α_τ	Connecting rod angular acceleration around centre of mass	(rad/sec^2)
ζ_{cylN}	Cylinder-N phase angle	(rad)
ψ_{cylN}	Cylinder-N crankshaft arm angle	(rad)
ω_τ	Connecting rod angular speed around centre of mass	(rad/sec)
ϕ_{BDC}	Angle of obliquity at BDC	(rad)
ϕ_{TDC}	Angle of obliquity at TDC	(rad)
B	Cylinder bore	(m)
K	Crankshaft arm radius	(m)

L	Connecting rod length	(m)
S	Piston stroke length	(m)
r	Compression ratio	
α	Crankshaft angular acceleration	(rad/sec^2)
ζ	Cylinder phase angle	(rad)
θ	Engine angle	(rad)
τ	Connecting rod angular position around centre of mass	(rad)
ψ	Crankshaft arm angle	(rad)
ω	Crankshaft angular speed	(rad/sec)

CHAPTER 5: Valvetrain

CA_f	Curtain flow area	(m^2)
CA_{f2}	Second curtain flow area	(m^2)
D_b	Lobe baseline diameter	(m)
D_i	Valve port diameter	(m)
H_{lobe}	Lobe height	(m)
H_{max}	Maximum camshaft lobe height	(m)
$L_{\max\ eff}$	Maximum effective valve lift	(m)
L_s	Valve lift switching to CA_{f2}	(m)
M_{in}	Lobe Cartesian coordinate matrix	(m)
M_{out}	Rotated lobe Cartesian coordinate matrix	(m)
PA_f	Port flow area	(m^2)
P_{cam}	Camshaft profile radius	(m)
R_{eff}	Effective torque radius	(m)
R_{lobe}	Lobe radius	(m)
T_{cam}	Camshaft torque	(Nm)
X_{cam}	X axis camshaft lobe drawing coordinate	(m)
Y_{cam}	Y axis camshaft lobe drawing coordinate	(m)
s_r	Sign of direction of rotation	
θ_{cr}	Rotation in crankshaft angle	(rad)
θ_d	Duration of lobe profile	(rad)
θ_r	Camshaft angle	(rad)
θ_s	Starting angle of lobe profile	(rad)
D	Valve diameter	(m)
F	Effective force acting on camshaft lobe	(N)
L	Valve lift	(m)

d	Valve stem diameter	(m)
u	Lobe profile smoothing factor	
θ	Valve seat angle	(rad)

CHAPTER 6: Throttle kinematics

h_p	Throttle plate height	(m)
A_{th}	Throttle flow area	(m^2)
A_{th}^{max}	Maximum effective throttle flow area	(m^2)
A_{th}^{plate}	Throttle plate area	(m^2)
D_p	Throttle plate diameter	(m)
D_{sh}	Throttle shaft diameter	(m)
D_{th}	Throttle bore	(m)
θ_{seg}	Segment area angle	(rad)
θ_{seg}^{plate}	Throttle plate segment area angle	(rad)
θ_{thC}	Closed throttle plate angle	(rad)
ψ_0	Closed throttle angle	(rad)
D	Throttle bore	(m)
d	Throttle shaft diameter	(m)
l	Ratio d/D: shaft diameter over throttle bore	
α	Throttle angle	(rad)
ψ	Throttle angle	(rad)

CHAPTER 7: Engine inertia

I_a	Known added inertia	(kg m^2)
I_e	Engine inertia	(kg m^2)
J_{crank}	Inertia of crankshaft assembly	(kg m^2)
J_{eff}	Effective engine inertia	(kg m^2)
J_{exh}	Inertia of exhaust camshaft assembly	(kg m^2)
J_{idle}	Inertia of idle gear assembly	(kg m^2)
J_{int}	Inertia of intake camshaft assembly	(kg m^2)
R_{crank}	Effective crankshaft sprocket/pulley radius	(m)
R_{idle}	Effective idle sprocket/pulley radius	(m)

T^N	Engine torque output at speed *N*	(Nm)
T_a	Engine torque output (with known added inertia)	(Nm)
T_{crank}	Net engine torque output	(Nm)
T_e	Engine torque output	(Nm)
m_{chain}	Mass of chain/belt	(kg)
α_a	Engine acceleration (with known added inertia)	(rad/sec^2)
α_e	Engine acceleration	(rad/sec^2)
α_e^N	Engine acceleration at speed *N*	(rad/sec^2)
α_α^N	Engine acceleration (with known added inertia) at speed *N*	(rad/sec^2)
θ_{crank}	Crankshaft rotation angle	(rad)

CHAPTER 8: Thermodynamic cycle modelling

C_p	Specific heat of constant pressure	(kJ/kg K)
C_v	Specific heat of constant volume	(kJ/kg K)
P_0	Known cylinder pressure	(kPa)
P_{new}	Unknown cylinder pressure	(kPa)
T_0	Known cylinder temperature	(°K)
T_C	Temperature in Celsius	(°C)
T_K	Temperature in Kelvin	(°K)
T_{new}	Unknown cylinder temperature	(°K)
$\dot{V}$	Cylinder volume rate of change	(m^3/sec)
V_0	Cylinder volume of P_0	(m^3)
V_{new}	Cylinder volume of P_{new}	(m^3)
r_{equ}	Compression ratio equivalence	
R	Gas constant	(kJ/kg K)
k	Ratio of working mixture's specific heats	

CHAPTER 10: EngMap framework development

V_{TPS}	TPS voltage	(V)
V_{TPS}^0	Closed TPS voltage	(V)
V_{TPS}^{WOT}	Wide open throttle TPS voltage	(V)
θ_{thC}	Closed throttle angle	(rad)
TPS	Closed to wide opened throttle %	

a	Throttle angle	(rad)

CHAPTER 11: Conclusion and future work

A_{exh}	Exhaust valve flow area	(m^2)
A_{int}	Intake valve flow area	(m^2)
A_v	Valve flow area	(m^2)
P_{cyl}	Cylinder pressure	(kPa)
P_{port}	Port pressure	(kPa)
V_{cyl}	Cylinder volume	(m^3)
N	Engine speed	(RPM)

CHAPTER 1: Introduction

Engine modelling is quite a large field with a plethora amount of knowledge available in literature. The main problem encountered is that the models are either too simple to allow the implementation of new control strategies or too specific as they were developed for a particular application. A process that has been found to be in need of improvement is the engine mapping and model calibration. The current use of mean-value engine models and mapping procedures result in data that can not be used on other engines while some engine phenomena can not be expressed at all. Thus, a physics based modelling approach has been chosen to mathematicaly represent the engine while developing a cycle-by-cycle engine model which can be used for any desired application such as engine simulation, virtual mapping procedure and flow models developement.

Assuming that a mathematical model about a process or system of interest is available in the literature, it is most of the time unclear or difficult to implement it in a particular simulation package. This problem is either the outcome of missing information while sometimes it is due to the absence of a complete model structure which correctly represents the interaction of all presented equations. The mathematical models presented in this work have been developed in such a way so that they can form an autonomous engine sub-system which allows them to be clearly presented, understandable, and easily implemented by the reader, In addition, their sub-system format facilitates the complete engine model development or future editing. The sections that follow are a brief

introduction to the mathematical modelling terminologies and their main applications for analysing SI engines.

1.1 Mathematical modelling

The mathematical representation of an actual system that is carried out by correlating input and output variables using equations is referred to "mathematical modelling". It is used on systems that need to be optimised, controlled or simulated. There is always a trade-off between the model accuracy, simplicity and simulation speed as more accurate models usually tend to be more complex.

The mathematical models are classified into different categories from which some are listed below.

Static vs. Dynamic: Static models do not take into account the time variable. Sometimes they describe a system at a particular moment in time or one that does not vary over time. On the other hand, dynamic models are mathematical expressions of a system over time and usually are represented by differential equations.

Continuous vs. Discrete: The term *"continuous"* is used to refer to the model ability to represent the system using a constant set of equations. On the other hand, "*discrete models*" variables and equations may switch when a system's process changes.

Linear vs. Non-linear: Linear models can be evaluated using the four fundamental mathematical operators, addition, subtraction, multiplication and division. A non-linear model can have any mathematical operation and non-linearities.

Black-box vs. White-box: The terminology *"black-box"* is used to describe a model that contains some unknown operations (Figure 1.1-a). There are cases which some experimental data are used within a model to replicate a physical phenomenon and because either the phenomenon is not needed to be further analysed or the knowledge is not available, then it is used as it is. An example of such a model is a trained neural network model which is representing a system. The system's mathematical model is not known but only its input-output relationships. On the other hand, a model is noted as *"white-box"* when everything is mathematically expressed and known (Figure 1.1-b). Practically, every model falls in an imaginary category between these two.

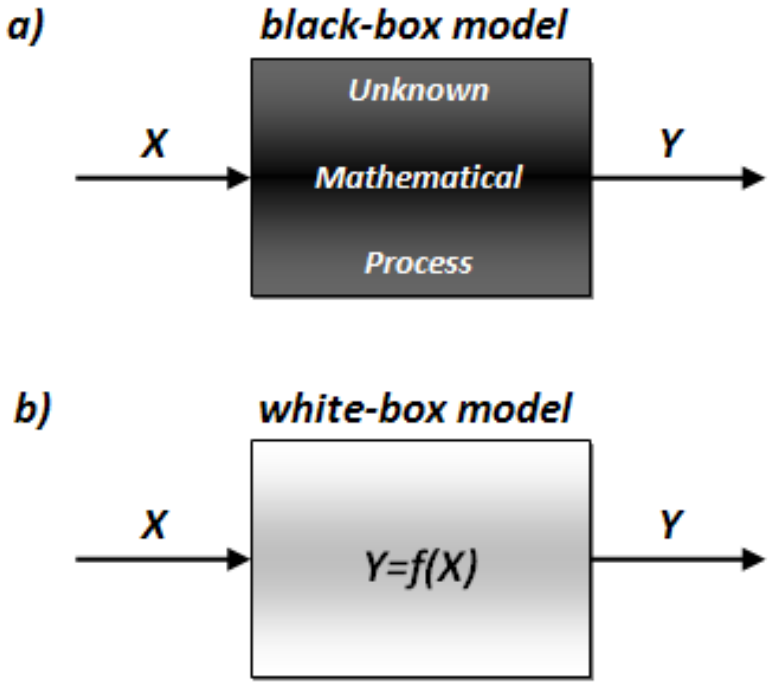

Figure 1.1: Black-box & white-box models

1.2 Engine modelling applications

The term engine modelling is used whenever an engine is modelled through the use of mathematical equations. These equations may describe a complete engine (virtual engine), an engine's process or just a variable. Below are some of the main applications an engine model can be used.

Engine design: Mathematical modelling is used for engine design in order to optimise some specific components or systems. Engine sub-systems are usually designed and *"tuned"* in specific softwares depending on the requirements. An intake manifold for example is likely to be designed and optimised in a Computational Fluid Dynamics (CFD) package while the material selection for the crankshaft mechanism will be done using Finite Element Analysis (FEA) software. Engine models can provide typical input data to softwares like these when experimental data is not available.

Mapping and calibration: The process of engine mapping (Figure 1.2) is mainly used by the automotive industry which consists of running a particular engine through all its operating range while collecting data from which *"maps"* can be build. The engine maps can then be used to build a model so that it can behave like that engine. This type of models is used to calibrate the Engine Control Unit (ECU). The equations that are in the engine model are used to collect the data and to evaluate variables in the ECU. It is common to have black-box models representing individual engine dynamics sub-systems as they are simpler and achieve a good accuracy. Due to the fact that it is an engine mapping process and not a physic based model parameterisation, the maps represent only the engine at the moment

and conditions of the mapping procedure. The engine calibration process includes the engine mapping procedure but has in addition the controller calibration parameters, sensor calibration and control verifications. Specialised hardware, software and services are provided by companies such as AVL[1] and FEV[2] for this purpose.

HIL and SIL: Software In-the-loop (SIL) is used to denote the interaction and simulation of two virtual systems. The simulation of a vehicle model connected to an engine model is an example of a software in the loop application. On the other hand, the term Hardware In-the-loop (HIL) is used when at least one system is a real hardware under testing through a simulation. An example of such a system is an ECU hardware connected to an engine model in order to evaluate the ECU's control algorithms (Figure 1.3). SIL applications and configurations are practicaly unlimited with engine modelling. Any engine or vehicle sub-system can be modelled and then simulated together depending on their developement objective. The same applies to HIL application. It can be as simple as a sensor testing, sensor algorith developement, any hardware or engine testing.

Virtual prototyping: All above are steps of the virtual prototyping procedure before manufacturing. Successful virtual prototyping procedures will normally lead to flawless products which will not have to be redesigned. Virtual prototyping has become very popular since the availability of personal computers which lead to a significant amount of software and hardware development intended for this sector.

[1] AVL Homepage: http://www.avl.com/
[2] FEV Homepage: http://www.fev.com/

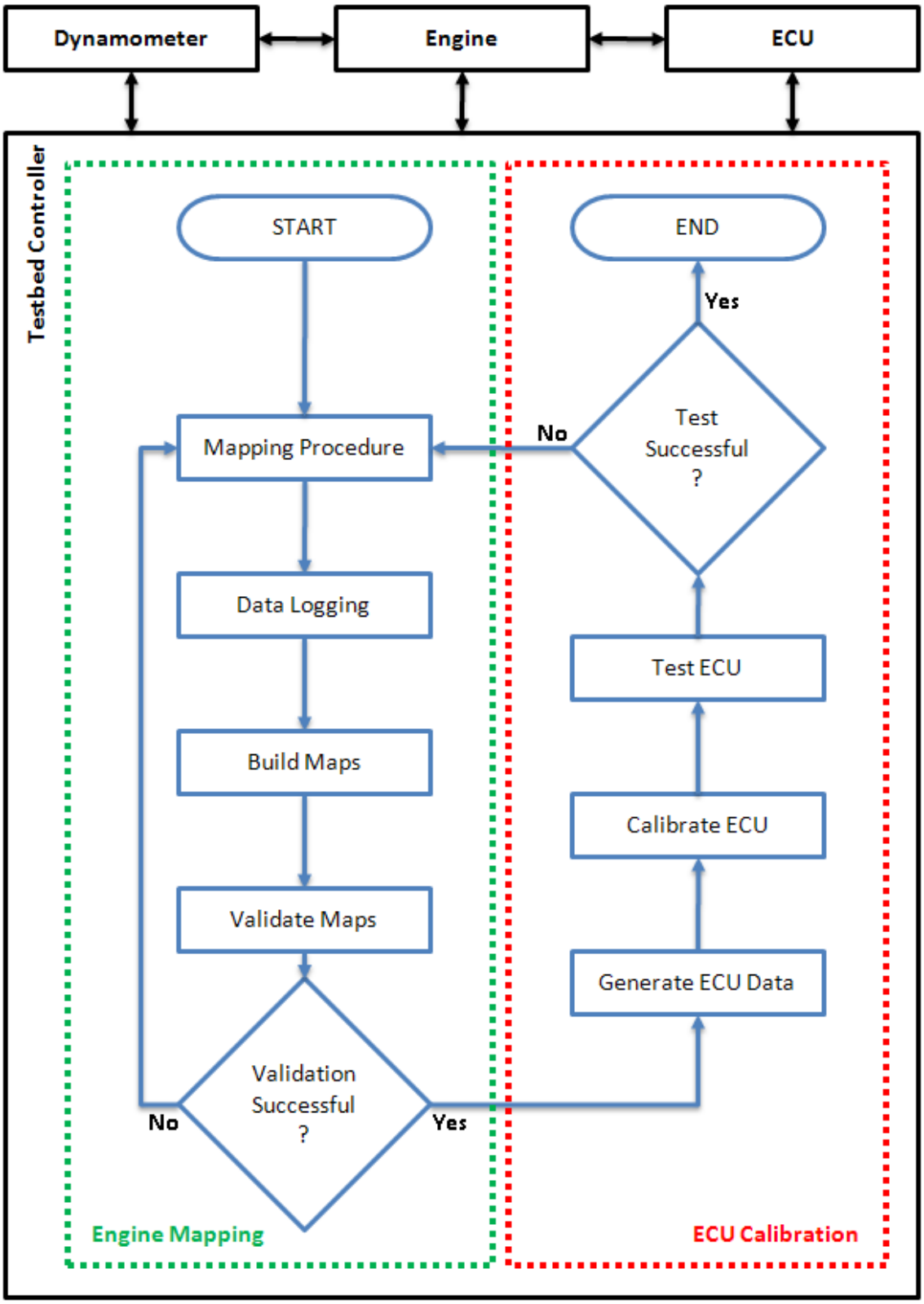

Figure 1.2: Typical engine mapping and ECU calibration process

a) HIL Configuration

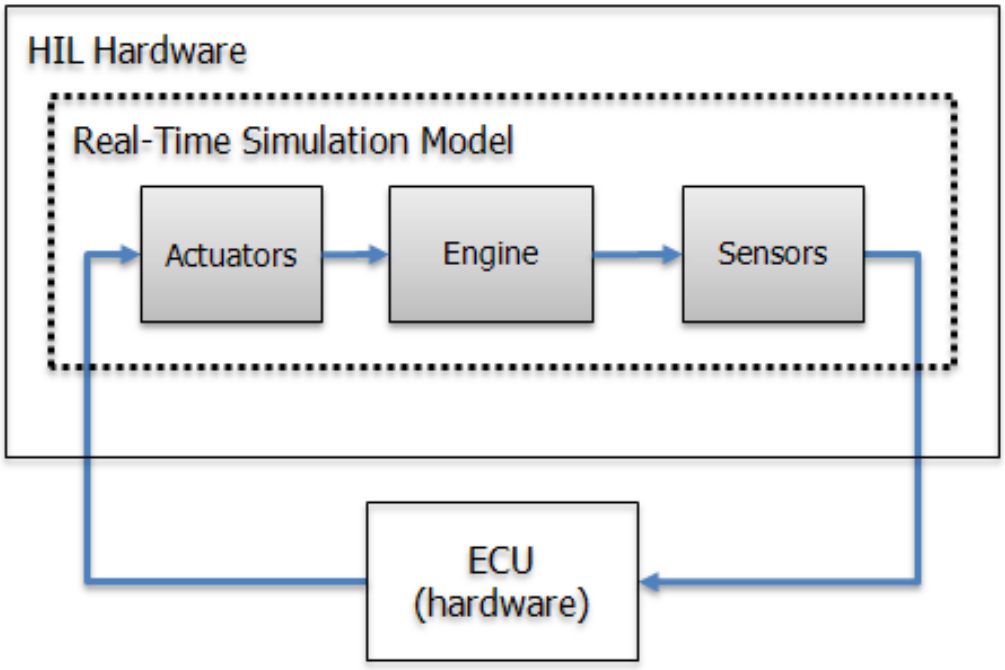

b) SIL Configuration

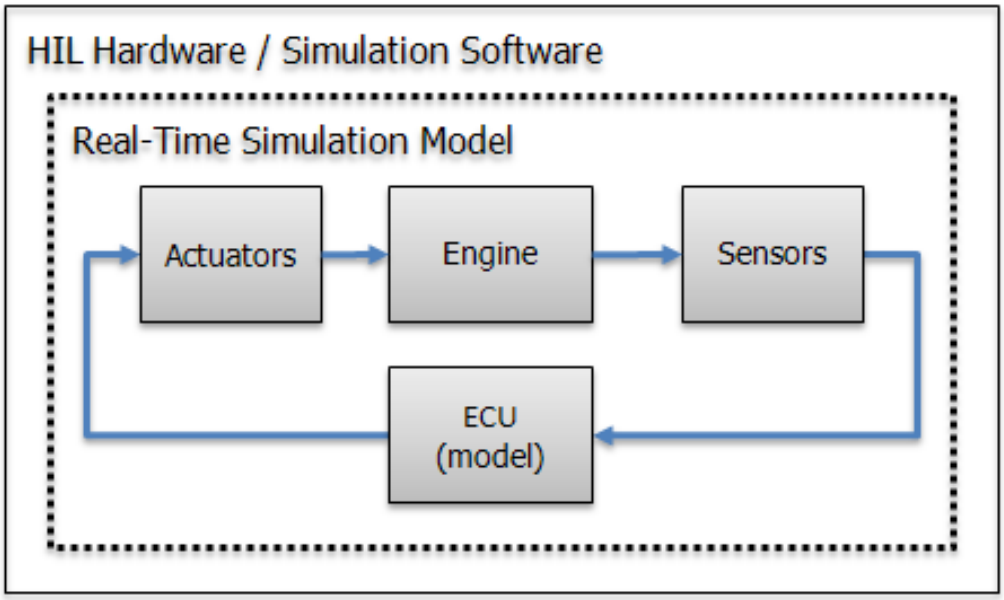

Figure 1.3: Typical HIL and SIL engine model configuration

Real-time: The main variable during a dynamic simulation is the time. If the time variable in the simulation can advance equally or faster than the real time, then the model and the simulation are said to have the ability to run in real time. This term is very important when an HIL application is required, as it means that the hardware can be used as it is, running at its nominal speed. If the model that it has to connect to is not real-time capable, then the hardware would have to run at a lower speed (down-clocked) which can compromise the hardware testing results. Caution must be taken whenever coming across with the term "real-time" as it is widely used these days due to its huge marketing advantage. An engine model can be for example real-time capable on a specific application and incapable on every other. This is mainly due to the simulation hardware, time step size or calculation accuracy used which are rarely presented.

1.3 Cycle-by-cycle modelling vs. mean value modelling

The main difference between cycle-by-cycle (cyclic) and mean value (MV) engine modelling is that the cyclic models require the crankshaft position as an input parameter while MV model evaluate all output variables averaged through either a crankshaft revolution (360°) or a complete engine cycle (720°). If an engine for instance is modelled using both the cyclic and MV type, and assuming all input parameters are constant; MV models output constant values while cyclic models produce constant output waveform patterns for each cycle. The engine's intake manifold pressure for example is pulsating due to the individual non-linear piston intakes. This pulsating flow can be only represented by a cyclic model (Figure 1.4).

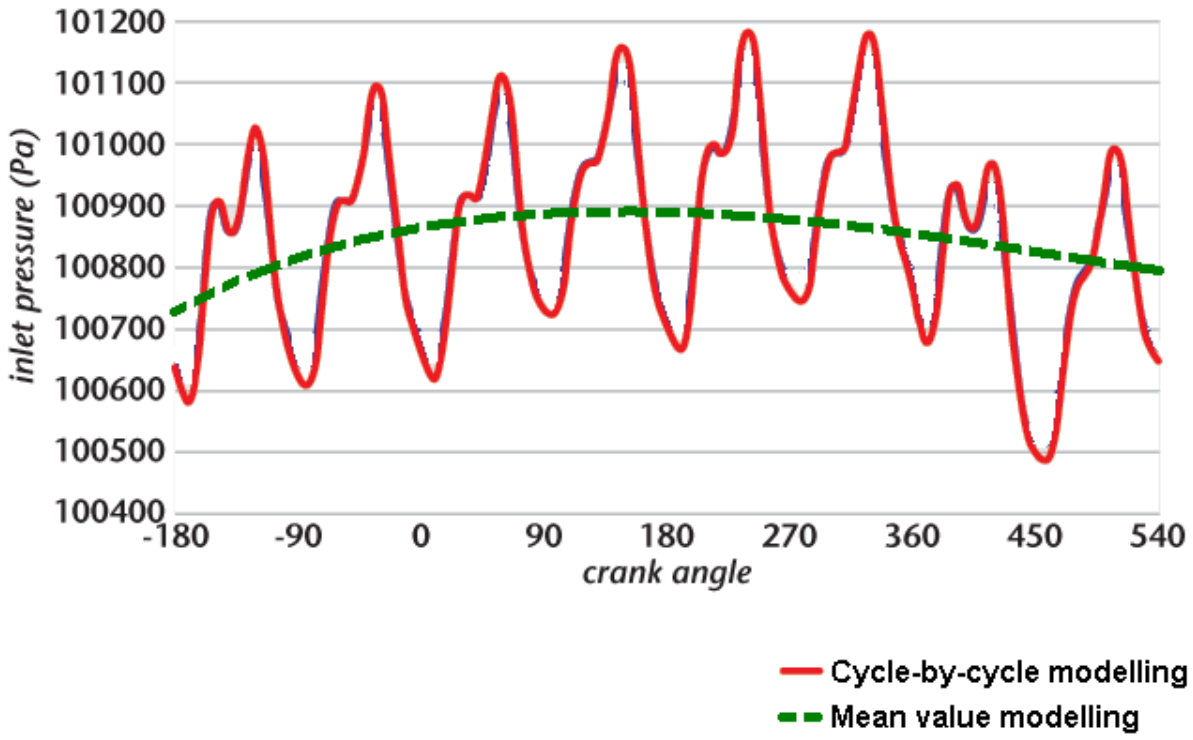

Figure 1.4: Cyclic and MV inlet pressure[3]

In some cases, the complete effect of a phenomenon may disappear with a MV model. Such an example is the inertial forces of the reciprocating components which affect the crankshaft as a torque. This torque can be simply explained as the force applied by the crankshaft to accelerate and decelerate the reciprocating components throughout a crankshaft rotation. The inertial torques of all reciprocating components in an engine are the cause of the cyclic engine speed fluctuations along with the cyclic cylinder pressures which created the need of a flywheel to be attached on the crankshaft to increase its rotational inertia.

[3] Edited from: *http://www.fluent.com/about/news/newsletters/04v13i2/a15htm*
Last time accessed: 23 October 2009

The total work done on the components, while neglecting frictions, is zero as they return to the exact same position in space after each revolution. The output of the inertial torque from a mean value model would be a constant zero value as it is the averaged value for each revolution which totally hides this phenomenon (Figure 1.5).

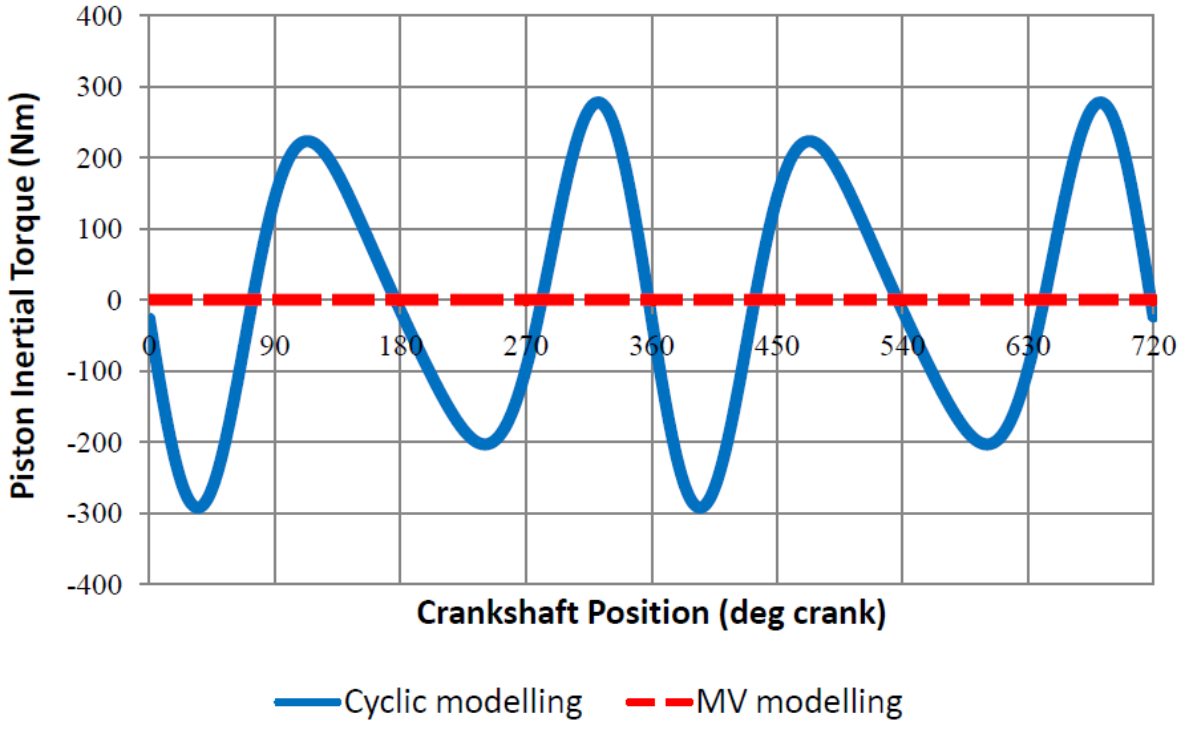

Figure 1.5: Piston inertia effect on the crankshaft (@ high speed)

One thing to have in mind is that different engines modelled using a MV type may produce the same mean value outputs at similar engine conditions while their cyclic values would be totally distinctive as each one will have a different pattern. Assuming a couple of turbocharged engines running at the same constant boost pressure; MV models will output this constant boost pressure value for their inlet manifold pressures, while cyclic models will

produce a unique pressure pattern for each engine with the boost pressure being their averaged.

The loss of information such as these described above is the major reason for choosing a cycle-by-cycle modelling type throughout this work. In addition, a cyclic engine model can be used to produce mean value outputs without any difficulty. A complete high fidelity cycle-by-cycle model could be used in a simulation package for example to evaluate all the desired mean value outputs which are needed for ECU calibration. As this process is basically the mapping of an engine model, the process can be named "*virtual mapping*".

1.4 Contribution

After studying the SI engine modelling literature, it was found that there is a lack of mean-value and cycle-by-cycle flow models that could describe a particular engine through all its operating range. In addition, the complexity of cycle-by-cycle engine processes is responsible for the discrete structure of cyclic models resulting in the difficulty of representing the engine in a dynamically continuous structure.

The current mean-value type of engine mapping is believed to have "flaws" as it has to be extensively repeated for every single engine [1, 2]. The problem arises as a result of the "mean-value" type of engine mapping and modelling.

The aim of this project is to develop a generic cycle-by-cycle model structure that can be used for cycle-by-cycle engine mapping; virtual engine model development and any other

application and configuration an engine model can be used including HIL, SIL and real-time applications [3]. This will hopefully facilitate the transition from mean-value engine mapping to a cycle-by-cycle mapping as the equations and complete sub-models that are going to be presented can be applied to any reciprocating SI engine. In addition to the equations, all the description of model parameter evaluation from a physical engine are explained, and specific tools were developed as standalone software to obtain typical valvetrain data for simulation, or fit the model with actual experimental data.

1.5 Structure of the thesis

CHAPTER 2: Literature review on engine modelling

A literature review on engine modelling is presented in order to understand the common types of modelling techniques currently used and the requirements of an engine model depending on its application. The focus then switches to the notation of the mapping technique and model structure commonly used which is thought to be the cause for the mapping and model calibration problems currently encountered.

CHAPTER 3: SI engine operation and control

A brief explanation of the spark ignition engine operation and control is introduced with the aim of explaining the components, processes and terms that are going to follow in the thesis.

CHAPTER 4: Crankshaft mechanism

The complete formulation of the piston and connecting rod kinematics are shown which form the base of cycle-by-cycle models. In addition, all reciprocating cylinder parameters are evaluated based on the piston motion.

CHAPTER 5: Valvetrain

A variable phasing and variable lift valvetrain model is presented in this chapter from which the effective valve flow areas are evaluated. A set of tools has been written as well in MATLAB which facilitate the valvetrain model calibration.

CHAPTER 6: Throttle kinematics

The formulation of the throttle effective flow area is presented as well as an approximation model which may find its use on real-time applications where the model execution speed can be crucial.

CHAPTER 7: Engine inertia

A mathematical rigid engine inertia model is derived as well as an experimental procedure to calibrate a model using transient speed measurements. This model takes into account all rotating components that have a constant speed ration with the crankshaft.

CHAPTER 8: Thermodynamic cycle modelling

An analysis is conducted to model the reciprocating motion continuously and the importance of using variable specific heats during a cycle-by-cycle simulation is evaluated in order to build an engine framework that can support this concept.

CHAPTER 9: SIES framework development

The development and structure of the Spark Ignition Engine Simulation (SIES v1.0) Framework is illustrated. The framework was developed in the MATLAB/SIMULINK[4] environment which has shown to be a flexible and invaluable tool for calculations and simulations.

CHAPTER 10: EngMap framework development

The development of the Engine Mapping (EngMap v1.0) Framework is presented which can form the base of the development of cyclic mapping procedures and data acquisition applications. The software used for this framework is the National Instruments LabVIEW[5] because of its flexibility and simplicity to acquiring sensor signals.

CHAPTER 11: Conclusions and future work

A further discussion is done around the subject of engine mapping procedures and possible improvements are explained. In addition, future framework developments are clarified.

[4] Mathworks Homepage: *http://www.mathworks.com/*
[5] LabVIEW Homepage: *http:/www.ni.com/labview/*

CHAPTER 2: Literature review on engine modelling

Mathematical modelling is used on engines since their first appearances. The main objective of early engine modelling was to increase the particular power output of an engine. The objectives switched to lower the fuel consumption and emissions due to the emission regulations introduced in recent years like the EURO 1 emission standards for passenger vehicles in 1992[6]. The regulations since then have not stopped becoming more severe which keep the field of engine modelling and control continuously evolving so that future vehicles can meet these standards.

The literature review has been divided into four different sections of focus interest. The first section deals with the main types of mathematical modelling techniques and structures used currently in engine modelling. A review of the engine model applications is following in order to understand the requirements needed depending on the model use. Then, the controversy between black-box and generic engine modelling is presented by denoting their advantages and weaknesses. Finally, the rationality and the ideas feeding this work are described as well as some important key elements that have been found in the literature that provided insight for the model structure development and application possibilities.

2.1 Engine modelling approaches

Over the past years, it can be said that the engine modelling approach switched from a mathematical to an experimental based. Literature shows that during the 60s and 70s, the

[6] *http://www.ceraclean.com/en/download/PKW_LightVehicles_EU.pdf*
Date last accessed: *15 July 2009*

cycle-by-cycle modelling approach was used in order to express the cylinder pressure and engine flow [4-9] while the researchers were trying to understand most of the processes occurring in the engine. In the beginning of the 80s, electronic advances allowed the electronic control units (ECU) to be cost viable for production and their low speed would require simple control algorithms [10]. The mean-value engine modelling became the only possible approach which could be implemented in the ECUs. Thus, the 80s would mark the transition to a mean-value engine modelling requirement, where all parameters and engine cyclic depended variables are tried to be expressed as averaged with the less possible calculations [11-13]. The installation of electronic controllers on engines increased the demand in engine control schemes development, engine mapping procedures, ECU calibration algorithms and structures.

In terms of literature availability between these model types, text books always present a more detailed and complete cycle-by-cycle model than journal/papers publications due to the complexity of such an entire engine model [14-18].

Another type of mathematical modelling used for non-linear models is soft computing algorithms. The components of soft computing are fuzzy logic, evolutionary algorithms and neural networks which have the ability to describe complex non-linear system input-output relationships quite accurately [19-22].

2.2 Applications of engine models

The applications possible of an engine model are almost unlimited. Computer engine models are helpful during the design process as they allow a simulation of the engine to be

built which speeds up the engine development process, reducing the trial-and-error changes before production. They serve as well as a tool to understand the processes and phenomena occurring, but can also be used for diagnostic algorithms development for on-board availability. A very important advantage is that a mathematical model of particular engine variable relationships can be developed to estimate quite accurately some variables which are difficult or even impossible to measure experimentally on an actual engine [6]. This approach can significantly reduce the cost of experimentation as more variables are estimated using a minimum amount of sensors and it would be correct to classify these engine models in the category of virtual sensors [23].

Engine models are widely used in the field of engine control as they facilitate the development and testing of control algorithms in real-time or not [24-26]. Sometimes, engine controller algorithms are such as that they require a version of the engine model to always be available in order to evaluate the control parameters. A real-time engine model is then embedded inside the controller. Powertrain controllers usually have an embedded vehicle model of which part of it is an engine sub-model providing the availability of estimating the particular effects between each vehicle sub-system has on the others [27].

The advances in electronics and personal computers gave birth to HIL and SIL simulations which can cut cost and production time significantly. A Powertrain Control Module (PCM) was connected to a mathematical model (SIMULINK[7]) of a throttle motor and TPS sensor in order to evaluate throttle responses [28]. ECU algorithms were tested in an automotive HIL

[7] SIMULINK Homepage: *http://www.mathworks.co.uk/products/simulink/*

platform (PiAutoSim[8]) to investigate its advantages which were very important as ECU signal noise levels and other problems could be identified during the testing [29]. A very good example of multiple HIL use in one application was the automated map-based ECU calibration by simultaneously controlling the engine ECU and dynamometer [30].

The type of engine model determines its application possibilities. Mean-value models are preferable wherever speed and simplicity is required. A mean-value engine model was used in a hybrid powertrain simulation to investigate the maximum allowable transients which do not produce irregularities and extreme excursions in the engine air-fuel ratio in order to keep the emissions within acceptable range [31]. Mean-value engine models have been developed as well for control algorithm developments where the required model inputs can be obtained from sensors that are available on engines and can predict engine behaviour with the less possible calculations and at an acceptable accuracy for control applications that do not require cyclic information [12, 32].

On the other hand, cycle-by-cycle modelling is used whenever cyclic data has to be estimated. One example is the cylinder pressure estimation that has been developed using custom heat release functions for the combustion which was validated to experimental pressure profile data [33]. The engine simulated was a direct injection methanol engine. Cycle-by-cycle gasoline direct injection (GDI) models have been developed as well for GDI torque control [34]. Another application of cyclic modelling has been the simulation of an engine model to obtain the variable valve timing (VVT) maps and visualise the effects of the VVT control strategy [35].

[8] PiAutoSim Homepage: *http://www.pi-shurlok.com/*

Powertrain modellers are interested mostly in cyclic torque as it can be used to predict oscillations, vibrations and speed fluctuations when the engine model is connected to a powertrain model. The speed fluctuations were successfully correlated to other engine variables as the speed is available on an engine due to the fast sampling rate of the crankshaft sensor which is used as well for crankshaft position estimation. A model was developed to relate the cylinder pressure variations to the speed fluctuations [36] and another for estimating the brake torque output in real-time for powertrain control [37]. The cyclic speed variations have been modelled as well for a single cylinder diesel engine which is designated for transient fuel control [38].

2.3 State models Vs generic models

Some of the literature encountered will be divided in this section into two categories in order to clarify the current techniques used. The first category includes the engine models encountered in which once the process of model calibration has been completed, it can only describe the particular engine from which the data was obtained and not even the same engine on some different conditions. Thus, these fitted models can describe only the "state of the particular engine" during the experimental data acquisition time. The naming convention "state models" has been selected for this reason.

On the other hand, the term "generic models" is going to be used to express the mathematical models that have to be calibrated for a particular engine but their model structure can still predict the same engine on a different state or on some cases another engine as well. Note that "state models" and "generic models" can be calibrated to estimate

variables for any engine; the difference comes in the allowable alterations that can be made on an actual engine that would require model re-calibration.

The main characteristic of "state models" is that they use multidimensional "black-box" calibration data. Another characteristic is that they are all mean-value engine models [39-40]. There is a huge amount of publications that present mean-value engine models due to the fact that they are preferred on different fields. An engine model developed in SIMULINK which can run in real-time was presented but its main disadvantage is that it requires a large model calibration procedure [27]. The same applies to an engine model used for an air-fuel ratio control using sliding mode technique [41], air-fuel ratio dynamics modelling on a sequentially injection engine [42], and in a diagnosis system which was described as a black-box type air flow model to evaluate sensor faults of the intake system [43].

The intake system mean value models are usually based on a manifold filling-emptying concept in which the intake manifold pressure is estimated by evaluating the mass change inside the manifold from the difference between the flow passing through the throttle and the air entering the cylinders [44] (Figure 2.1).

Filling – emptying manifold model

$$\frac{dP_m}{dt} = \left(\dot{m}_{thr} - \dot{m}_{cyl}\right)\frac{RT_m}{V_m} \qquad \text{(Eq. 2.1)}$$

Where:

P_m, T_m andV_m: Intake manifold pressure, temperature and internal volume respectively

$\dot{m}_{thr}$: Mass air flow through the throttle

$\dot{m}_{cyl}$: Mass air flow into the cylinders

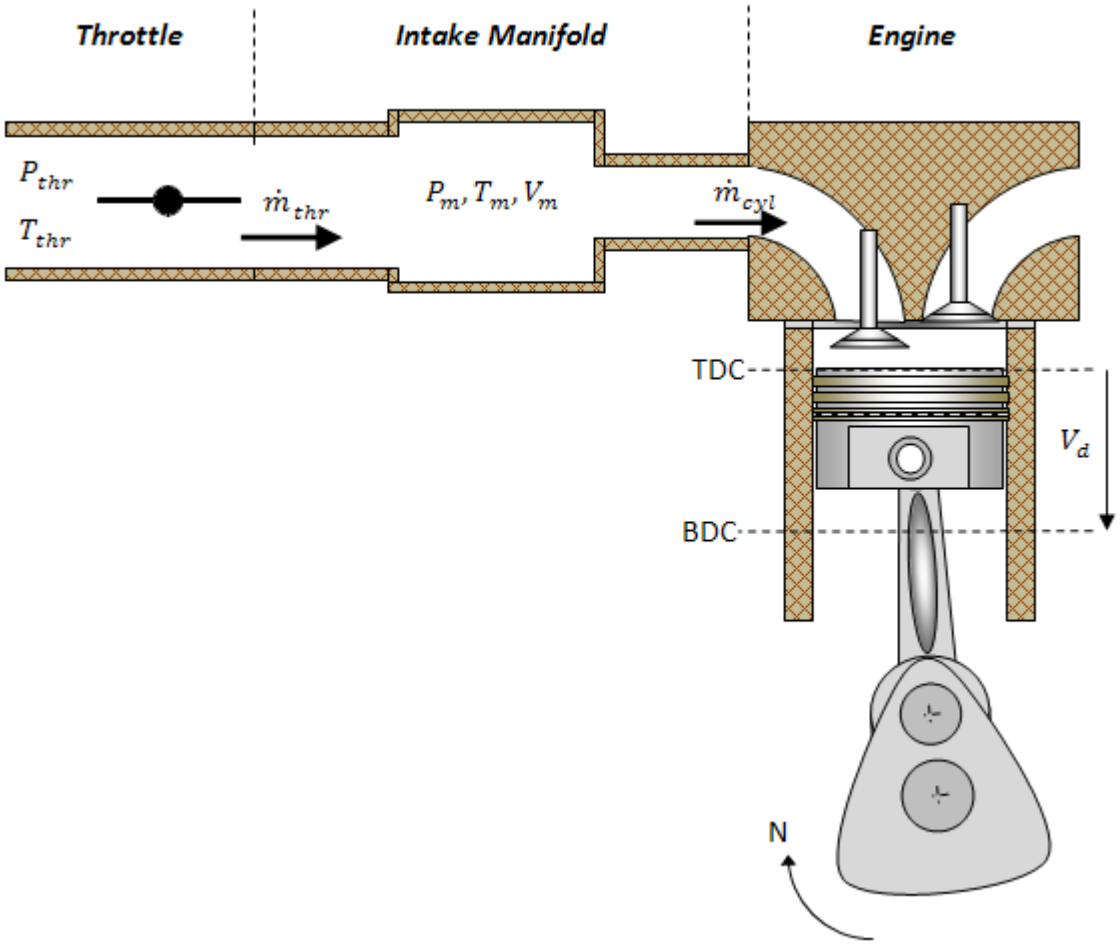

Figure 2.1 Intake air flow dynamics

Note that multi-dimensional mapped variables are added to (Eq. 2.1) to include the effects of the EGR system. The standard orifice isentropic compressible fluid flow equation is usually used to describe the flow through the throttle by mapping the discharge coefficient $\boldsymbol{C_D}$ as a function of throttle angle and pressure ratio across the throttle [32, 39, 42, 45-47].

Mass air flow through the throttle [32]

$$\dot{m}_{thr} = \frac{\boldsymbol{C_D} A_{thr} P_{thr}}{\sqrt{R T_{thr}}} \left(\frac{P_m}{P_{thr}}\right)^{1/\gamma} \Upsilon \qquad \text{(Eq. 2.2)}$$

With Υ*:*

Un-chocked flow : $\frac{P_m}{p_{thr}} > \left(\frac{2}{\gamma+1}\right)^{\frac{\gamma}{\gamma-1}}$

$$\Upsilon = \left\{ \frac{2\gamma}{\gamma - 1} \left[1 - \left(\frac{P_m}{P_{thr}}\right)^{\frac{\gamma-1}{\gamma}} \right] \right\}^{\frac{1}{2}} \qquad \text{(Eq. 2.3)}$$

Choked flow: $\frac{P_m}{P_{thr}} \leq \left(\frac{2}{\gamma+1}\right)^{\frac{\gamma}{\gamma-1}}$

$$\Upsilon = \left(\frac{2}{\gamma + 1}\right)^{\frac{\gamma+1}{2(\gamma-1)}} \qquad \text{(Eq. 2.4)}$$

Where:

$\boldsymbol{C_D}$: Discharge coefficient obtained experimentally

$A_{thr}, P_{thr}, T_{thr}$: Throttle effective flow area, pressure and temperature respectively

P_m: Intake manifold pressure

γ: Gas specific heat ratio

The mass air flow entering the cylinders is evaluated using the volumetric efficiency pumping equation [40, 47, and 48] which requires the mapping of the engine's volumetric efficiency as a function of at least intake manifold pressure and engine speed [22].

Mass air flow into the cylinders

$$\dot{m}_{cyl} = \boldsymbol{\eta_V} \frac{P_m V_d}{R T_m} \frac{N}{120} \qquad \text{(Eq. 2.5)}$$

Where:

$\dot{m}_{cyl}$: Mass air flow into the cylinders

P_m and T_m: Intake manifold pressure and temperature respectively

V_d and N: Engine's displacement volume and speed respectively

$\boldsymbol{\eta_V}$: Volumetric efficiency obtained experimentally (multi-dimensional)

A fuel wall wetting model is required whenever transient engine operations are considered. This is due to the fact that some of the injected fuel sticks on the manifold walls and intake valves and ports because ECUs inject the fuel when the intake valves are closed [49]. This fuel mass is referred as *"puddle mass"*. Whenever a flow change occur, the amount deposited on the walls change as for example during a throttle step which leads to air-fuel ratios excursions. This effect is not new but was tried to be mechanically solved on carburetted engines using exhaust heat to vaporise the fuel before mixing it with air[50, 51].

The puddle mass wall wetting model (Figure 2.2) is described by the following equations and requires the mapping of the time constant for fuel vaporisation $\boldsymbol{\tau_f}$ and proportion of the fuel that is depositing on the manifold $\boldsymbol{X_f}$. [10, 19, 40, 41, 45]

Fuel wall wetting model

$$\dot{m}_{ff} = \frac{1}{\boldsymbol{\tau_f}}\left(-\dot{m}_{ff} + \boldsymbol{X_f}\dot{m}_{fi}\right) \quad \text{(Eq. 2.6)}$$

$$\dot{m}_{fv} = \left(1 - \boldsymbol{X_f}\right)\dot{m}_{fi} \quad \text{(Eq. 2.7)}$$

$$\dot{m}_f = \dot{m}_{fv} + \dot{m}_{ff} \quad \text{(Eq. 2.8)}$$

Where:

m_{fi}: mass of fuel injected

m_{ff}: mass of fuel film (puddle)

m_{fv}: mass of fuel injected reaching the intake valve

m_f: mass of fuel entering the cylinder

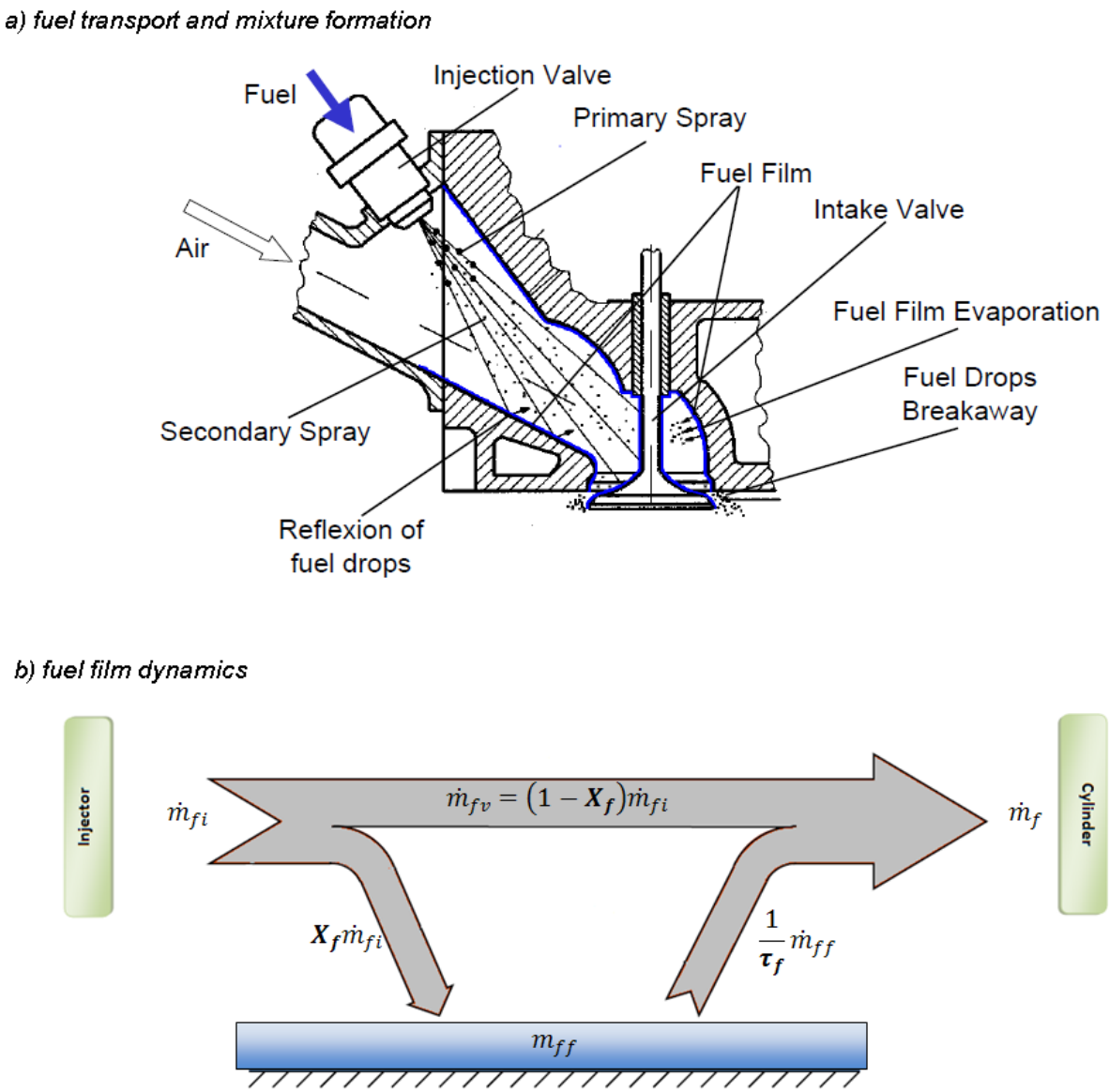

Figure 2.2: Fuel flow dynamics (adapted from [52])

The exhaust pressure mapping is tried to be avoided due to the cost of sensory equipment needed for the measurement of exhaust gases. This is the reason why the exhaust pressure is estimated using the air intake information. Different methods can be used to evaluate the exhaust pressure, the intake air flow model [53], the engine's residual gas map or

volumetric efficiency [54]. The downside is that these methods are not applicable when the engine is turbocharged.

The amount of data that has to be collected from an engine just to represent the air and fuel flow as shown is immense and usually multidimensional. These multidimensional maps increase in complexity whenever a components or effect that is in *"contact"* to the air, fuel or exhaust path can be altered on the engine such as compression ratio, valvetrain components and timings [17]. This is the reason why the mapping procedure is reduced by mapping the engine on steady state conditions while transient operations are assumed to have the same maps.

On the other hand, cyclic modelling is more generic as it requires less model calibration data. Cycle-by-cycle models can simulate for example engine pressure and combustion without the need of much of a model calibration. This is due to the fact that the model parameters are mostly gas properties and combustion coefficients which are more or less same on every engine of the same type. If these parameters were to be mapped, they would never exceed a 2-dimensional map. A great example is the Wiebe function heat release model which is widely used to model the combustion in cycle-by-cycle models [8, 55-58]. The only parameter that has to be mapped here is the duration of combustion.

Wiebe heat release function:

$$f_{b(\theta_c)} = e^{\propto\left(\frac{\theta_c-\theta_s}{\theta_d}\right)^n} \quad \text{(Eq. 2.9)}$$

This heat release function evaluates the mass fraction of fuel burnt $f_{b(\theta_c)}$ at θ_c which is the crankshaft angle at which the calculation is done, while θ_s and θ_d is the crankshaft angle at which the combustion starts and the duration of the combustion in crankshaft angle respectively. The terms $\propto$ (usually=5) and n (usually=2 to 3) are coefficients defining the shape of the function curve.

One dimensional gas and fluid dynamic numerical models are used as well for engine design and simulation of engine processes [59-61] but their disadvantage is that they are complex and the complete air and gas flow paths have to be divided into small pieces (mesh) to evaluate the flow. Their calculation usually requires a large amount of time as it is an iterative process.

2.4 Cycle-by-cycle modelling and mapping

The current engine modelling and mapping method preferred (mean-value) looks like it has reached a critical point. At the beginning of its use, almost no engine had variable air/gas flow parameters except maybe an exhaust gas recirculation (EGR) valve and rarely a camshaft phasing. Thus, the maps were quite simple compared to what they should be for let's say an engine with variable lift, variable phasing, etc. In addition, control algorithms always evolve, becoming more complex, and requiring more accuracy from the engine model. Taking the intake system for instance, the unavailability of a proper model to predict the flow mixing during the valve overlap period was stated by the authors of [59, 62] and the unavailability of an accurate intake manifold dynamic model during warm-up periods in [63] which would not have been a problem for a proper cycle-by-cycle model.

A cycle-by-cycle modelling approach will facilitate the understanding of the processes occurring in the engine. For example, the intake air charge was found to be proportional to the intake manifold pressure in [39] and the authors stated that it was a "surprisingly simple relationship". They also denoted that the intake air charge per stroke is the variable that has to be modelled for cylinder intake and not the volumetric efficiency. This simple relationship was hidden all this time in the volumetric efficiency maps. A more detailed physics based modelling is going to reveal other correlations that will reduce the complexity and dimensions of maps required to represent an engine on a mathematical model. As correctly stated in [10] mathematical model complexity simplifies the mapping and model calibration procedures, which will reduce the ECU calibration costs [12, 31].

A more detailed fuel wall wetting model was developed in [64] which resulted in an easier calibration. It is my understanding that the models are going to be continuously extended to a more physics based approach until they are going to end up to a high fidelity cycle-by-cycle structure in the future. The future trends were denoted in [65] as being automated calibration and adaptive control on a cycle-by-cycle basis. The automated self-learning ECU calibration is an attractive field and looks promising [30, 66-69] while the adaptive controllers difficulty in the development phase and great potential is stated in [70]. The availability of an *"engine simulation framework"* would facilitate the development and algorithm testing. In addition, control engineers, would not have to go through the complete cycle-by-cycle modelling as they could directly select the engine variables of interest in the model.

The GDI control model requirements are a bit different than the port injection engines. The moment of fuel injection in a port injection engine is affecting the fuel flow into the cylinder and the manifold pressure which rephrases to intake air flow. On a GDI engine, the moment of injection in addition affects the fuel flow through the injectors due to the difference in cylinder pressure which makes it an important parameter.

The cycle-by-cycle mapping of an engine may be more expensive due to the need of cyclic sensory equipment such us cylinder pressure sensor. The development of new low cost cylinder pressure sensors [8] that can be even used for production purposes [71] have made this mapping method viable.

2.5 Guidelines

The key elements that served as guidelines which were found in the literature are presented below. The inlet and exhaust flows are affected by the in-cylinder gas motion, port design [72] and manifold sizes [45] while the valve lift affects the intake port speed which leads to affecting the fuel vaporisation [73]. In addition, the valve lift undergoes three flow regimes as stated in [7, 15, 16] and was experimentally confirmed in [7, 73] which denotes the importance of using three different effective flow area models during a complete valve lift event. Another important parameter stated in [9] during the intake and exhaust flows is the instantaneous piston speed.

If any engine model must be developed, an EGR system is mandatory sub-model to meet current and future emission regulations [74]. In addition, the crankshaft would have to be modelled as a flexible component if the model is to be used for cyclic variations [75].

A cycle-by-cycle model structure would have to be continuous for simplicity and calculation speed [76] and its accuracy may be increased by the use of variable specific heats for the modelled gases [14, 77].

New designs on engine sub-systems or complete engines could be easily simulated on a complete cycle-by-cycle engine model. For example, the potential use of the Atkinson cycle on a diesel engine was simulated in [78].

A cycle-by-cycle simulation framework will be able to output the maps doing a virtual engine mapping to map mean-value engine models [40]. An engine model developed using the GT Power was successfully used to obtain optimum camshaft profiles for a particular engine [56].

Two identical engines require different fuel and spark advance maps on a map based ECU. This is mainly due to the manufacturing tolerances of each individual component and maybe assembly variation (i.e. one may have a camshaft timed half a degree differently). A virtual engine model can provide insights to which component tolerances compromise these variations, and which in what amount.

The study of the literature inspired the creation of a cycle-by-cycle spark ignition simulation framework in MATLAB/SIMULINK which will provide the base of a complete cyclic model that could be for any desired application. The structure will have to be modular such as different sub-models could be easily implemented and compared.

In parallel, a cyclic engine mapping framework is being developed in National Instruments LabVIEW for engine flow model development and mapping. Both frameworks have to be developed using the same model equations so that the data obtained experimentally calibrates correctly the simulation models. The unavailability of a proper light valve flow model to be used in cycle-by-cycle simulation explains the reason that the isentropic flow equations (Eq. 2.2 - 2.4) are used instead [34, 58], while others totally neglect the intake and exhaust flow during simulations [37, 79].

CHAPTER 3: SI engine operation and control

The internal combustion engines have been chosen for road transportation over the years due to their high efficiency and low production cost. They can be classified using different factors such as displacement volume, number of cylinders, number of valves, cylinder orientation, camshaft position, valve train type, etc. There is also a classification depending on the type of fuel they are burning. The two main types of road vehicle engines used are the spark ignition engine (SI engine) and the Diesel Engine.

The Diesel Engine and fuel was named after its inventor (Rudolf Christian Karl Diesel) which included his work and invention in a publication and formed the basis of his work. The diesel engine which is also called the Compression Ignition engine (CI engine) causes enough pressure and temperature on the fuel to start a spontaneous fuel combustion by auto-ignition. On the other hand, the SI engine uses a spark to ignite the fuel following the Otto cycle named after Nicolaus Otto which was the first to develop a working engine, although he didn't hold the patents.

Internal combustion engines haven't stop evolving since their first appearance. While the main objective on earlier years was to increase the power output and reliability, their design and electronic control strategies have switched to decrease emissions output and fuel consumption over the past years while trying not to compromise the power output.

The fact that electronic fuel injection systems have been installed on SI engines allowed the development of control schemes and algorithms which are since then a constantly evolving

field as it allows an on-board real-time processing unit which by reading the engine's sensory system it then evaluates the required actuation for a particular desired effect.

A brief description of the SI engine components, operation and control is going to be presented below as it is always better to understand the subject system before modelling it.

3.1 SI engine operation

The SI engine is operating following a repeating cycle of four-strokes which are the intake, compression, expansion (or power) and exhaust stroke.

Intake Stroke: The piston is currently at TDC (Top Dead Centre) with the intake valve open, as the piston moves towards BDC (Bottom Dead Centre) fresh air is drawn inside the cylinder through the open intake valve. This process (TDC to BDC) is called the intake stroke (Figure 3.1). If it is a direct injection engine, meaning that the fuel is injected inside the cylinder, then only fresh air is drawn in otherwise it is a mixture of air and fuel. It is important to note that on actual engines, not only fresh air is usually drawn in, but in some cases (depending on valve timing) exhaust gases may be inducted inside the cylinder through the intake valve.

Compression Stroke: The intake valves close a bit after BDC enclosing the mixture inside the cylinder and the piston moves from BDC to TDC increasing the pressure and temperature of the mixture (Figure 3.1). The only flow out of the cylinder during this process if the engine and components operate correctly may be the flow through the piston rings which is referred to as "blow-by" losses. This effect is happening because the pressure inside the

cylinder is significantly higher than the crankcase pressure and the piston rings cannot perfectly seal the cylinder.

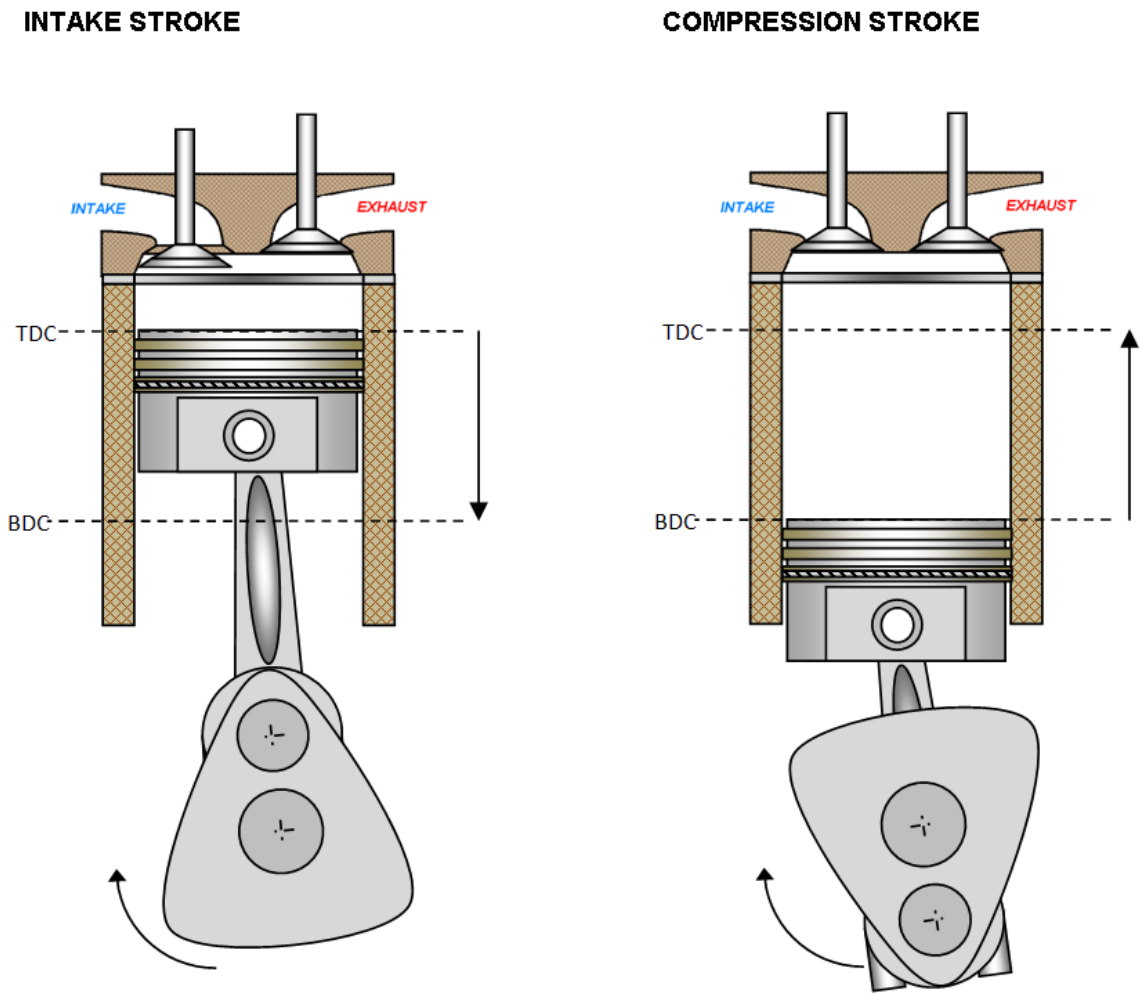

Figure 3.1: Intake and compression strokes

Expansion or Power Stroke: Towards the end of the compression stroke, the spark plug is fired which ignites the mixture and the combustion process starts. As the piston passes TDC, the gas pressure pushes the piston towards BDC and the cylinder volume is expanded

(Figure 3.2). This stroke is usually the only one producing useful work and thus also called the “power stroke”. The highest value of cylinder pressure during a cycle usually occurs on the first quarter of this stroke.

Exhaust Stroke: The exhaust valve opens just before BDC to take advantage of the higher cylinder pressure which creates momentum in the exhaust manifold and reduces the amount of work needed to remove the exhaust gases from the cylinder. Then, the rest of the exhaust gases are pushed out by the piston as it moves to TDC (Figure 3.2).

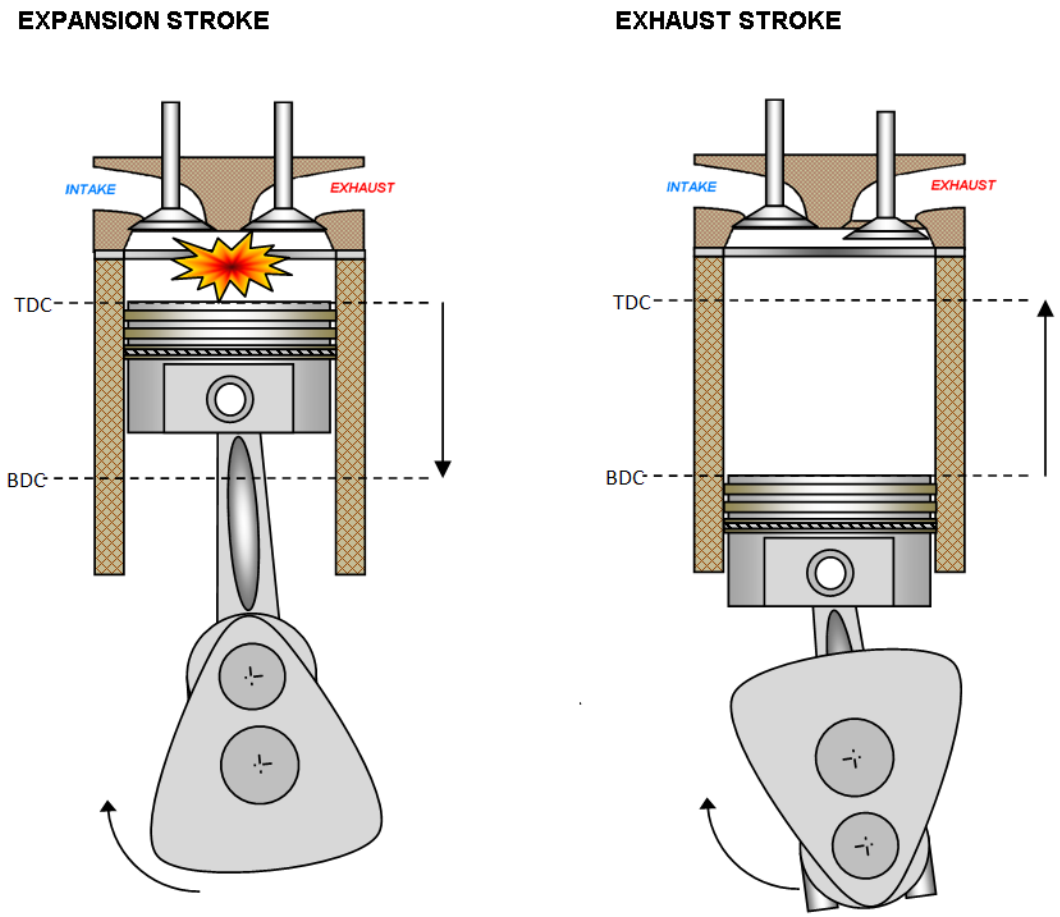

Figure 3.2: Expansion and exhaust strokes

The intake valve is opened before TDC for the intake stroke which produces a duration which is called “the valve overlap” as both intake and exhaust valves are simultaneously open. The remaining gases inside the cylinder are named “residual gases”. They occur firstly because at TDC the cylinder volume is not zero, and secondly because a portion of the exhaust gases sometimes exit through the intake valves during overlap and low engine speeds. These are drawn back inside on the next intake stroke.

3.2 SI engine control

The spark ignition engine has evolved from a simple mechanical controlled system to a complex electronically controlled when the emission requirements became more demanding. In addition, the market competition and environmental global warming over the past years have set an aim to reduce the fuel consumption to the minimum possible.

There are engines that have a large amount of control systems working simultaneously to achieve a smooth operation, efficiency and comfort. These can be variable valve timing control, idle speed control algorithms, exhaust gas recirculation, spark timing, fuel injection, etc. Nevertheless, every control system named above is a field of its own and thus only the control of fuel injection and spark timing is going to be described as they are the two fundamental control systems found in every today’s vehicle.

3.2.1 Fuel injection

Over the years, quite a number of injection systems have been used on spark ignition engines. When the transition from carburettors to injection systems was under way, the most common injection systems were the single point injection systems which generally

consisted of a throttle plate valve along with an injector. Their advantage at their time was that they could directly replace the carburettor on a specific engine design without the need of any significant intake manifold, or vehicle design alteration.

The multi-port injection systems that followed and that are still today the most commonly found, have one injector (sometimes two) per cylinder placed on the intake manifold closed to the cylinder head intake port. The injection events are either sequentially, simultaneously (all injector fired simultaneously) or batched (pairs of cylinders).

When the injected fuel reaches a closed inlet valve, the mixing is done inside the manifold volume and the fuel wetting phenomenon is an important phenomena to consider modelling.

The latest injection system used commercially on spark ignition engines is the direct injection system, the concept which is to inject the fuel directly inside the cylinder during the compression, and thus totally cancelling the effect of fuel wetting inside the manifold.

The proper simulation and modelling of a generic fuel wetting model can be done only in a cycle-by-cycle engine model structure due to the fact that the crankshaft position at the moment of injection is important. The same applies for a direct injection system as the timing of injection inside the cylinder defines along with the duration the amount of fuel that is going to be injected and the air-fuel mixing process. The objective of the fuel injection is to accurately control the air fuel ratio by keeping it as close as possible to the stoichiometric value (14.7 kg air/ kg fuel) for which the 3-way catalysts operate at its higher efficiency.

A richer mixture should be used in the case of maximum power output requirements. On moderns 4-valve per cylinder naturally aspirated engines, the maximum power output is usually achieved at a mixture ratio between 12.8-13.2 kg air/kg fuel.

3.2.2 Spark timing

The second important control parameter in a SI engine is the spark timing. It is needed due to the fact that the combustion requires an amount of time to complete and in addition, the effect of knocking occurring.

The flame of the combustion starts at the spark location and propagates fast thorough the whole cylinder volume with its speed usually referred as “flame speed”. The pressure and temperature inside the cylinder rise rapidly during this period. If the un-burnt mixture’s temperature surpasses a limit, it will self-ignite. A spontaneous self combustion is occurring which creates large pressure oscillations and temperatures which can damage engine components.

The maximum pressure and temperatures of the combustion have then to be kept below the knock limit which is possible by altering the moment of spark firing. The spark timing is also named as “Spark Advance” (SA) and its units are in degrees of crankshaft before TDC. (i.e. 25° SA means 25° before the end of the compression stroke).

There is a value of SA for every engine operating condition that produces the maximum brake torque output which is called the “Maximum Brake Torque” timing (MBT). Any advance or retardation from that timing will reduce the brake torque output.

The generic modelling of the spark advance effect on engine variables and knocking can as well only be achieved using a cycle-by-cycle engine model structure.

3.2.3 ECU

The Electronic Control Unit (ECU) has the task to control the engine actuators to achieve specific goals. It is able to evaluate the correct actuation quantities by monitoring the engine sensors.

A typical list of the most common sensors (Figure 3.3) and reasons the ECU is monitoring them is given below:

Mass Air Flow (MAF): It is used to measure the intake air flow between the filter and the throttle using the hot-wire measurement method. This sensor is an important reading that the ECU has available for closed-loop control.

Manifold Absolute Pressure (MAP): The manifold absolute pressure is used for the evaluation of the air flow and sometimes it is used as well for applying correction factors on the actuations.

Lambda sensor: It provides a signal from which it can be identified if the mixture burnt was rich or lean and is also called a narrowband O2 sensor.

Wideband O2 Sensor: It is able measure accurately the exact air-fuel ratio of the mixture burnt usually between the range: 10-18 kg air/kg fuel.

Air temperature: The measurement of the intake manifold air temperature along with the pressure can be used to evaluate the air density value by the ECU. Programmable ECUs uses

this measurement to apply the appropriate correction factor on spark advance and fuel injection.

Coolant temperature: The coolant temperature is the closest reference to the engine components temperature and thus cylinder temperature. It is used as well to evaluate the desired actuation amounts.

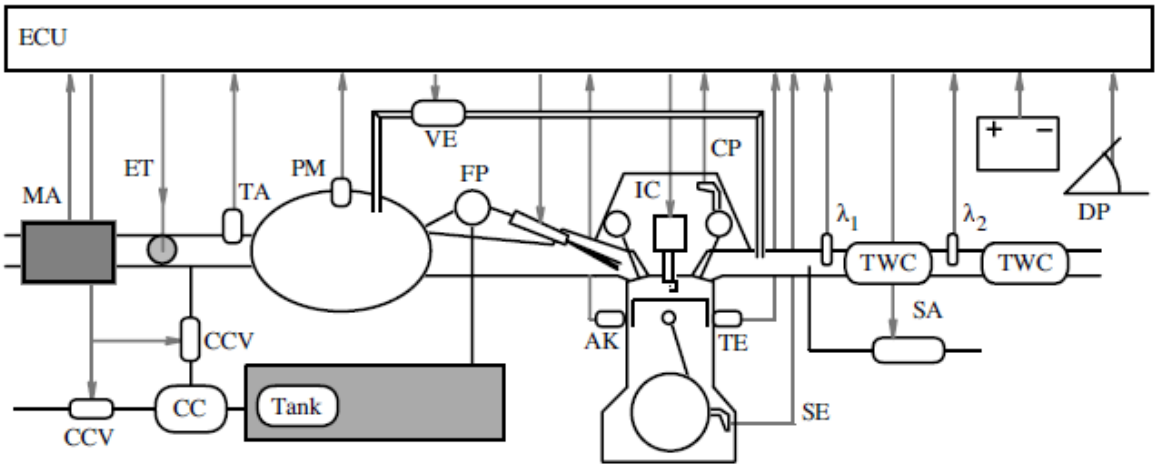

AK	knock sensor	PM	manifold pressure sensor	VE	EGR valve
CP	camshaft sensor	ET	electronic throttle	SA	secondary air valve
IC	ignition command	TA	intake air temperature sensor	TWC	3-way catalyst
MA	air mass-flow sensor	TE	cooling water temperature sensor	ECU	controller
SE	engine speed sensor	CC	active carbon canister	CCV	CC control valves
FP	fuel pressure control	$\lambda_{1,2}$	air/fuel ratio sensors	DP	driver pedal

Figure 3.3: Schematic representation of the sensors and actuators present in modern gasoline engines [65]

Crankshaft & camshaft sensor: The crankshaft sensor signal is a frequency wave from which the ECU can evaluate the actual engine position, speed and acceleration. This signal is very important for the spark timing as it is the reference point. The camshaft sensor is needed to

evaluate the next firing cylinder on a sequential injection engine and the individual piston strokes if needed, as well as the engine speed.

Knock Sensor: The knock sensor outputs a high frequency signal when the engine is knocking and thus the ECU can retard the spark timing until knocking stops.

The ECU algorithms can be classified into two main categories, closed-loop and open loop. A closed-loop control scheme is a control structure in which the actuations are evaluated dynamically by monitoring all sensors and the response of the desired variable. The controller tries to minimise the error between the desired value and the actual. Taking as an example the air-fuel ratio control, the signal from the exhaust lambda sensor is the response that the ECU tries to correct. The open-loop control applies to a controller that sets the desire value but do not have a feedback to determine in reality if it has achieved its goals.

An interesting thing to note at this point is that even without an open-loop control, an engine can be controlled perfectly. Programmable aftermarket ECUs if calibrated properly, can achieve an accurate operation. Their main structure usually consists of 2-D data tables for injection duration and spark advance. Once the engine condition is obtained, the ECU retrieves the actuation values from the tables and then applies corrections based on the sensor signals. The actuation calculations in a map based ECU structure are non dynamic input-output functions.

3.3 Summary

The engine goes through an extensive testing to evaluate the effect of all control parameters from which maps are developed. These are then used by the ECU alongside with the feedback of the lambda sensor to calculate the control parameters such as spark advance and injection duration. The mathematical models used in the ECU are MV models which limit the control possibilities (i.e. injection moment). The ECU usually has a large amount of algorithms for controlling different engine parameters such as idle control and boost control. It may have as well specific algorithms to control the engine on different regimes. An example is the warm-up regime which main purpose is to quickly warm-up the catalyst converter so that it does not operate on low conversion efficiency for a long period of time.

CHAPTER 4: Crankshaft mechanism

The kinematic motion of the piston is without a doubt the starting point of all cycle by cycle reciprocating engine models. It is an important part as it forms the basis of a cycle-by-cycle dynamic engine model due to the fact that cylinder geometry is related to the piston position. In addition, all cyclic variables such as torque, cylinder pressure, manifold pressure, etc, are affected by the crank mechanism. The work that follows describes the formulation and development of a complete reciprocating crankshaft mechanism dynamic mathematical model so that it can form the basis of a complete cycle-by-cycle engine model. In addition, the crankshaft mechanism's piston pin offset which is usually neglected on similar cyclic equations has been taken into account and has shown that in some cases its absence may produce significant errors.

4.1 Crankshaft dynamics

Although a large amount of literature exists on the subject of cycle-by-cycle modelling, it is hard to come across the equations of motion for the piston and connection rod which would evaluate their instantaneous speed and acceleration while the piston pin offset parameter is totally neglected even when evaluating the piston position. The effect of this parameter becomes noticeable when the inertial forces of the connecting rod and piston are evaluated as it is noticeably affecting the acceleration of the piston and connecting rod. The piston pin offset is usually only referred on literature on engine noise reduction as it is one of the parameters optimised to reduce piston slap which occurs when switching from

the compression to the expansion stroke [80]. The calculation errors than can occur by neglecting the piston pin offset in cycle-by-cycle simulations are clearly stated in [18].

An effect that is produced by offsetting the reciprocating mechanism is that the strokes become uneven. This results in unequal stroke durations in time units when an engine is rotating at constant speed. The uneven stroke lengths can be seen in the operation of free piston engines [81, 82] which can be thermodynamically optimised by producing a faster expansion which increases the efficiency [83].

The mean piston speed is usually used to map the intake flow processes as it has shown to fit better experimental data than the crankshaft speed [17]. Although better, it is still not perfect as different engine may have the same mean piston speed. Their distinctive variable is the instantaneous speed which should be used for intake flow mapping.

Piston position and velocity equations usually do not include the piston pin offset [16, 79, 84]. An exception is present in [38] which takes into account the piston pin offset to evaluate the piston position which in turn is used in a prediction model of cyclic speed variations on a single cylinder diesel engine.

4.2 Parameters of the crankshaft mechanism

The piston motion can be derived by analysing the geometry of the crank mechanism. The analysis that is going to follow is based on the assumption that the piston pin has an offset relative to the cylinder centre line of piston motion. It is important to have in mind that a crankshaft axis offset has exactly the same effect as both analysis lead to the same result.

Thus, at this point a new parameter has to be introduced in order to take into account the total offset of the crank mechanism during the mathematical analysis.

The total crank mechanism offset affecting the piston motion is given by:

$$O_t = O_c + O_p \qquad \text{(Eq. 4.1)}$$

O_t is the total crankshaft mechanism, O_c is the crankshaft offset and O_p the piston pin offset in meters.

A representation of crankshaft mechanisms having a crankshaft and piston pin offset as well as their positive assumed directions is shown in Figure 4.1. The clockwise rotation is chosen to be the positive direction for angular motions throughout this work.

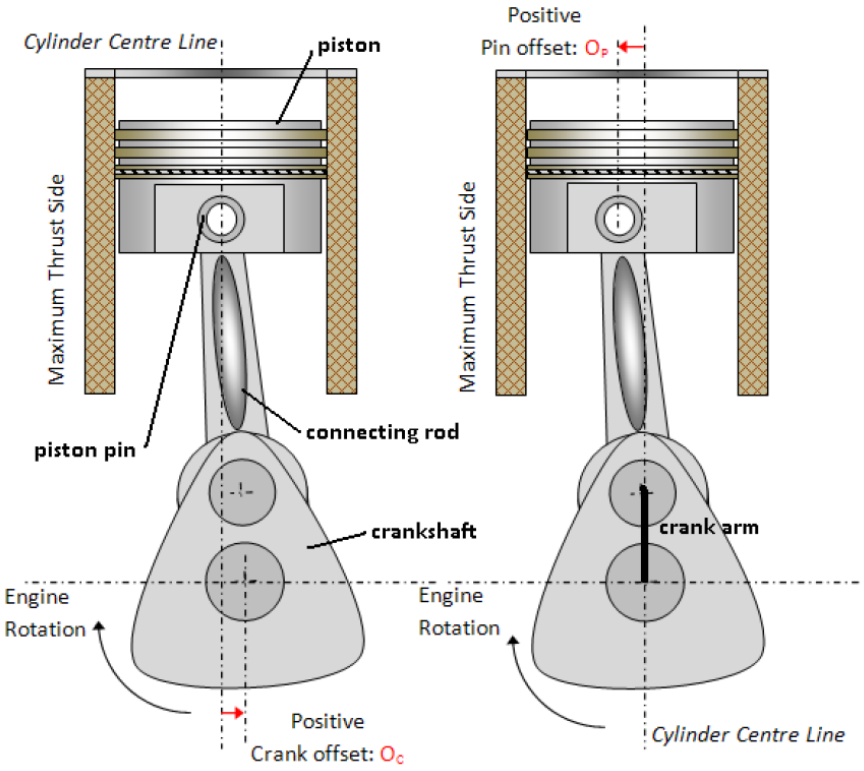

Figure 4.1: Crankshaft and piston pin offsets

The crank arm angle is zero at TDC and the piston stroke is twice the crank arm radius when the crank mechanism does not have an offset. In the other hand, when there is an offset, everything is different. The piston stroke and crank arm angle at TDC become a function of the offset.

The only problem rising at this point is the choice of reference point. It is not practical to use the crank arm angle as an input to the equations as TDC occurs at a no zero angle due to the offset (Figure 4.2). This can be solved by introducing another parameter named "*engine angle*" which will have a value of zero at TDC.

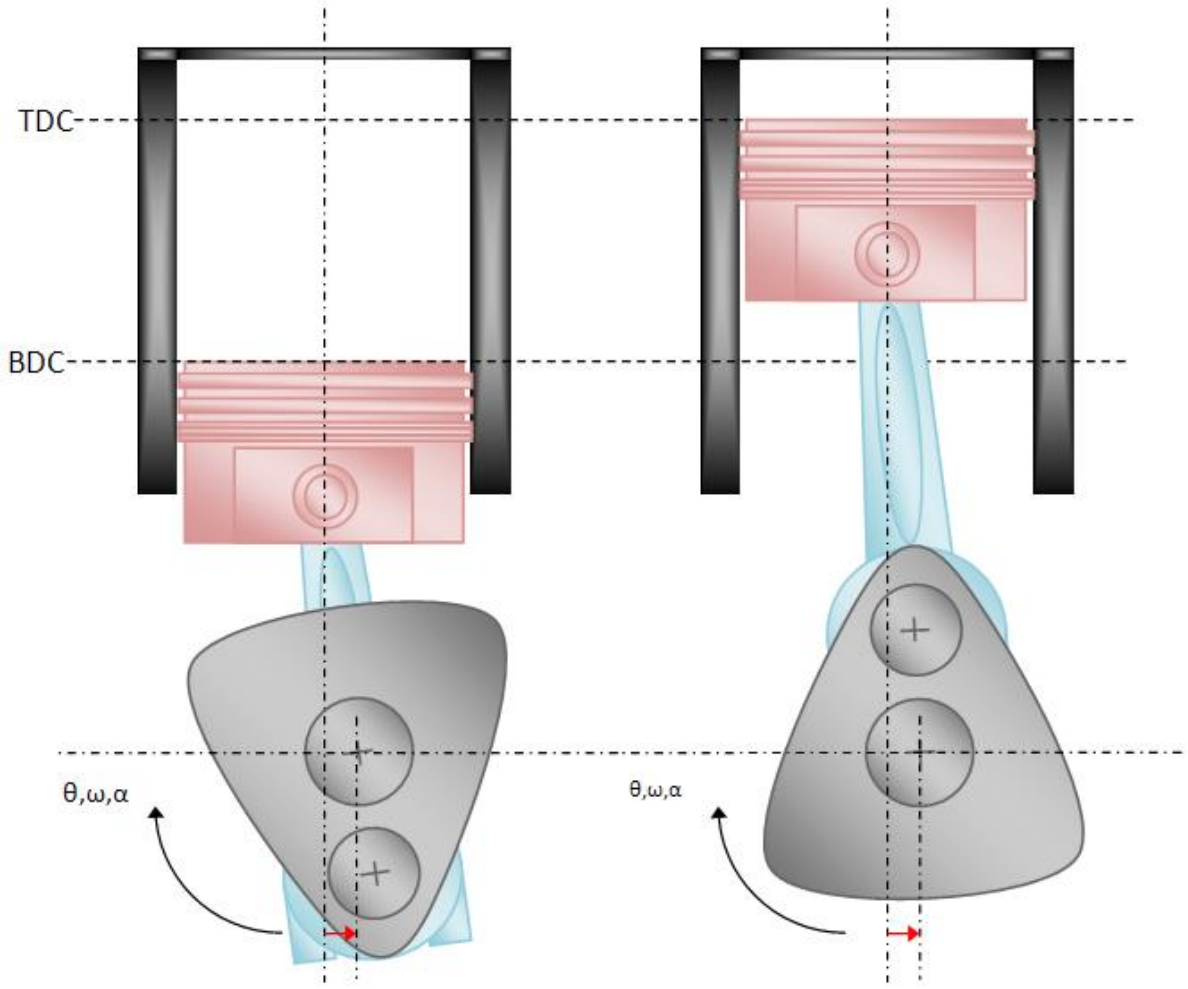

Figure 4.2: Crankshaft mechanism BDC and TDC positions with offset

The position angle of the crank arm rotating the end of the connecting rod is going to be denoted as ϕ and the engine angle as θ. BDC & TDC piston positions on a positive total offset can be seen in (Figure 4.3). It is understandable from the picture that the stroke of the piston is no longer twice the crank arm and that the TDC and BDC positions are no longer at 0° and 180° crank arm angle respectively.

Inspecting the diagram (Figure 4.3), the crank arm positions for TDC and BDC can be evaluated using trigonometry[9]. TDC and BDC crank arm angles (ϕ_{TDC} *and* ϕ_{BDC}) are referred to as angles of obliquity [18] and are given by:

$$\phi_{TDC} = -\sin^{-1}\frac{O_t}{L+K} \qquad \text{(Eq. 4.2)}$$

$$\phi_{BDC} = 180 - \sin^{-1}\frac{O_t}{L-K} \qquad \text{(Eq. 4.3)}$$

L is the connecting rod length (m) and K is the crank arm radius (m).

As referred previously, the engine stroke is not anymore twice the crank arm length when an offset is present. The following equation (Eq. 4.4) gives the piston stroke of an engine with an offset piston motion.

Piston stroke:

$$S = Xp_{TDC} - Xp_{BDC} = \sqrt{(L+K)^2 - {O_t}^2} - \sqrt{(L-K)^2 - {O_t}^2} \qquad \text{(Eq. 4.4)}$$

[9] *0 reference shown on the diagram Figure 4.3 as Φ=0°.*

The interesting effect of an offset reciprocating motion is the unequal stroke durations which are given below (Eq. 4.5 & Eq. 4.6) using (Eq. 4.2 & Eq. 4.3).

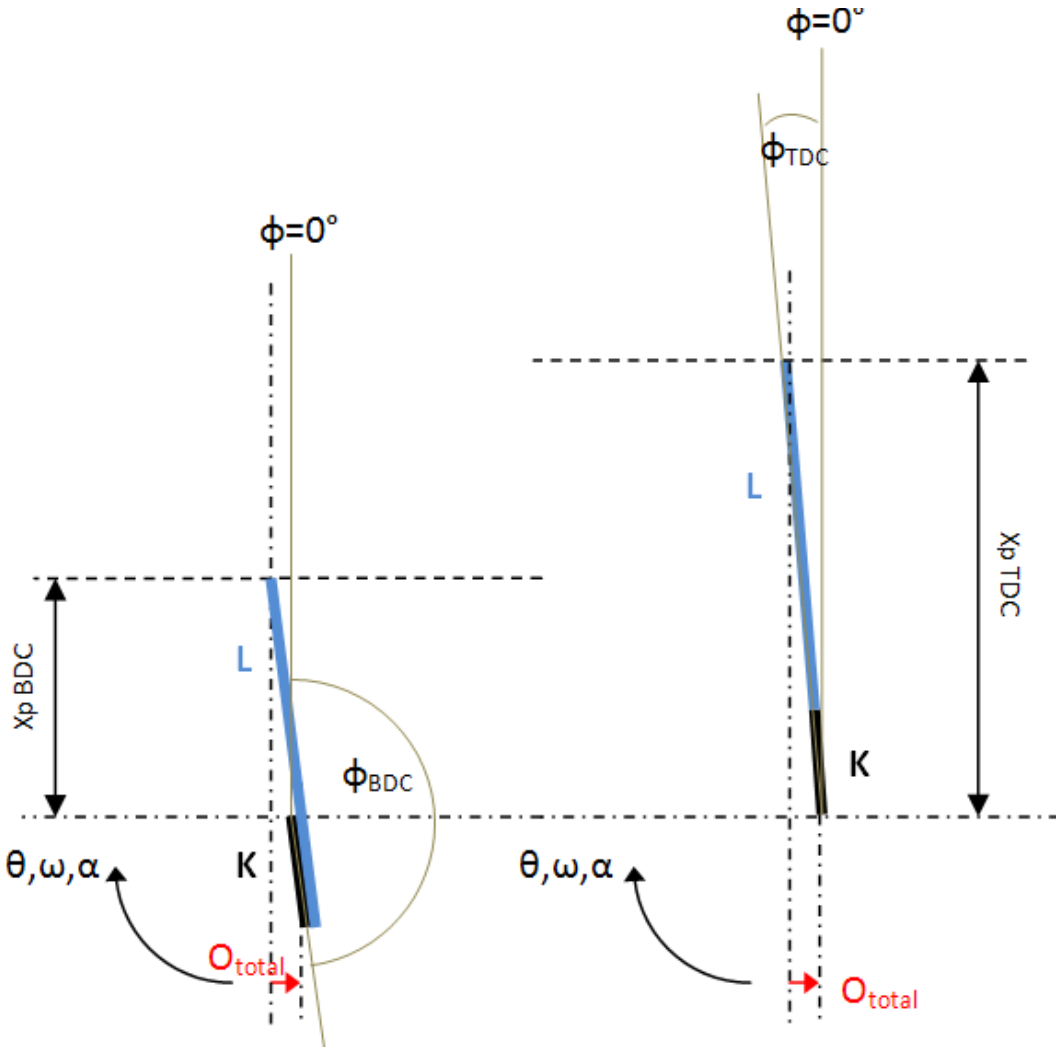

Figure 4.3: BDC and TDC positions diagram

Stroke durations:

$$\phi_{TDC-BDC} = \phi_{BDC} - \phi_{TDC} \quad \text{(Eq. 4.5)}$$

$$\phi_{BDC-TDC} = 360 - \phi_{BDC} + \phi_{TDC} \quad \text{(Eq. 4.6)}$$

$\phi_{TDC-BDC}$ is the stroke duration in crankshaft angle from TDC to BDC (deg), (Intake & Expansion Stroke) and $\phi_{BDC-TDC}$ is the stroke duration in crankshaft angle from BDC to TDC (deg), (Compression & Exhaust).

The possibility of designing an engine with unequal stroke durations can improve some engine behaviour on different areas. The first thing to have in mind in order to understand this concept is that assuming a constant engine speed during the cycle, a longer stroke duration angle would result in a longer stroke duration in time units. This provides the ability to vary the time duration of the strokes.

Examining the case that the TDC to BDC stroke duration is longer (Expansion & Intake), the effect is that the same work during the expansion is transferred to the crankshaft on a longer rotation which would result in lowering the peak to peak cyclic torque amplitudes. In addition, the piston speed is lower on this case which increases the volumetric efficiency of the engine as more time is available for intake resulting in a larger amount of air in the cylinder by the end of the intake stroke.

4.3 Piston motion

The piston pin position is a function of the crank arm angle, while its velocity is a function of both crank arm position and speed. The piston pin acceleration is an important variable to evaluate as it is the parameter along with the mass of the piston that produces the inertial forces on the crankshaft.

Due to the fact that TDC is no longer at crank arm angle 0° but Φ_{TDC} when a total offset on the reciprocating motion is present, a need to shift the crank arm angle so that TDC will

occur at an angle of 0°. Top dead centre has been chosen to be as the zero reference as it is the primary reference point used for different timings on the engine as spark timing, intake and exhaust camshaft timings. Thus, the new term that is going to be introduced at this point is called the "*engine angle*" θ which is used to evaluate the crank arm angle ψ, and it is given by:

$$\psi = \phi_{TDC} + \theta \qquad \text{(Eq. 4.7)}$$

The cylinder axial distance of the piston pin relative to the crankshaft or piston pin position is given below:

$$x_{pin}(\psi) = K\cos\psi + \sqrt{L^2 - (K\sin\psi + O_t)^2} \qquad \text{(Eq. 4.8)}$$

The piston pin velocity and acceleration can be derived by differentiating the equation (Eq. 4.8).

Piston pin velocity:

$$v_{pin}(\psi, \omega) = -\omega A(\psi) \qquad \text{(Eq. 4.9)}$$

Piston pin acceleration:

$$a_{pin}(\psi, \omega, \alpha) = -aA(\psi) - \omega^2[B(\psi) + C(\psi)] \qquad \text{(Eq. 4.10)}$$

Where:

$$A(\psi) = K\sin\psi + \frac{K^2\sin\psi\cos\psi + O_t K\cos\psi}{\sqrt{L^2 - (K\sin\psi + O_t)^2}} \quad \text{(Eq. 4.11)}$$

$$B(\psi) = K\cos\psi + \frac{K^2\cos^2\psi - K^2\sin^2\psi - O_t K\sin\psi}{\sqrt{L^2 - (K\sin\psi + O_t)^2}} \quad \text{(Eq. 4.12)}$$

$$C(\psi) = \frac{K^4\sin^2\psi\cos^2\psi + 2K^3 O_t\sin\psi\cos^2\psi + K^3{O_t}^2\cos^2\psi}{[L^2 - (K\sin\psi + O_t)^2]^{3/2}} \quad \text{(Eq. 4.13)}$$

ω is the crankshaft/engine angular speed (rad/sec) and α is the crankshaft/engine angular acceleration (rad/sec^2).

4.4 Crankshaft mechanism model validation

The equations above have been validated by building an offset crankshaft mechanism model in the dynamic simulation package MSC ADAMS[10]. It was found that the equations produce the same results as the model built in MSC ADAMS. Table 4.1 shows the crankshaft parameters used in the ADAMS model (Figure 4.4) and in equations (Eq. 4.1 to Eq. 4.13).

Table 4.1: Crankshaft mechanism parameters used for validation

Crank arm radius	K	0.027	m
Connecting rod	L	0.13	m
Total offset	O_t	0.005	m
Engine speed	ω	9000	RPM
	ω	942.4778	rad/sec
Engine acceleration	α	0	RPM/sec

[10] MSC ADAMS Homepage: *http://www.mscsoftware,com/products/adams.cfm*

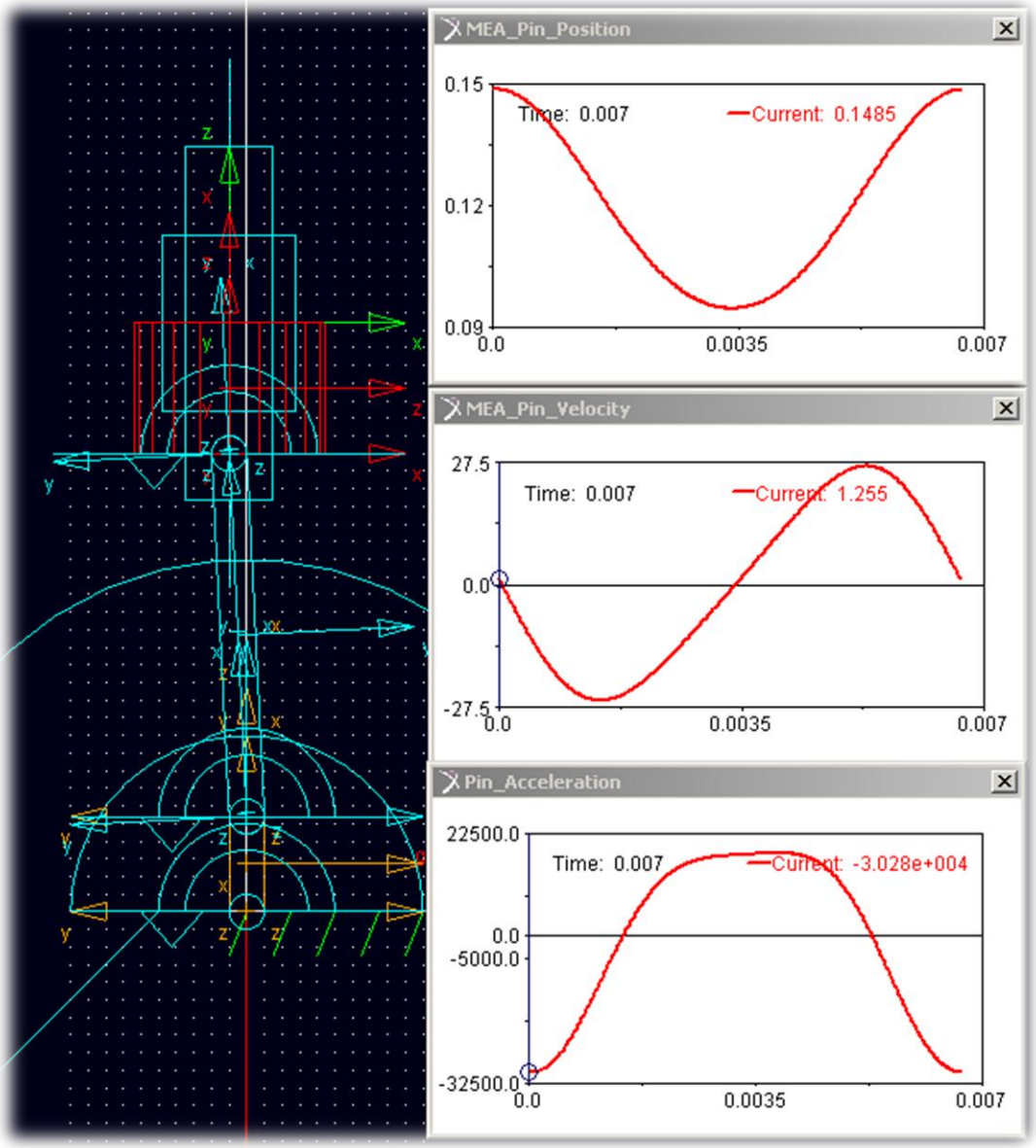

Figure 4.4: MSC ADAMS simulation model for validation

The piston has the same kinematics as the piston pin assuming that it follows a linear motion inside the cylinder. Although same, the positive direction is going to be defined as opposite to the pin motion. By doing so, the cylinder properties and rates can be defined from the piston motion in Figure 4.5.

The distance between the piston top and the highest cylinder point (TDC), velocity and acceleration are given below.

$$x_{cyl}(\psi) = Xp_{TDC} - x_{pin}(\psi) \quad \text{(Eq. 4.14)}$$

$$x_{cyl}(\psi) = \sqrt{(L+K)^2 - {O_t}^2} - \left[K\cos\psi + \sqrt{L^2 - (K\sin\psi + O_t)^2}\right] \quad \text{(Eq. 4.15)}$$

$$v_{cyl}(\psi, \omega) = \omega B(\psi) \quad \text{(Eq. 4.16)}$$

$$a_{cyl}(\psi, \omega, \alpha) = aA(\psi) + \omega^2[B(\psi) + C(\psi)] \quad \text{(Eq. 4.17)}$$

$A(\psi)$, $B(\psi)$ and $C(\psi)$ are given in equations Eq. 4.11 to Eq. 4.13. ψ is the actual crank arm angle given by equation Eq. 4.7 and ω and α are the angular speed (rad/sec) and acceleration (rad/sec2) respectively.

4.5 Compression ratio

The compression ratio is the ratio of the BDC cylinder volume over the TDC volume. This engine design specification can be said to define the compressibility of an engine. The compression ratio affects engine operation such as knocking, power output and other parameters directly or indirectly related.

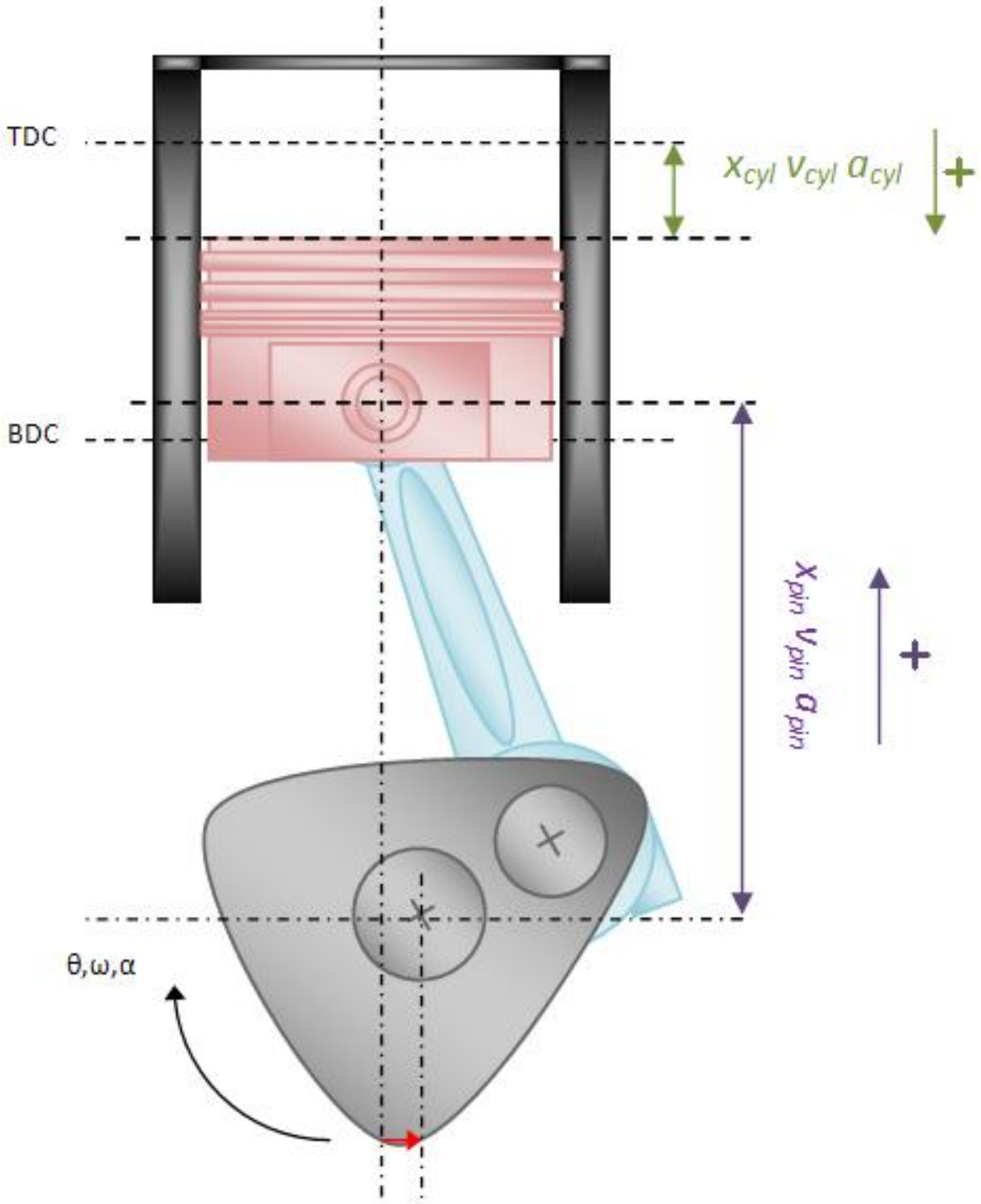

Figure 4.5: Positive directions for piston pin and piston kinematics

If the compression ratio r, cylinder bore B and swept volume V_{swept} of a cylinder are known for a particular engine, then the cylinder volumes at TDC and BDC can be evaluated. The swept volume is the cylinder volume between TDC and BDC, thus:

$$V_{swept} = \frac{\pi B^2}{4} S \quad \text{(Eq. 4.18)}$$

The compression ratio is:

$$r = \frac{V_{BDC}}{V_{TDC}} = \frac{V_{TDC} + V_{swept}}{V_{TDC}} \quad \text{(Eq. 4.19)}$$

Solving above gives the cylinder volumes at TDC and BDC:

$$V_{TDC} = \frac{\pi B^2 S}{4r - 4} \quad \text{(Eq. 4.20)}$$

$$V_{BDC} = \frac{\pi B^2 S r}{4r - 4} \quad \text{(Eq. 4.21)}$$

4.6 Cylinder area

The cylinder area is a parameter required when evaluating the engine heat transfer to the cylinder block and coolant fluid. It is usually difficult to know the cylinder area at TDC as the combustion chamber geometry vary from one engine to another except if a CAD model exists. Although, it can be approximated by assuming a perfect cylinder with a diameter

identical with the cylinder bore. This will produce an effective TDC cylinder height of the combustion chamber which is given by:

$$h_{TDC} = \frac{S}{r-1} \quad \text{(Eq. 4.22)}$$

The total cylinder height as a function of engine/crankshaft angle is then:

$$h_t = h_{TDC} + x_{cyl}(\psi) \quad \text{(Eq. 4.23)}$$

The velocity and acceleration that this cylinder height varies over crankshaft angle, speed and acceleration are the same as v_{cyl} (Eq. 4.15) and a_{cyl} (Eq. 4.16) respectively. Having in mind that the total area of the cylinder will be its parametrical area and two circular areas with a diameter equal to the cylinder bore, the following equations can be evaluated.

$$\begin{aligned} A_{cyl}(\psi) &= \pi B h_t + 2\frac{\pi B^2}{4} = \pi B\left(h_t + \frac{B}{2}\right) \\ &= \pi B\left(h_{TDC} + \frac{B}{2} + x_{cyl}(\psi)\right) \end{aligned} \quad \text{(Eq. 4.24)}$$

Thus the total cylinder area and rates of change are given below.

$$A_{cyl}(\psi) = \pi B\left(\frac{S}{r-1} + \frac{B}{2} + x_{cyl}(\psi)\right) \quad \text{(Eq. 4.25)}$$

$$\frac{d}{dt}A_{cyl}(\psi,\omega) = \pi B v_{cyl}(\psi,\omega) \quad \text{(Eq. 4.26)}$$

$$\frac{d^2}{dt^2}A_{cyl}(\psi,\omega,a) = \pi B a_{cyl}(\psi,\omega,a) \quad \text{(Eq. 4.27)}$$

4.7 Cylinder volume

The cylinder volume and its rate of change as a function of crankshaft angle have to be evaluated as they are needed for the calculation of the cylinder pressure. Following a similar approach as for the calculation of the cylinder area previously described, it can be shown that:

$$V_{cyl}(\psi) = \frac{\pi B^2}{4}\left(\frac{S}{r-1} + x_{cyl}(\psi)\right) \quad \text{(Eq. 4.28)}$$

$$\frac{d}{dt}V_{cyl}(\psi,\omega) = \frac{\pi B^2}{4}v_{cyl}(\psi,\omega) \quad \text{(Eq. 4.29)}$$

$$\frac{d^2}{dt^2}V_{cyl}(\psi,\omega,a) = \frac{\pi B^2}{4}a_{cyl}(\psi,\omega,a) \quad \text{(Eq. 4.30)}$$

4.8 Cylinder phasing

Most engines are multi-cylinder to provide more power output relative to their size and weight. The additional advantage is that the cyclic torque is smoothed and the peak to peak height reduced due to cylinder phasing. In order to be equally phased, each firing cylinder must be phased by an equal amount of crankshaft angle from the previous firing cylinder.

This phase angle ζ (deg) is given by:

4-stroke engine: $\zeta = \frac{720}{\mathrm{n_{cyl}}}$ (Eq. 4.31)

2-stroke engine: $\zeta = \frac{360}{\mathrm{n_{cyl}}}$ (Eq. 4.32)

n_{cyl} is the total umber of cylinders.

Assuming now a 4-cylinder 4-stroke engine equally phased with a 1-3-4-2 cylinder firing order, the following table (Table 4.2) can be made:

Table 4.2: Firing order example

Cylinder #	**1**	**2**	**3**	**4**
Firing Order ***FO_N***	1st	4th	2nd	3rd
Phase Angle (deg) ***ζ_{cyl}***	0	540	180	360
Cylinder Volume	V_{t1}	V_{t2}	V_{t3}	V_{t4}

The phases of each cylinder ζ_{cylN} relative to cylinder 1 are given by:

$$\zeta_{cylN} = \zeta(FO_N - 1) \qquad \text{(Eq. 4.33)}$$

FO_N is the cylinder's N firing order (i.e. 1st=1, 2nd=2 ...)

The actual crank arm angle $\psi_{cylN}(\theta)$ of each individual cylinder will then be:

$$\psi_{cylN}(\theta) = \phi_{TDC} + \zeta_{cylN} + \theta \qquad \text{(Eq. 4.34)}$$

Solving the engine example shown on Table 4.2 will produce:

$$\psi_{cyl\,1}(\theta) = \phi_{TDC} + 0 + \theta \qquad \psi_{cyl\,2}(\theta) = \phi_{TDC} + 540 + \theta$$

$$\psi_{cyl\,3}(\theta) = \phi_{TDC} + 180 + \theta \qquad \psi_{cyl\,4}(\theta) = \phi_{TDC} + 360 + \theta$$

These actual crank arm angles have to be used to evaluate individual cylinder, piston and connecting rod motion on the previously described equations containing ψ.

For example, the individual cylinder volumes of the engine used above (Table 4.2**Error! Reference source not found.**) are given by:

$$V_{cyl\,1}(\psi_{cyl\,1}) = \frac{\pi B^2}{4}\left[\frac{S}{r-1} + x_{cyl}(\psi_{cyl\,1})\right]$$

$$V_{cyl\,2}(\psi_{cyl\,2}) = \frac{\pi B^2}{4}\left[\frac{S}{r-1} + x_{cyl}(\psi_{cyl\,2})\right]$$

$$V_{cyl\,3}(\psi_{cyl\,3}) = \frac{\pi B^2}{4}\left[\frac{S}{r-1} + x_{cyl}(\psi_{cyl\,3})\right]$$

$$V_{cyl\,4}(\psi_{cyl\,4}) = \frac{\pi B^2}{4}\left[\frac{S}{r-1} + x_{cyl}(\psi_{cyl\,4})\right]$$

Note that V_{cyl1}=V_{cyl4} on this example as their crank arms are phased by 360° thus 0°. Same applies for V_{cyl2}=V_{cyl3}

4.9 Crankcase volume

Another important engine parameter which is neglected is the crankcase volume. Most models assume that an atmospheric pressure inside the cylinder will result in no work/force on the piston. Although, this would be correct only if the pressure inside the crankcase is as well atmospheric. To demonstrate the concept the following picture can be observed (Figure 4.6).

The force acting on the piston F_p is due to the pressure difference between both sides of the piston and is given by:

$$F_p = \left(P_{cyl} - P_{case}\right)\frac{\pi B^2}{4} \qquad \text{(Eq. 4.35)}$$

P_{cyl} and P_{case} are the pressures inside the cylinder and crankcase respectively in Pa.

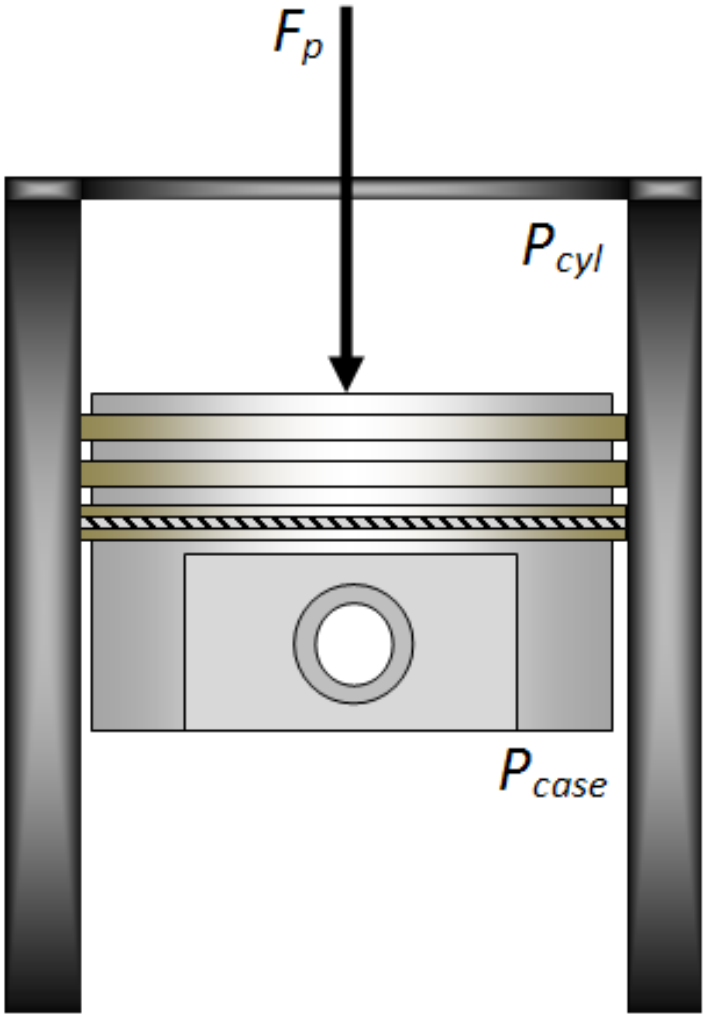

Figure 4.6: Piston force

Figure 4.7 shows the crankcase air volume which pressure fluctuates as it is affected by the followings:

1. Amount of lubricant leaving this container through the oil pump
2. Amount of lubricant returning
3. Amount of gases entering this volume through the piston *(blow-by)*
4. Air flow through the crankcase breather (usually connected to the intake manifold)
5. Crankcase volume change due to piston motion

This section will deal with the evaluation of the crankcase volume change due to piston motion. This effect is diminishing with the increase of cylinder numbers in an engine considering they are equally phased. On the other hand, the crankcase pressure is kept close to atmospheric by the crankcase breather connected to the intake manifold and some times to open air. The crankcase breather is usually on the top of the cylinder head cover which results in a lower breathing effect as the distance is longer for the pressure to equalise.

Assuming the crankcase internal volume V_{cTDC} is known at TDC then, the crankcase volume V_c and rate of change as a function of crankshaft angle for the engine described on Table 4.1 are given by:

$$V_c(\theta) = V_{cTDC} - \frac{\pi B^2}{4} x_{Tcyl}(\psi) \qquad \text{(Eq. 4.36)}$$

$$\frac{d}{dt} V_c(\theta) = -\frac{\pi B^2}{4} v_{Tcyl}(\psi) \qquad \text{(Eq. 4.37)}$$

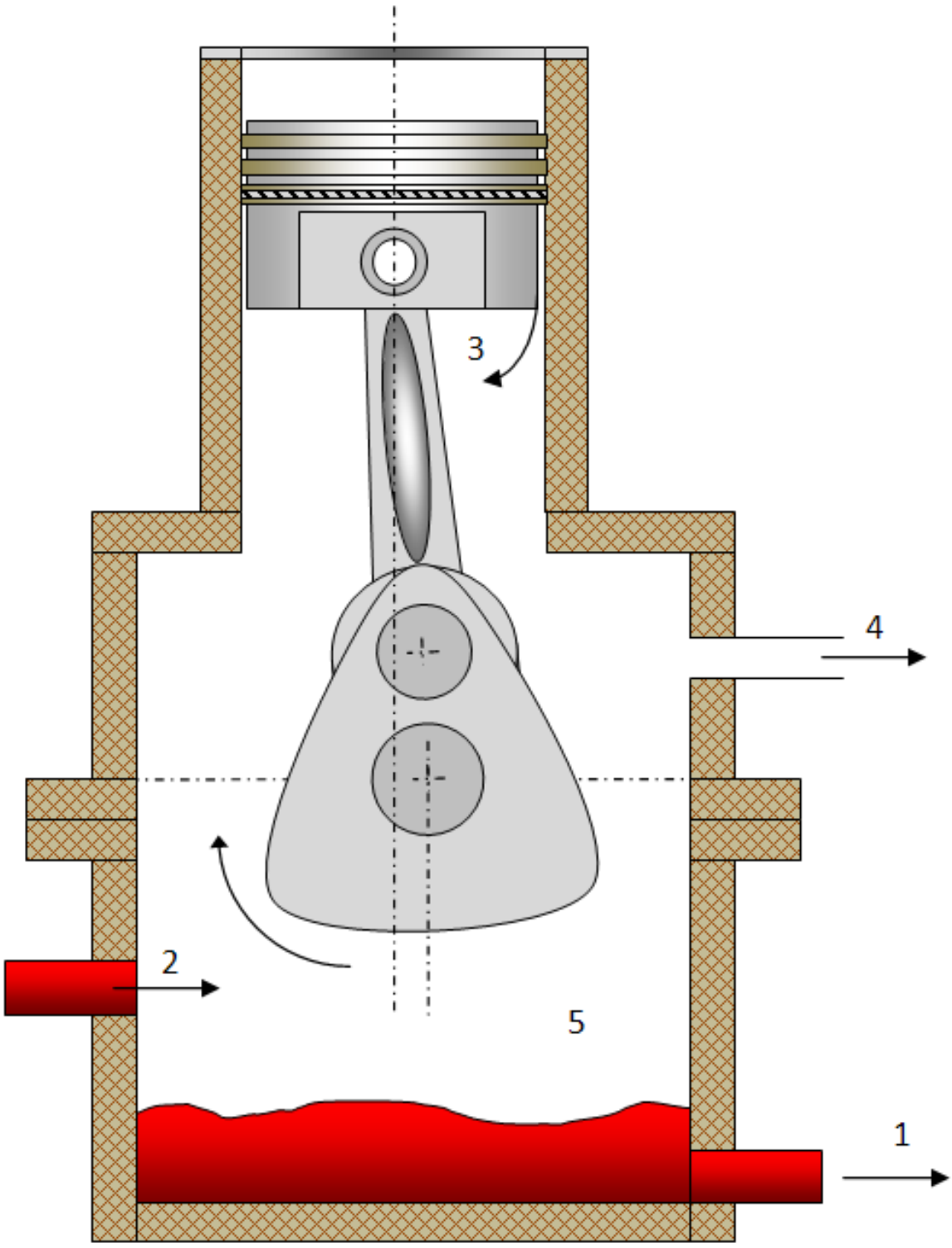

Figure 4.7: Crankcase air volume

4.10 Connecting rod motion

The motion of the connecting rod's centre of gravity has to be evaluated as the equations are needed for the calculation of the inertial forces. This is needed mainly because even at a constant engine speed, the connecting rods are following an acceleration/deceleration cycle which is repeated for every engine revolution.

The centre of gravity of most connecting rods is usually on the crank arm side as that side has usually the largest diameter so that a bearing can be fitted. In addition, almost all connecting rods have an axis of symmetry along their length, thus only a position along this axis is chosen to define the position of its centre of gravity which is L_c as shown in Figure 4.8. The connecting rod's centre of mass kinematics are analysed on a Cartesian coordinate system thus each variable is evaluated for the X and Y axis. The analysis can be done by applying trigonometry which results for the centre of mass kinematics are given below.

Centre of mass position:

$$x_G(\psi) = K\,sin\,\psi - \frac{L_c}{L}(K\sin\psi + O_t) \qquad \text{(Eq. 4.38)}$$

$$y_G(\psi) = K\,cos\,\psi + \frac{L_c}{L}\sqrt{L^2 - (K\,sin\,\psi + O_t)^2} \qquad \text{(Eq. 4.39)}$$

Centre of mass velocity:

$$v_G^x(\psi,\omega) = \omega\left(1 - \frac{L_c}{L}\right)K\cos\psi \qquad \text{(Eq. 4.40)}$$

$$v_G^y(\psi,\omega) = -\omega\left(K\sin\psi + \frac{K^2 L_c \sin\psi\cos\psi + O_t L_c K\cos\psi}{L\sqrt{L^2-(K\sin\psi + O_t)^2}}\right) \quad \text{(Eq. 4.41)}$$

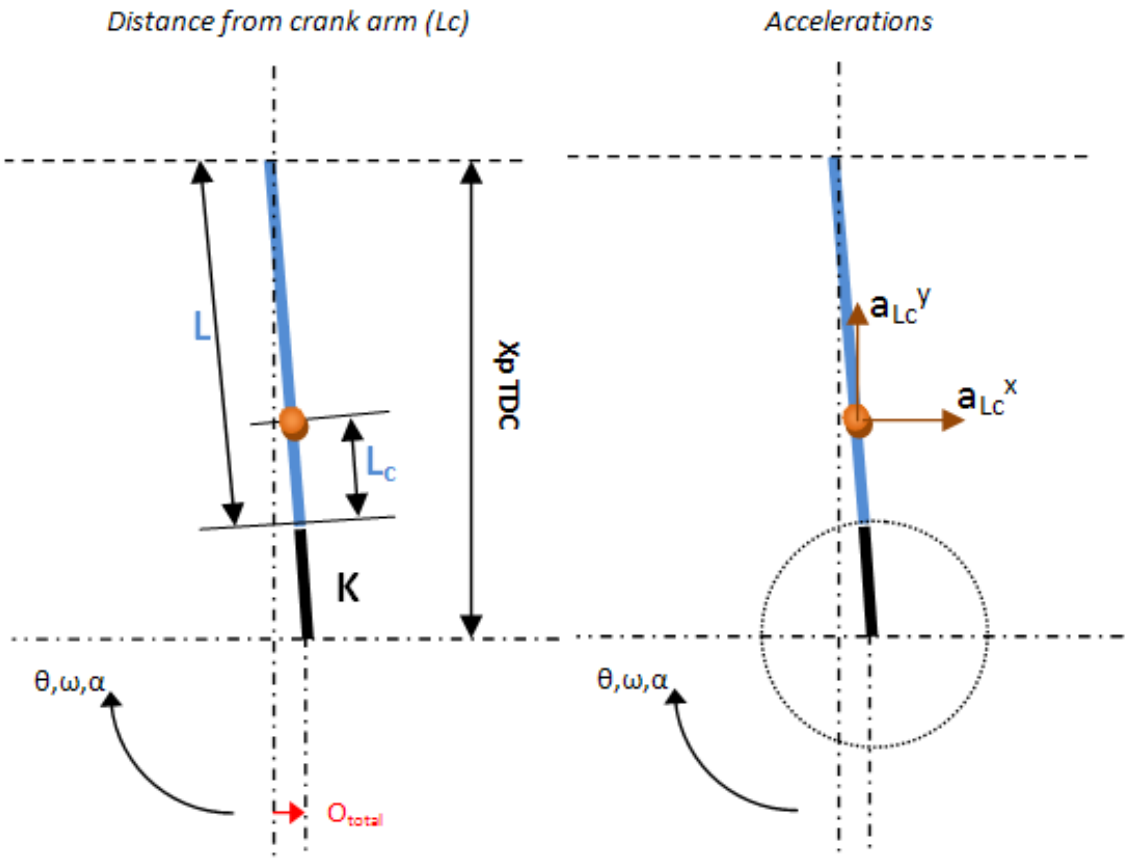

Figure 4.8: Connecting rod centre of mass

Centre of mass acceleration:

$$\alpha_G^x(\psi,\omega,\alpha) = (aK\cos\psi - \omega^2 K\sin\psi)\left(1-\frac{L_c}{L}\right) \quad \text{(Eq. 4.42)}$$

$$\alpha_G^y(\psi,\omega,\alpha) = -aA_G(\psi) - \omega^2[B_G(\psi) + C_G(\psi)] \quad \text{(Eq. 4.43)}$$

Where:

$$A_G(\psi) = K\sin\psi + \frac{L_c}{L}\frac{K^2\sin\psi\cos\psi + O_t K\cos\psi}{\sqrt{L^2 - (K\,sin\,\psi + O_t)^2}} \quad \text{(Eq. 4.44)}$$

$$B_G(\psi) = K\cos\psi + \frac{L_c}{L}\frac{K^2\cos^2\psi - K^2\sin^2\psi - O_t K\sin\psi}{\sqrt{L^2 - (K\,sin\,\psi + O_t)^2}} \quad \text{(Eq. 4.45)}$$

$$C_G(\psi) = \frac{L_c}{L}\frac{K^4\sin^2\psi\cos^2\psi + 2K^3 O_t\sin\psi\cos^2\psi + {O_t}^2\cos^2\psi}{[L^2 - (K\,sin\,\psi + O_t)^2]^{3/2}} \quad \text{(Eq. 4.46)}$$

The connecting rod's angular motion around its centre of mass ***G*** is required for the evaluation of the components inertia torque on the crankshaft. It is given by (Figure 4.9):

Angular Motion about centre of mass:

$$\tau(\psi) = -\sin^{-1}\frac{K\sin\psi + O_t}{L} \quad \text{(Eq. 4.47)}$$

$$\omega_\tau(\psi,\omega) = -\omega\frac{K\cos\psi}{L\sqrt{1 - \frac{(K\sin\psi + O_t)^2}{L^2}}} \quad \text{(Eq. 4.48)}$$

$$\alpha_\tau(\psi,\omega,\alpha) = -\alpha A_\tau(\psi) - \omega^2 B_\tau(\psi) \quad \text{(Eq. 4.49)}$$

Where:

$$A_\tau(\psi) = \frac{K\cos\psi}{L\sqrt{1 - \frac{(K\sin\psi + O_t)^2}{L^2}}} \quad \text{(Eq. 4.50)}$$

$$B_\tau(\psi) = -\frac{K\sin\psi}{L\sqrt{1-\frac{(K\sin\psi+O_t)^2}{L^2}}} + \frac{K^2\cos^2\psi\,(K\sin\psi+O_t)}{L^3\left[1-\frac{(K\sin\psi+O_t)^2}{L^2}\right]^{3/2}} \qquad \text{(Eq. 4.51)}$$

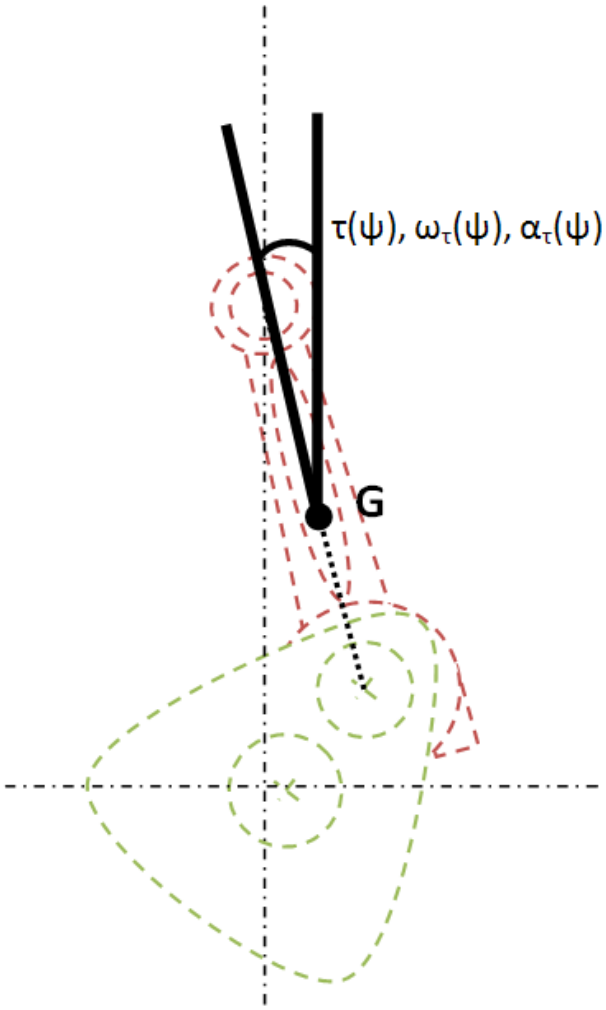

Figure 4.9: Connecting rod angular motion

A complete model structure of the crankshaft mechanism dynamics is shown in Figure 4.10. The equation interactions can be clearly observed while the main inputs of this system are the crankshaft dynamics as usually all other model parameters remain constant for a specific engine as they depend only on the component geometry.

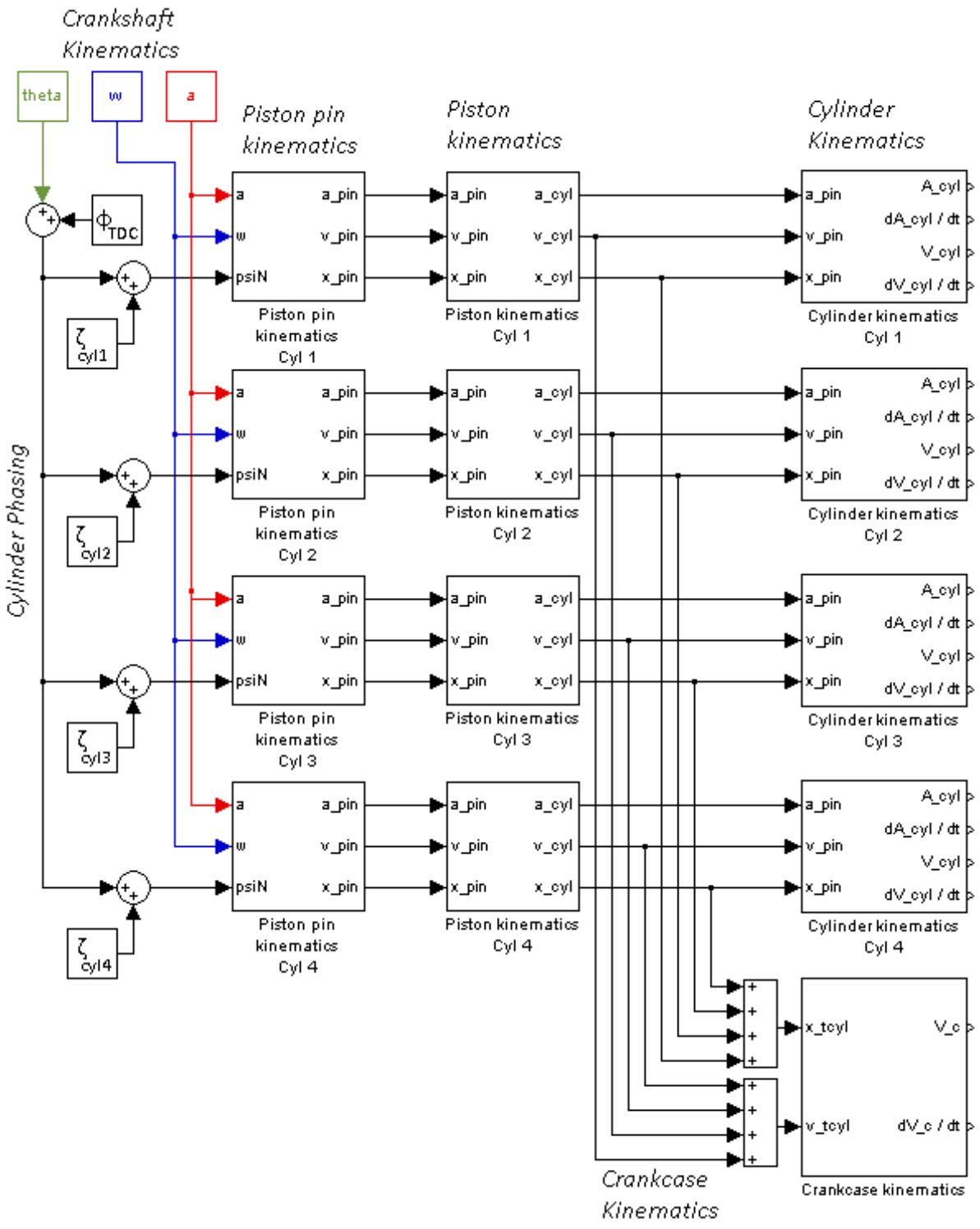

Figure 4.10: 4-cyl crankshaft kinematics model structure

4.11 Results and conclusions

The typical engine data of Table 4.1 has been used to demonstrate the effects of engine acceleration and crankshaft mechanism offsets. The piston acceleration was found to be affected on some conditions by the crankshaft acceleration which depends on crankshaft mechanism parameters and acceleration amplitude. Although affected, the error is quite minimal on engines that do not have immense accelerations. A typical value for acceleration has been used from a 2-stroke V6 Mercury marine engine. These engines can accelerate from idle to maximum (around 10000 RPM) in a fraction of a second which was evaluated to be in the order of 25000 to 30000 rad/sec2; thus this engine's acceleration can be used in an example to illustrate the effect of a large crankshaft acceleration. The piston acceleration is affected only at low engine speeds by the crankshaft acceleration due to the fact that the velocity is the main source of the piston acceleration. The worst case scenario has been chosen for illustration which is a huge acceleration or deceleration during low engine speed (Figure 4.11).

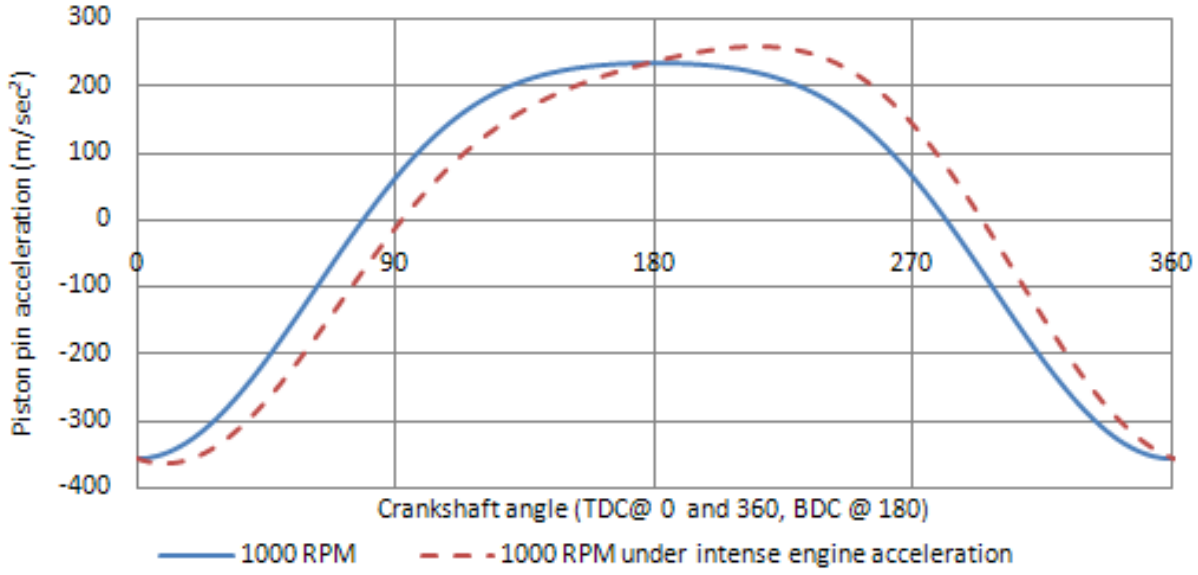

Figure 4.11: Crankshaft acceleration effect on piston acceleration

An offset on the other hand, has shown to affect noticeably the piston kinematics and stroke length. A calculation has been done for a zero, a positive and a negative total crankshaft mechanism offset which can be seen in Figure 4.12. The total offset of a crankshaft mechanism should not be neglected as it can lead to large calculation errors as inertial forces, cylinder area and cylinder volume scale from the piston and piston pin kinematics.

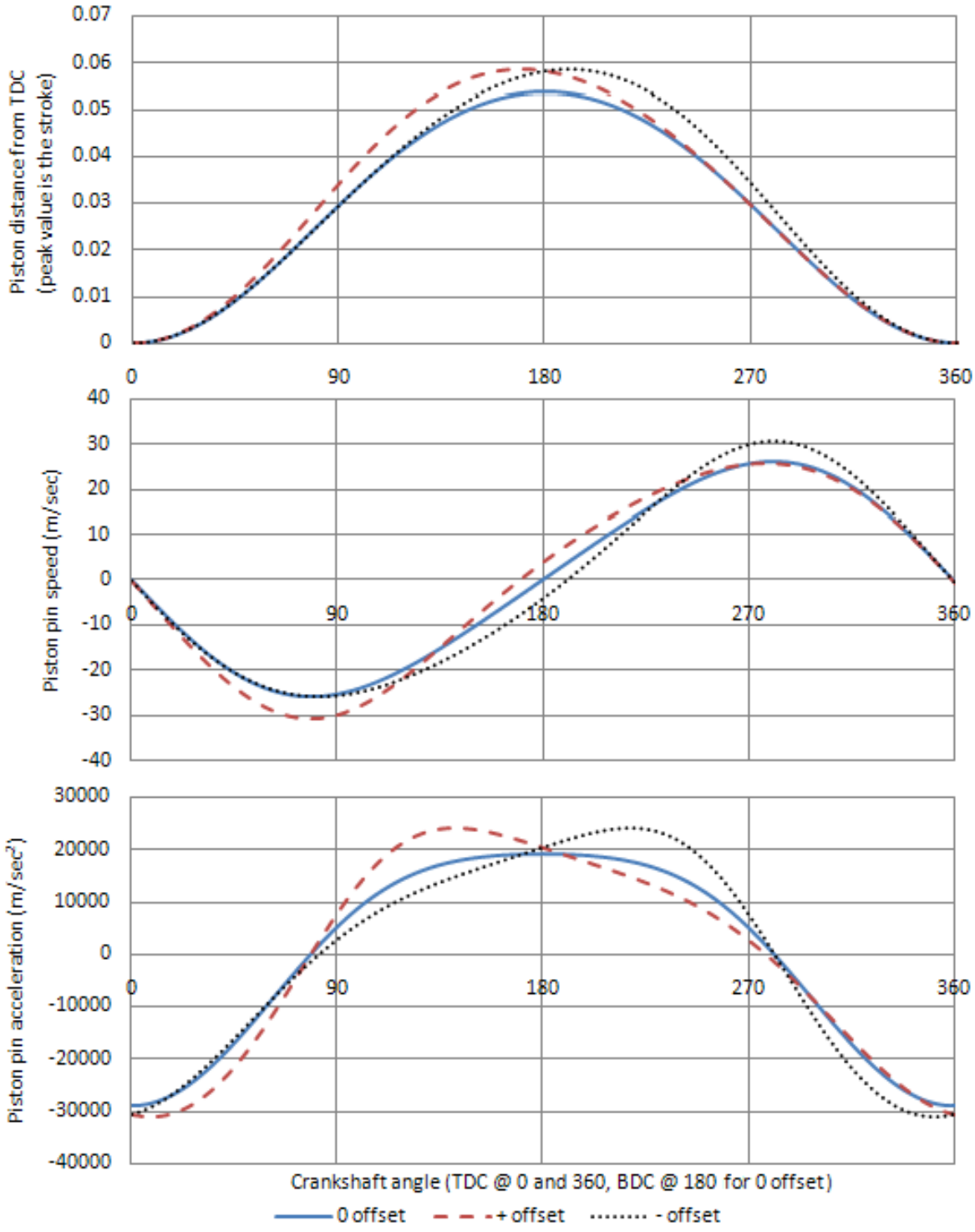

Figure 4.12: Crankshaft mechanism positive and negative offset effects @ 9000 RPM

CHAPTER 5: Valvetrain

It is quite difficult to obtain accurate valve flow area data as they depend on the valvetrain mechanism geometry and timings. It is common on cycle-by-cycle simulation to assume typical lift curves which lead to inaccurate model simulations. The valvetrain mechanism and timing are important factors which affects all engine parameters such as performance, emissions, fuel consumption, etc.

The valve flow area is the smaller cross sectional area along the path of the flow that acts as the restriction on the gas flow through the valve ports. This area is only a function of crankshaft position if the valve is always in contact with the camshaft. In the other hand, if the contact is lost, then the component masses, valve spring properties and engine speed become variables.

Variable valve timing mechanisms (VVT) are very common these days [15, 85], thus any valvetrain model should provide the ability to simulate any kind of VVT mechanism. The objective is to end up with a valve flow restriction area model that can be used on most VVT engines for simulation or cycle-by-cycle engine mapping.

The following sections show the complete process starting by the correct way to measure an actual engine camshaft and the calculations that have to be done in order to end up with the valve flow area for a direct acting valve train system.

5.1 Camshaft profile

The camshaft lobe shape is the main parameter which affects the valve opening curve. The drawback is that except for the designer of a particular camshaft, probably no one else knows the mathematical equation that describes its shape.

The camshaft lobe height is the increase in radial distance from the camshaft base diameter as a function of the angle theta around the camshaft shape. While the camshaft profile is the actual radius of the camshaft lobe material around the same angle theta. It is preferred to use the camshaft profile to publish or share camshaft data as it includes as well the base diameter and thus all lobe shape parameters. The camshaft profile is the representation of the camshaft lobe in the Polar coordinate system. Note that an identical camshaft lobe height curve on a different camshaft base diameter results in a totally different camshaft. The two terms that are going to be used can be seen on Figure 5.1.

5.1.1 Experimental measurement

It is usually easy to obtain the camshaft profile curve experimentally from measurements. On most OHC engines, the measurement can be made once the cylinder head cover is removed providing visibility to the camshafts. Following is a detailed procedure to measure the camshaft height, base diameter and thus obtain the profile. The tools required are a dial indicator to measure the lobe height, a calliper for the base diameter and a crankshaft protractor for the angle. The measurement procedure starts by assuming that the crankshaft protractor is already installed. Firstly, the camshaft has to be rotated so that its peak lift is facing away of the indicator's axis. This is done to ensure that the indicator is touching the base diameter.

Secondly, the indicator's measuring axis must be aligned with the centre axis of the camshaft rotation (Figure 5.2).

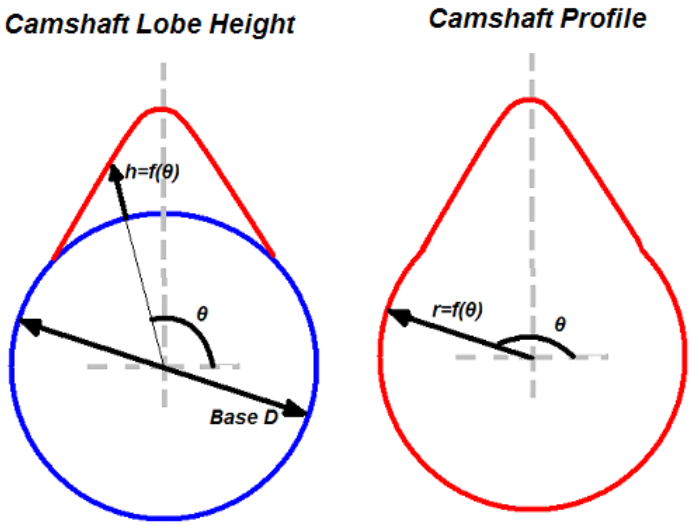

Figure 5.1: Camshaft lobe height and profile

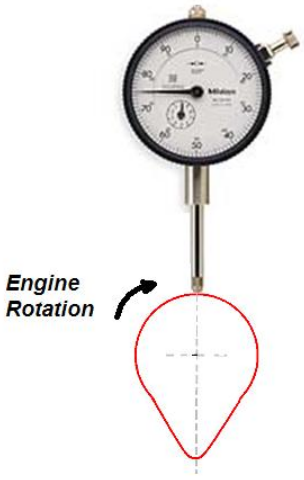

Figure 5.2: Camshaft lobe height measurement[11]

[11] Dial indicator image source: *http://www.drillspot.com/*

At this point the dial indicator should be reset to a zero reading and then the data collection can start. The procedure is to record the reading on the indicator then rotate the crankshaft on the engine's rotation direction. Repeat the procedure for two crankshaft revolutions which equals one camshaft revolution. Note that the crankshaft should be rotated only in one direction during this procedure in order to keep the timing chain/belt tension on the same side for all the measurement as a change in tension side may give inaccurate readings. The following graph (Figure 5.3) shows an actual lobe height measurement (BMW E30 318is intake camshaft) for 10 deg crankshaft step with measurement errors added on purpose to demonstrate a solution. It can be seen that data on the closing side are not accurate as they are clearly not forming a smooth curve. The base diameter of the measured camshaft is 38mm.

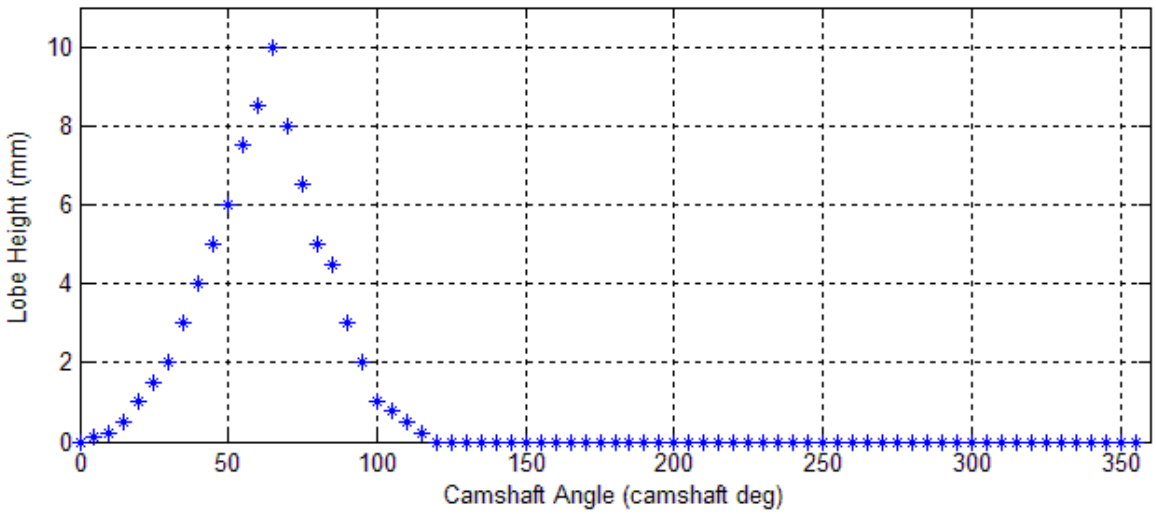

Figure 5.3: Camshaft lobe height measurement

The camshaft profile curve can be obtained by adding the radius of the camshaft base to the above value (Figure 5.4).

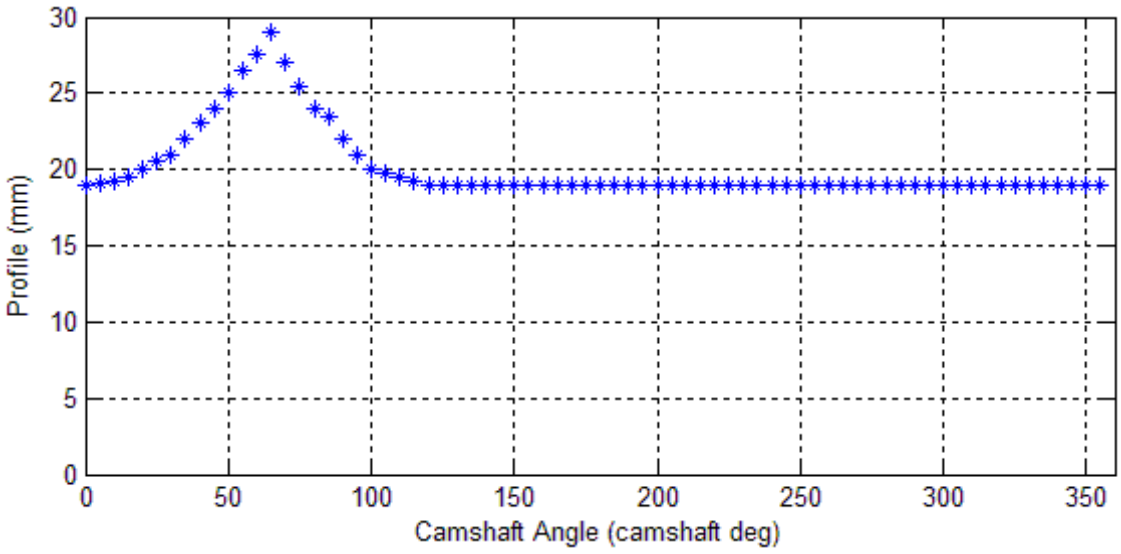

Figure 5.4: Camshaft profile

5.1.2 Camshaft lobe graphical representation

In case that a polar plot software is not available, the Cartesian graphical representation of the actual camshaft lobe (Figure 5.5) can be obtained using the following equations. This is actually a transition from the Polar coordinate system to the Cartesian.

$$X_{cam}(\theta_r) = \cos\theta \, P_{cam}(\theta_r) \qquad \text{(Eq. 5.1)}$$

$$Y_{cam}(\theta_r) = \sin\theta \, P_{cam}(\theta_r) \qquad \text{(Eq. 5.2)}$$

θ_r is the camshaft angle and $P_{cam}(\theta_r)$ is the camshaft profile radius at θ_r (profile Vs θ_r curve).

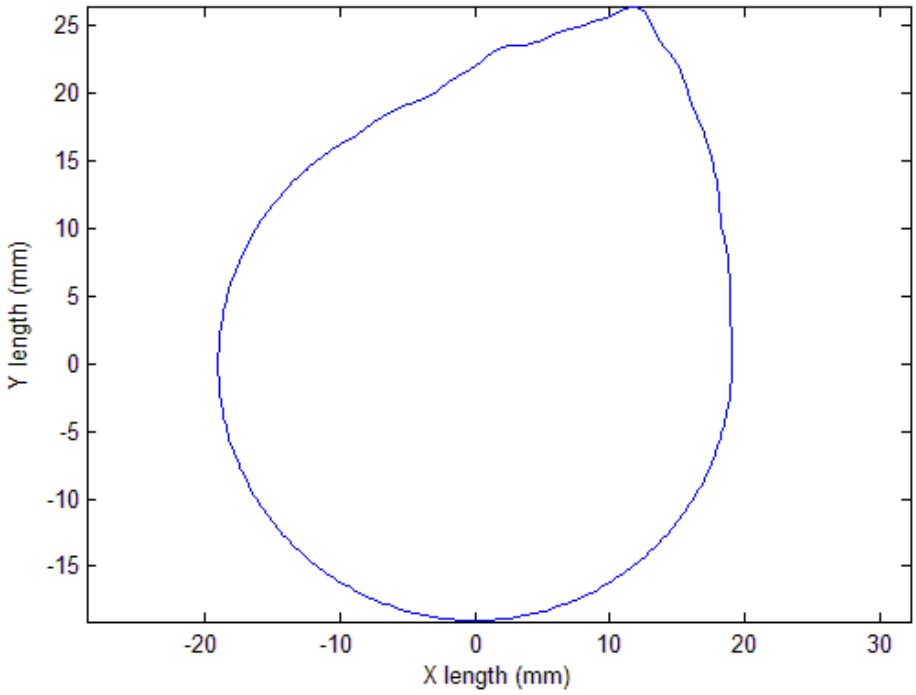

Figure 5.5: Camshaft lobe drawing

The error in the data introduced now can clearly be observed as it produces an unsmooth lobe surface (Figure 5.5). This can result in a severe problem depending on the type of model that this data is going to be used for. For example, if this camshaft data is to be used to evaluate the valve lift dynamics, the acceleration magnitude will be increased on the points where the error in the measurement was made resulting in large inertial forces.

5.1.3 Data processing

There may be need to increase the data points of the camshaft profile curve in order to use them for calculations in a step model. An interpolation can be used for this purpose as long as it is a shape preserving interpolation. The respective MATLAB function is the ***'interp1'*** function using the ***'pchip'*** method.

As noted earlier, errors were introduced in the measurement so that a solution can be demonstrated. A solution to this is to smooth the data points using a smoothing mathematical function.

The smoothing can be done using the MATLAB function '***smooth'*** while the method tested to produce the best results for this kind of application is the ***'sgolay'*** method using a span of 3-5 and a degree of 2 (Figure 5.6). If smoothing is inadequate, it is possible to smooth a couple of times in series as long as the maximum camshaft lobe profile is checked to be intact. Over-smoothing will result in reducing the maximum profile peak.

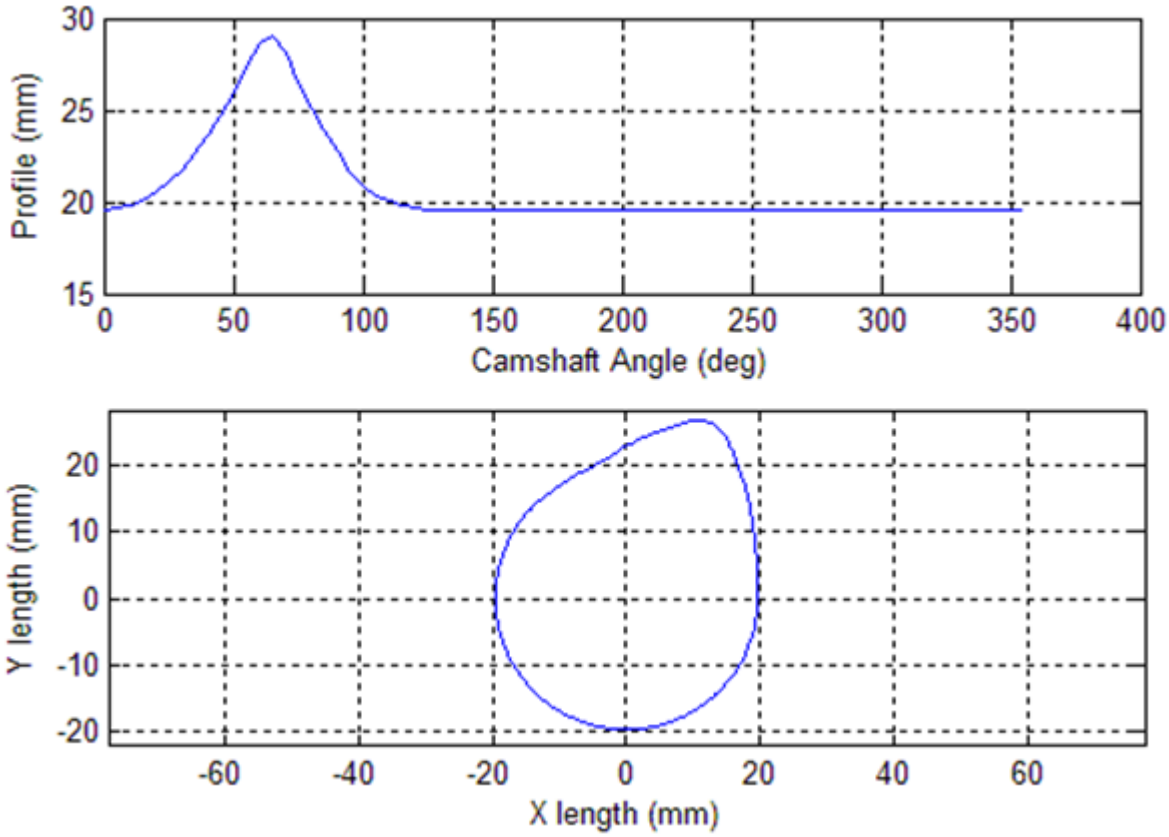

Figure 5.6: Camshaft profile data smoothing

5.1.4 Mathematical model

There are a lot of variables that define a camshaft profile. Some of the most important are, the total duration of the camshaft lobe, the opening duration and closing duration. Camshaft durations are referred in crankshaft degrees, mostly to have a common reference point with the crank mechanism rotation. Another parameter is the maximum lobe height, which defines the maximum valve lift ignoring the valve clearance.

Having all of the above in mind, and after experimenting with different functions that would produce a variety of acceptable camshaft profiles, an easy way to model the profile has been found by generating some curve functions from 0 to 1. Then, this curve once multiplied by the desired maximum lobe height can produce an acceptable camshaft profile.

The following picture shows the difference between an acceptable camshaft lobe result (smooth) and one that should be rejected because if it was to be installed on an engine, it would result in an increase in component stress and accelerations (Figure 5.7).

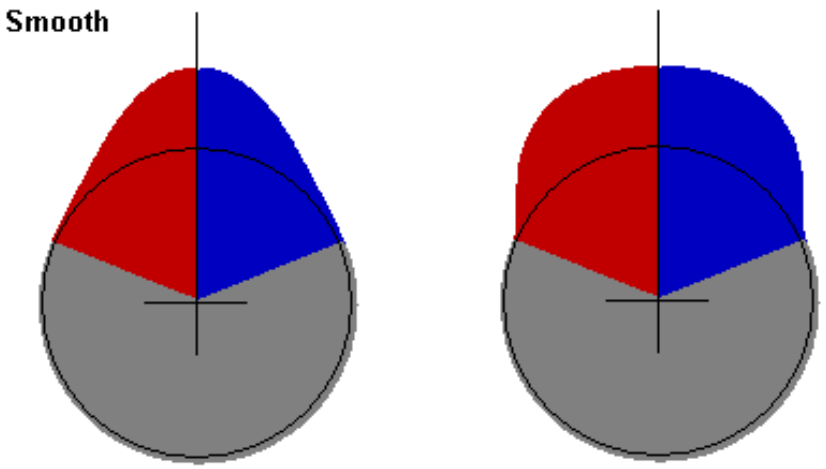

Figure 5.7: Acceptable (smooth) and incorrect camshaft lobes

The functions found by trial and error to have the ability to produce a smooth profile are given below:

$$fstep_{up}^{sin}(\theta_r) = \frac{sin\left[\frac{180(\theta_r - \theta_s)}{\theta_d} - 90\right] + 1}{2} \quad \text{(Eq. 5.3)}$$

$$fstep_{down}^{sin}(\theta_r) = \frac{sin\left[\frac{180(\theta_r - \theta_s)}{\theta_d} + 90\right] + 1}{2} \quad \text{(Eq. 5.4)}$$

$$H_{lobe}(\theta_r) = \frac{H_{max}\left[1 - fstep_{down}^{sin}(\theta_r)\right]u^{fstep_{up}^{sin}(\theta_r)}}{u} \quad \text{(Eq. 5.5)}$$

$$R_{lobe}(\theta_r) = \frac{D_b}{2} + H_{lobe}(\theta_r) \quad \text{(Eq. 5.6)}$$

θ_r is the camshaft angle of calculation, θ_s is the starting angle of lobe profile (opening or closing), θ_d is its duration, u is the smoothing factor, $H_{lobe}(\theta)$ is the camshaft lobe height at θ_r, $R_{lobe}(\theta)$ is the camshaft lobe radius at θ_r, D_b is the lobe's baseline diameter and H_{max} is the maximum camshaft lobe height. Typical values for u can range from 1-100 depending on desired profile and base diameter.

These functions have been incorporated into a program interface for fast visualization of the camshaft lobe result. Once the desired camshaft lobe is produced, the data can be exported.

The program was written in Visual Basic as it allows the program to run without the need of any additional software; complex real-time plotting can be developed onto the interface and can output any desired file format (Figure 5.8).

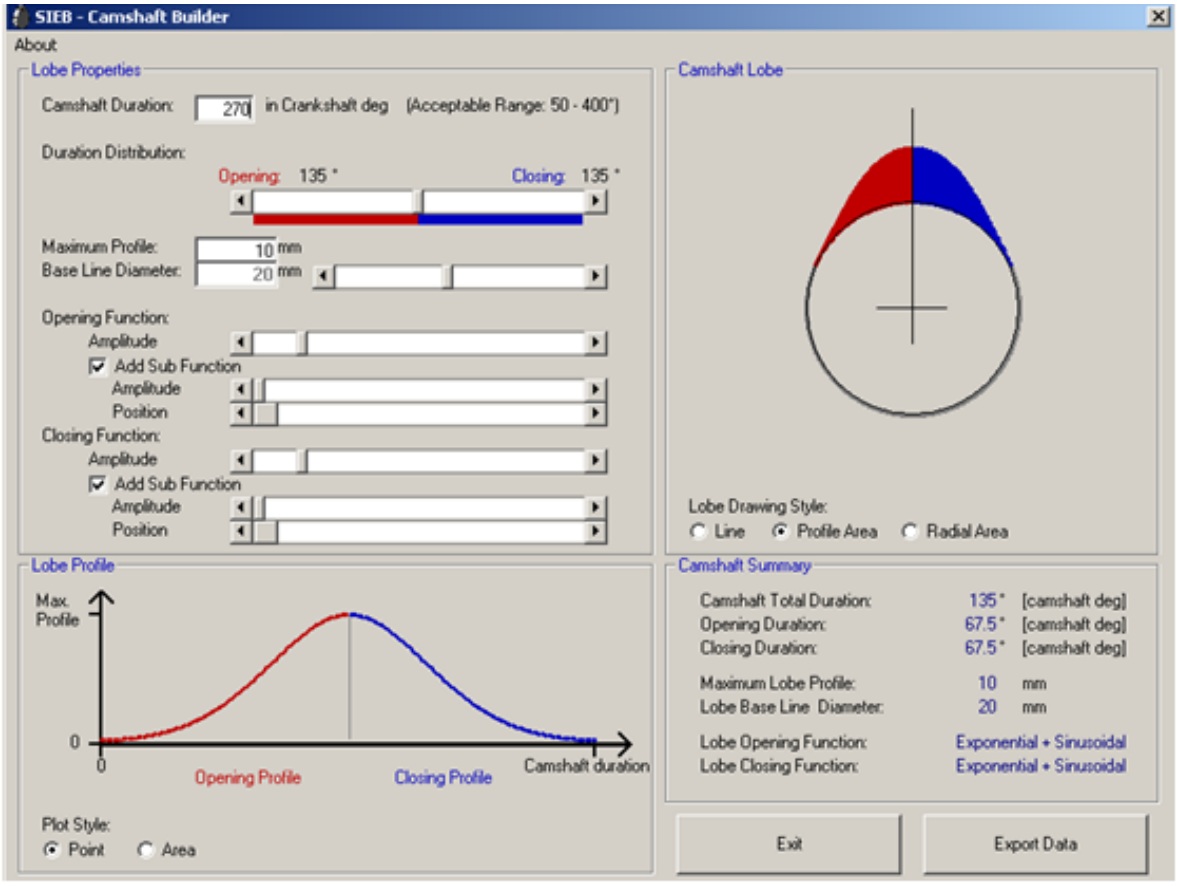

Figure 5.8: Developed camshaft builder software

5.2 Flat follower

Assuming at this point that the camshaft profile data is available, the next step is to evaluate the static position of the camshaft flat follower (direct acting system). This position defines the valve position when the follower is in contact with the camshaft as it can be seen in the figure below (Figure 5.9).

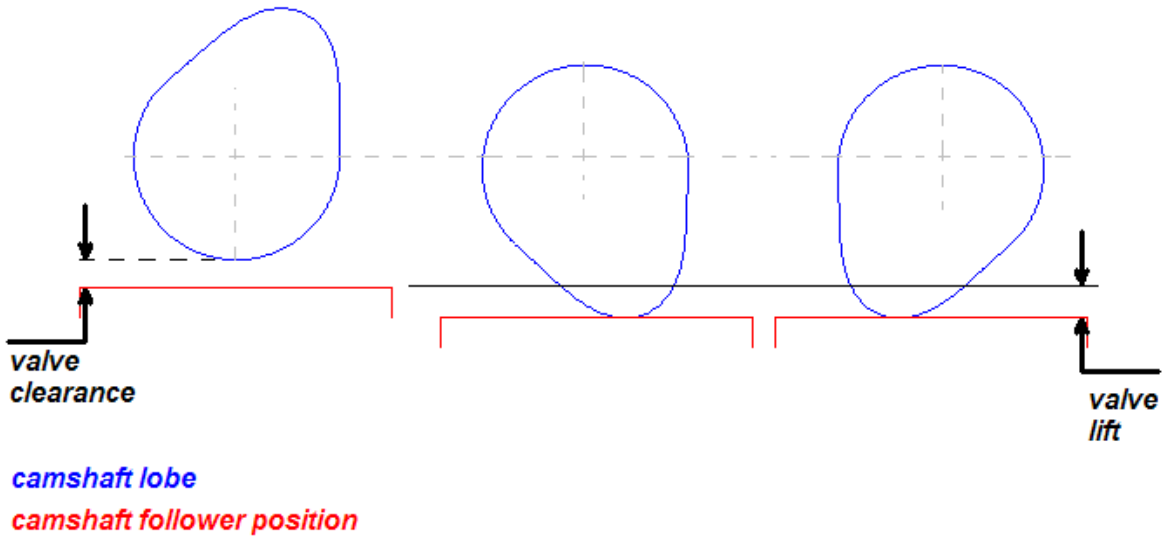

Figure 5.9: Flat follower position

The developed contact solver working principle is based on matrix rotation. First, the camshaft lobe Cartesians coordinates are loaded into a matrix and then this matrix is rotated for desired steps of crankshaft angle using the 2-dimensional matrix rotation formula below.

$$M_{out}(\theta_{cr}) = M_{in} \times \begin{bmatrix} \cos\theta_r & \sin\theta_r \\ -\sin\theta_r & \cos\theta_r \end{bmatrix} \quad \text{(Eq. 5.7)}$$

The camshaft rotation angle is given by the following equation as it is half of the desired crankshaft rotation.

$$\theta_r = s_r \frac{\theta_{cr}}{2} \quad \text{(Eq. 5.8)}$$

M_{in} is the lobe's Cartesian coordinates (X, Y), M_{out} is the rotated lobe Cartesian coordinates (X, Y), θ_{cr} is the desired rotation angle in crankshaft degrees, θ_r is the rotation angle in

camshaft degrees and s_r is the sign for the rotation direction (-1 for clockwise, +1 for anti-clockwise).

The point of contact can be easily found then as it is the lowest Y Cartesian coordinate of the M_{out} matrix.

5.2.1 Camshaft torque effective radius

The camshaft requires torque during the opening of the valves due to the fact that it is compressing the valve springs. On the other hand, during the closing period, torque is generated on the camshaft as the valve spring forces are pushing the camshaft lobe towards its direction of rotation (Figure 5.10).

The fact that the solver is a Cartesian representation of the mechanism produces directly an additional useful valve train result which is the effective radius of camshaft torque application. It can be seen in Figure 5.10 that the effective radius R_{eff}, is the Cartesian X coordinate of the contact location.

The camshaft torque is then given by:

$$T_{cam}(\theta) = -R_{eff}(\theta_{cr}) \times F \qquad \text{(Eq. 5.9)}$$

R_{eff} is the effective radius of torque generation/application (m), F is the valve spring reaction force (N) and T_{cam} is the reaction torque acting on the camshaft (Nm).

Figure 5.11 shows the evaluation of the effective torque radius for a typical camshaft lobe. The negative sign during the opening duration denotes the effect of the torque on the

camshaft, thus the requirement of torque. While on the other hand during the closing period, the positive sign represents the torque generation to the system by the valve spring.

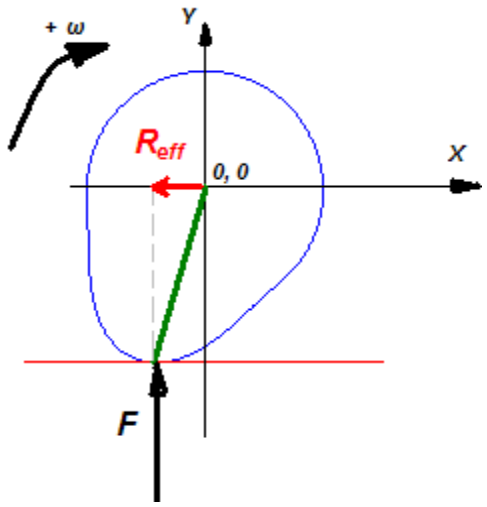

Figure 5.10: Camshaft torque effective radius

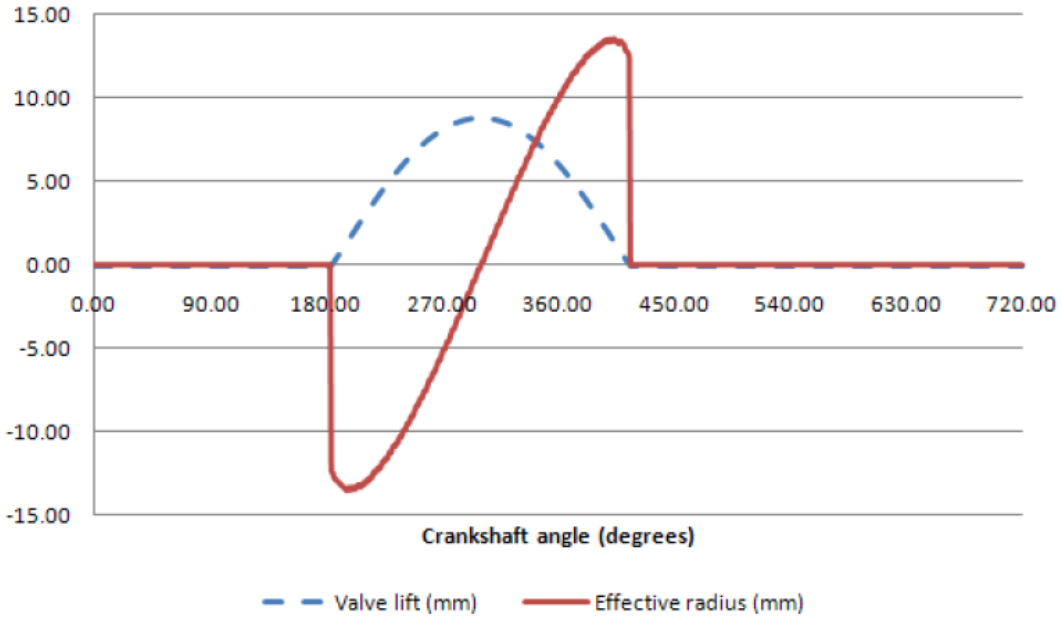

Figure 5.11: Valve position and effective torque radius (Contact Solver output)

5.2.2 Contact solver

A contact solver has been developed in MATLAB GUIDE which evaluates the valve position and effective torque radius for a direct acting valve train system with flat followers. Screenshots of the actual program can be seen on Figure 5.12 and Figure 5.13.

The program requires a tab delimited input text file of the camshaft profile with the following format.

Column 1: camshaft angle in constant steps from 0-360

Column 2: camshaft radius (mm)

Once the camshaft profile is loaded, smoothing can be applied and the result visualised. Then, the program rotates the camshaft lobe for a complete revolution during which it evaluates the valve position and effective torque radius.

The valve clearance is an important parameter as an increase in valve clearance reduces the effective camshaft duration and peak lift as it can be seen in the graphs on Figure 5.14.

The file output of this solver is a tab delimited file with the following format:

Column 1: crankshaft angle 0-720

Column 2: static valve/follower lift (mm)

Column 3: effective camshaft lobe radius (mm)

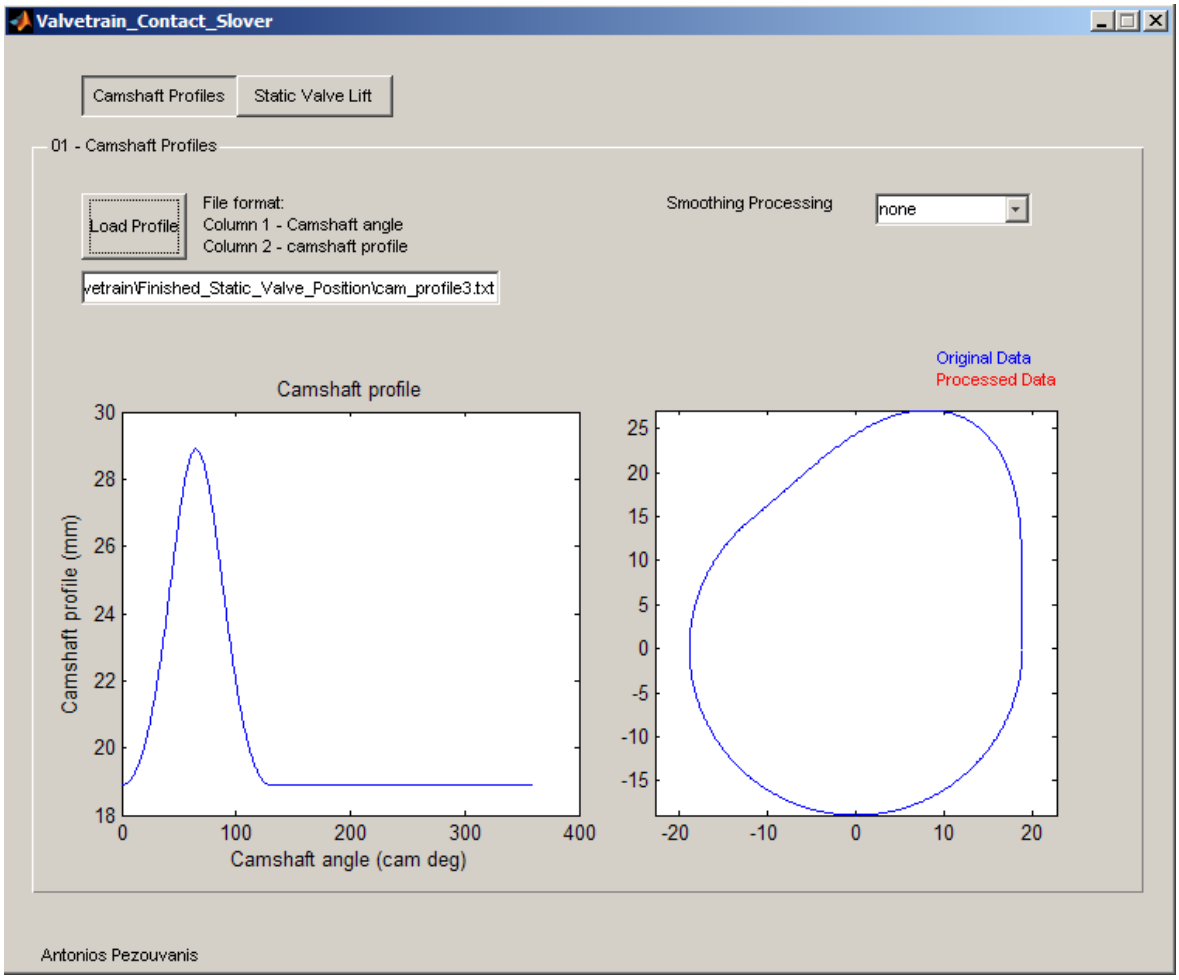

Figure 5.12: Camshaft contact solver (loading page)

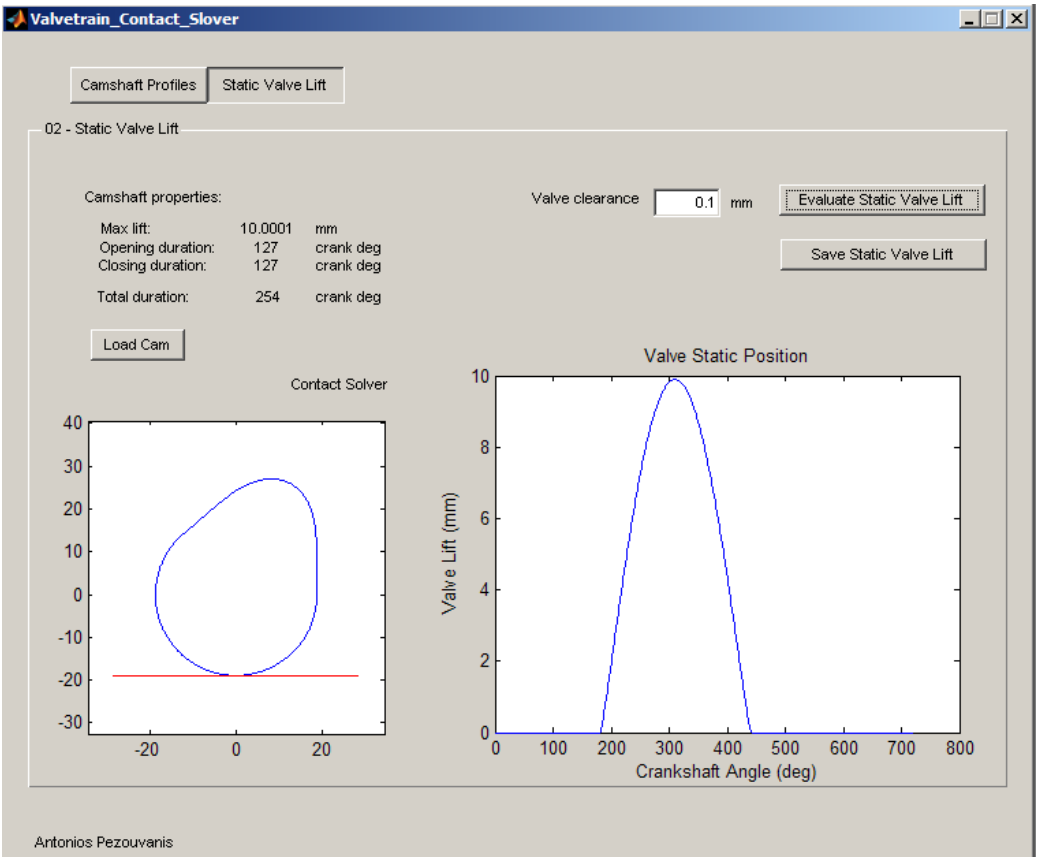

Figure 5.13: Camshaft contact solver (solver page)

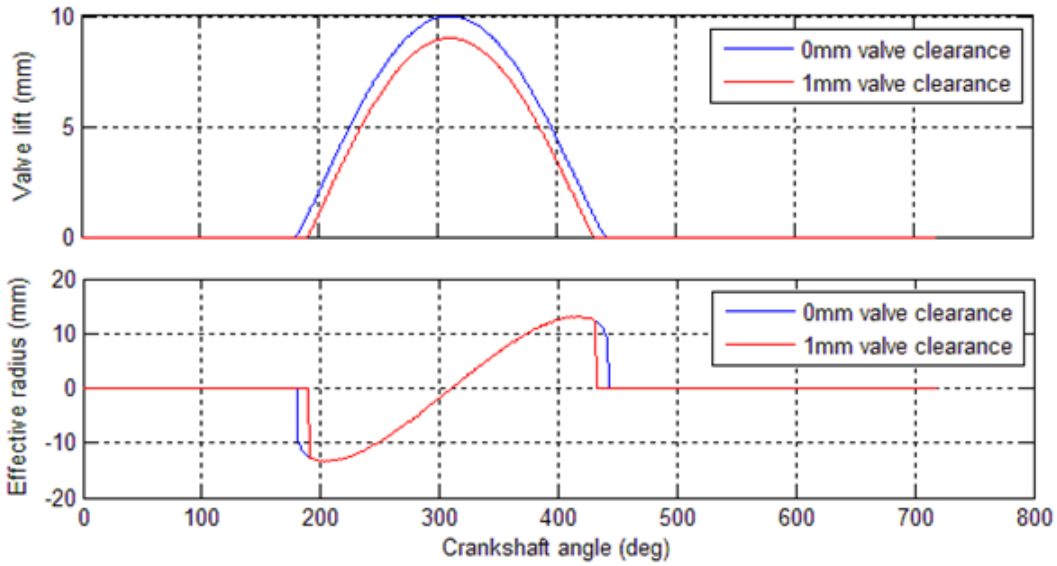

Figure 5.14: Effect of valve clearance

5.3 Valve timing

The valve timing affects the gas exchange process of the engine. Assuming at this point that the static valve lift is known, the next step is to time the data relative to the crankshaft angle and thus relative to the cycle of the engine. It is exactly the same process as timing the camshafts on an actual engine.

If an engine is to be modelled, then the actual IVO, IVC, EVO and EVC positions should be measured so that they can be replicated in the model. The process of the timing in the model is a simple phase shift of the valve static lift matrix by an amount of desired crankshaft angle.

Although it is simple, is quite a challenge to produce a simple application to facilitate the model timing due to the fact that the valve opening and closing positions have to be scanned and retrieved from the data.

The following picture (Figure 5.15) is a screenshot of the valve timing application. It allows the input of two static valve lift files and upon loading, it shifts the relative lifts to the proper engine stroke. Then, the user is able to time the valve opening and closing position by selecting the appropriate crankshaft phasing.

The input file format is given below:

Intake file:

Column 1: crankshaft angle (crank deg)

Column 2: intake static valve lift (mm)

Column 3: intake camshaft lobe effective radius of torque application (mm)

Exhaust file:

Column 1: crankshaft angle (crank deg)

Column 2: exhaust static valve lift (mm)

Column 3: exhaust camshaft lobe effective radius of torque application (mm)

As this application is the following step to the contact solver developed, the input format is the same as the solver's output. Thus, facilitating the process of data generation as the file can be loaded directly without any alteration.

The output format of the valve timing application is given below:

Column 1: crankshaft angle (crank deg)

Column 2: timed intake static valve lift (mm)

Column 3: timed exhaust static valve lift (mm)

Column 4: timed intake camshaft lobe effective radius of torque application (mm)

Column 5: timed exhaust camshaft lobe effective radius of torque application (mm)

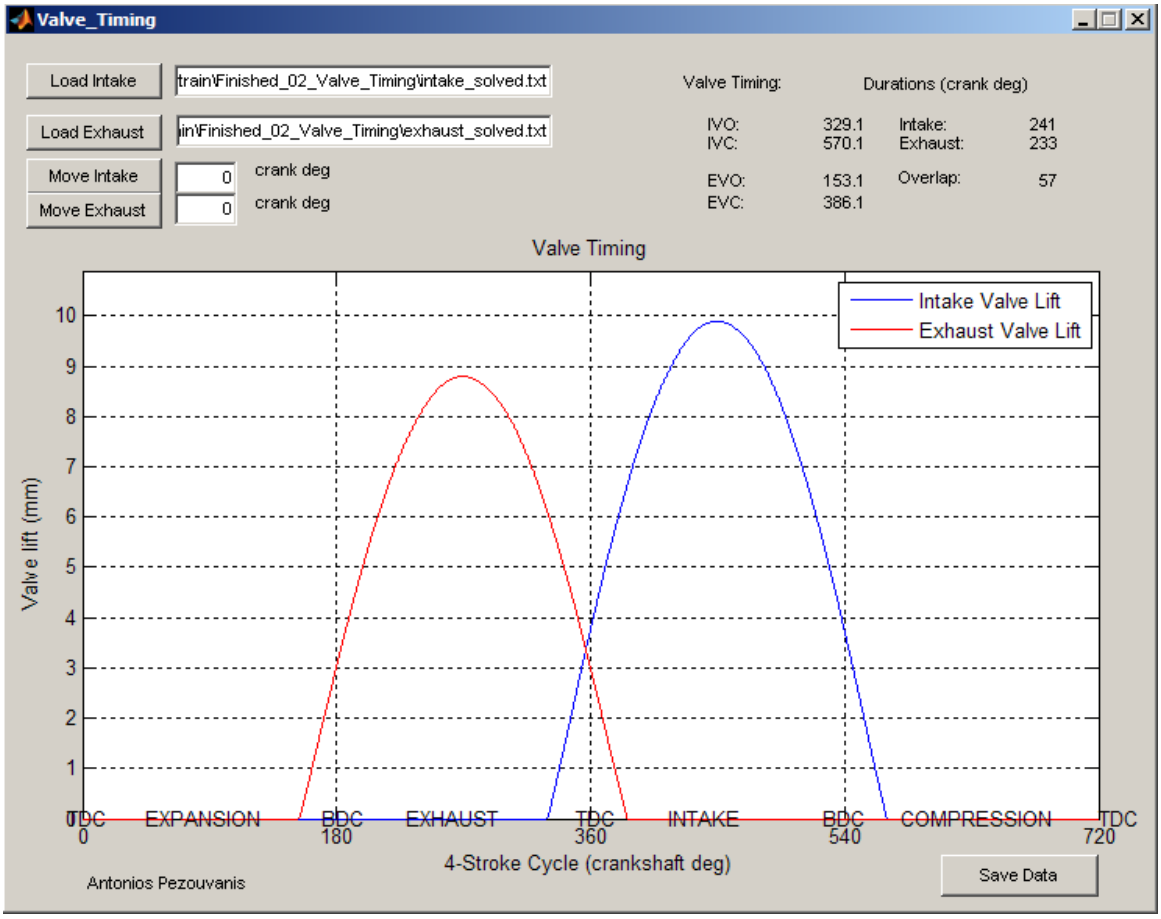

Figure 5.15: Valve timing application

5.4 Valve flow area

The calculations preceding this section were all done to obtain the static lift of the valves or flat followers and to time them at a specific crankshaft angle. The next step is to evaluate the restriction area along the path of the flow during the gas exchange process.

Two valve flow area models were found in the literature and provide the base for developing an improved version which takes into account additional parameters which are important when dealing with experimental discharge coefficient estimation.

The three models are presented below to show their differences and individual calculations involved.

5.4.1 Model 1 – Curtain area

The first model is a simple area evaluation based only on the valve head diameter D and port diameter (assumed to be equal to the valve head diameter) which evaluates an area created by the perimeter of the valve and its valve lift L [16] (Figure 5.16).

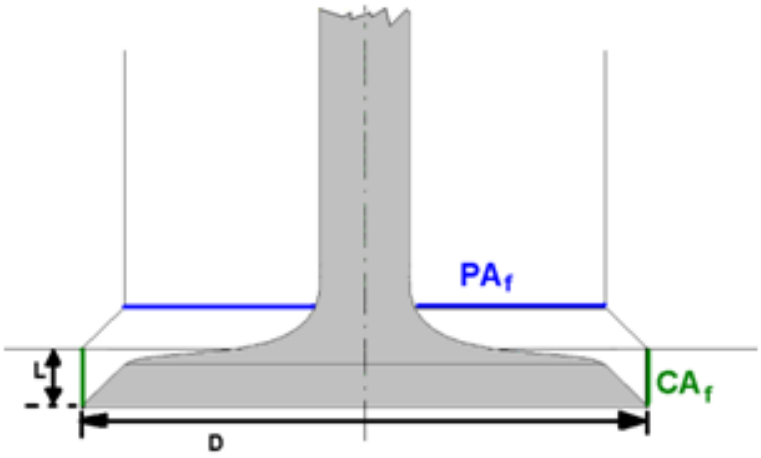

Figure 5.16: Model 1 - Curtain area

The curtain area (CA_f) and the port area (PA_f) are given by:

$$CA_f = \pi DL \qquad \text{(Eq. 5.10)}$$

$$PA_f = \frac{\pi D^2}{4} \qquad \text{(Eq. 5.11)}$$

The restricting flow area is the smaller output of these two equations (Eq. 5.10) and (Eq. 5.11). In other words, starting from a closed valve, the restricting area is the curtain area. As

the valve lift is increasing, at a point the curtain area will be larger than the port area. At that moment, the port area becomes the restriction.

The valve lift ($L_{\max\ eff}$) at which this transition occurs is given by:

$$L_{\max\ eff} = \frac{D}{4} \qquad \text{(Eq. 5.12)}$$

5.4.2 Model 2 – Gap area

The second model presented in [15] takes into account in addition to "model 1" the valve seat angle θ (Figure 5.17).

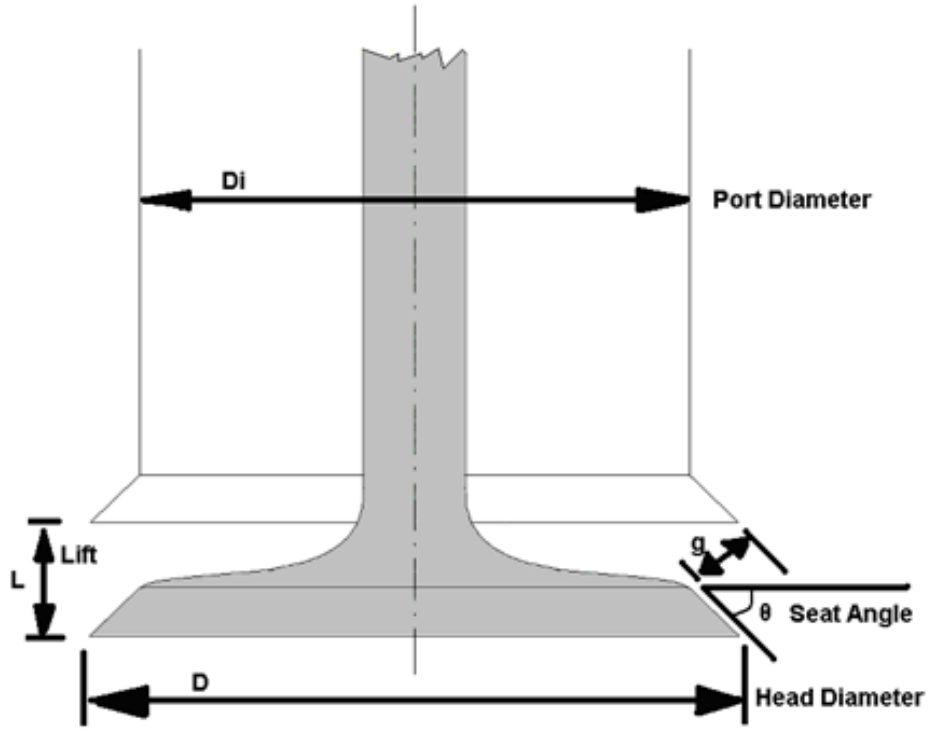

Figure 5.17: Model 2 - Gap area

The required cross-section on this model is the gap g between the valve and the valve seat. The actual curtain area (CA_f) and port area (PA_f) available to the flow are given by:

$$CA_f = \pi \frac{D + D_i}{2} g = \pi \frac{D + D_i}{2} L \cos\theta \quad \text{(Eq. 5.13)}$$

$$PA_f = \frac{\pi D_i^2}{4} \quad \text{(Eq. 5.14)}$$

The valve lift ($L_{\max\ eff}$) at which the port area becomes the flow restriction is given by:

$$L_{\max\ eff} = \frac{D}{4} \frac{\left(\frac{D_i}{D}\right)^2}{\cos\theta \frac{1 + \frac{D_i}{D}}{2}} \quad \text{(Eq. 5.15)}$$

5.4.3 Model 3 – Restriction area

The mapping of the discharge coefficients for poppet valves has shown that three different flow regimes exist during a valve lift event [7, 15-17]. Thus, the flow goes through three different valve flow area shapes. An accurate flow area should then be evaluated using three different set of equations. The three flow areas in question can be seen on the 3D representation on Figure 5.18. A more accurate model can be formulated by introducing the valve stem diameter d and examine the gap area as the lift is increased (Figure 5.19).

In this model, the port area (PA_f) is given by:

$$PA_f = \pi \frac{D_i^2 - d^2}{4} \quad \text{(Eq. 5.16)}$$

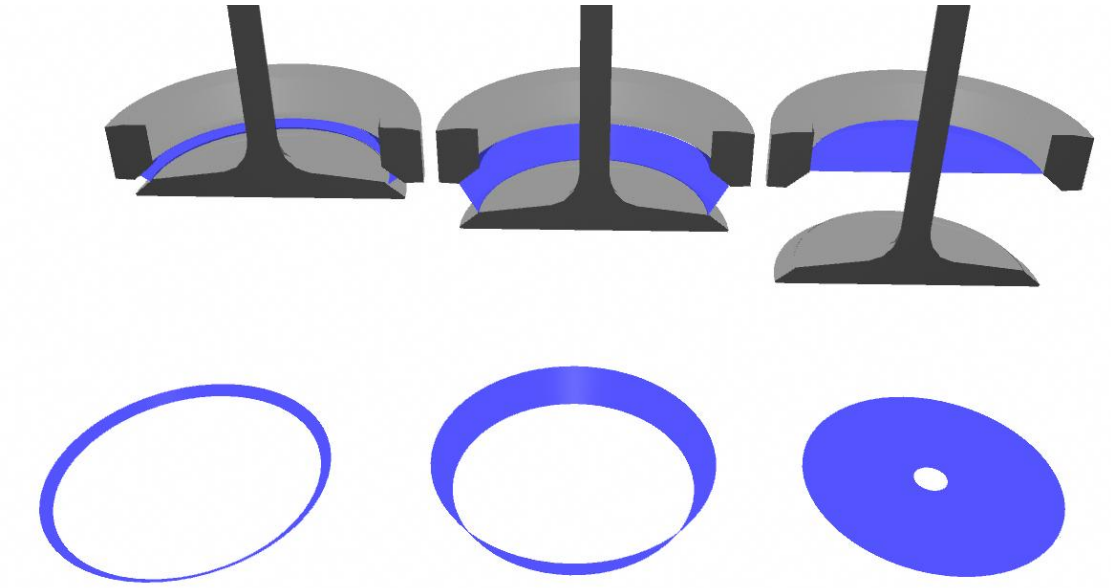

Figure 5.18: The three different restriction areas taking place during a valve lift event

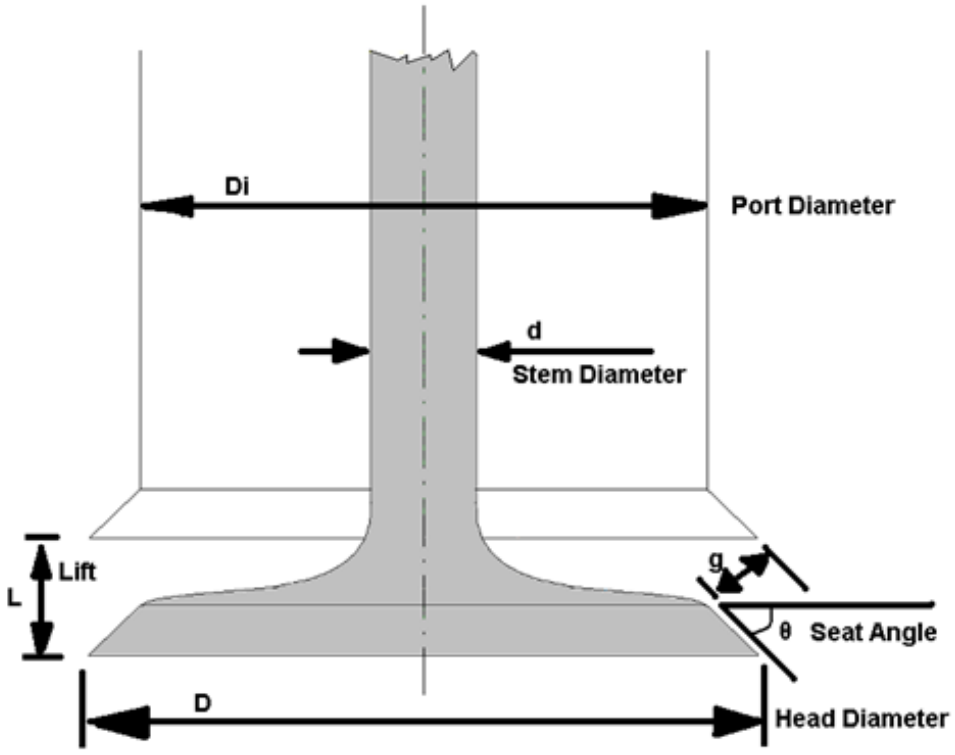

Figure 5.19: Model 3 - Restriction area

In order to calculate the curtain area (CA_f) an examination is needed of the gap (g) created between low lift and higher lift.

Low lifts

As it can be observed in Figure 5.20, the curtain area (CA_f) is given by:

$$CA_f = \pi \frac{D + D_i}{2} g = \pi \frac{D + D_i}{2} L \cos\theta \qquad \text{(Eq. 5.17)}$$

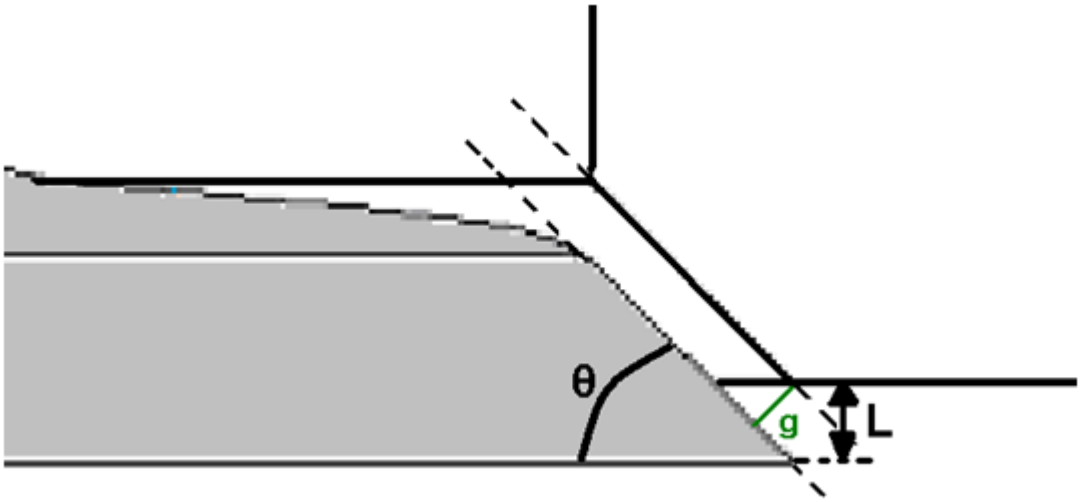

Figure 5.20: Gap area created at low lifts

High lifts

When the lift is increased, the restriction is not anymore the gap (g) as it can be seen in Figure 5.21. A second gap ($g2$) has to be introduced at this point which is the cross-section of the area between the corners of the higher point on the valve seat to the bottom end point of the cylinder-head seat.

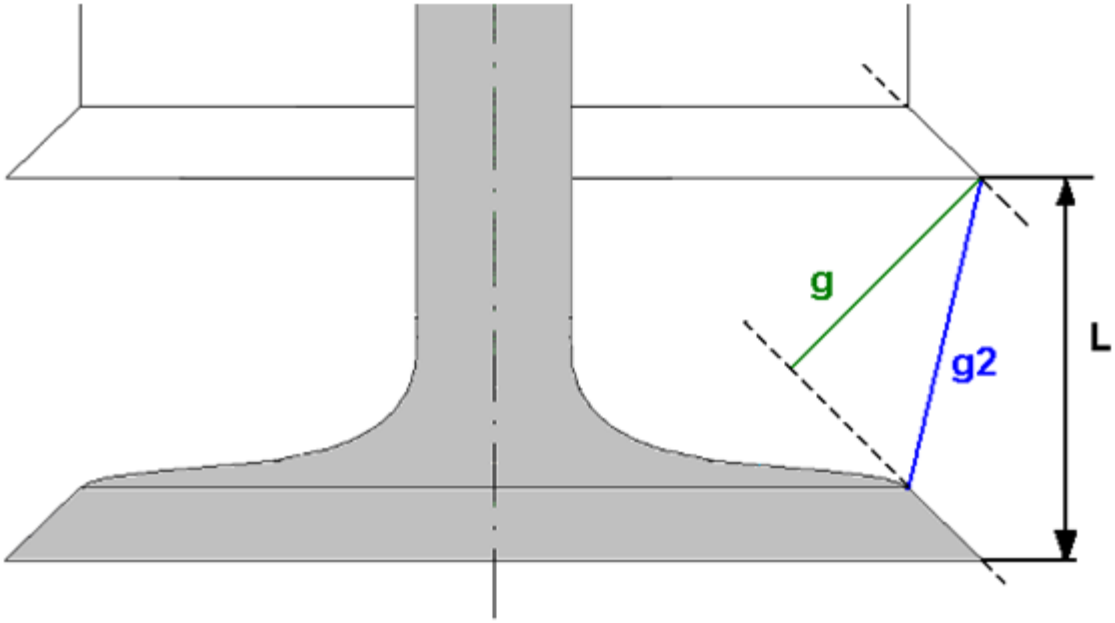

Figure 5.21: Gap area created at high lifts

The curtain area (CA_{f2}) at this cross section ($g2$) is given by:

$$CA_{f2} = \pi \frac{D + D_i}{2} \sqrt{\left(L - \tan\theta \left(\frac{D - D_i}{2}\right)\right)^2 + \left(\frac{D - D_i}{2}\right)^2} \qquad \text{(Eq. 5.18)}$$

The valve lift (L_s) at which the flow restriction area is switching from CA_f (Eq. 5.17) to CA_{f2} (Eq. 5.18) is given by:

$$L_s = \frac{D - D_i}{2 \sin\theta \cos\theta} \qquad \text{(Eq. 5.19)}$$

5.4.4 Comparison

The first model is very simple by taking into account only the valve head diameter. There is a difference in the maximum flow area between the three models due to the amount of inputs provided (Table 5.1). The maximum area is actually the port area which is a constant output and that is the reason for the horizontal limits on the plots as it can be seen in (Figure 5.22). The difference between Model 2 and Model 3 does not seem significant, but it has a larger effect when the valve opening duration is added as well. There is no point in increasing the valve more than the maximum effective valve lift as the flow area does not increase. Although, all engines have their camshafts designed so that the lift is higher than this value. This is done to maximise the flow area during the cycle as the engine has the maximum possible area available for that specific port design for a long duration. This is the reason that the correct calculation of this model is important for a correct estimation of the total flow area available during the cycle.

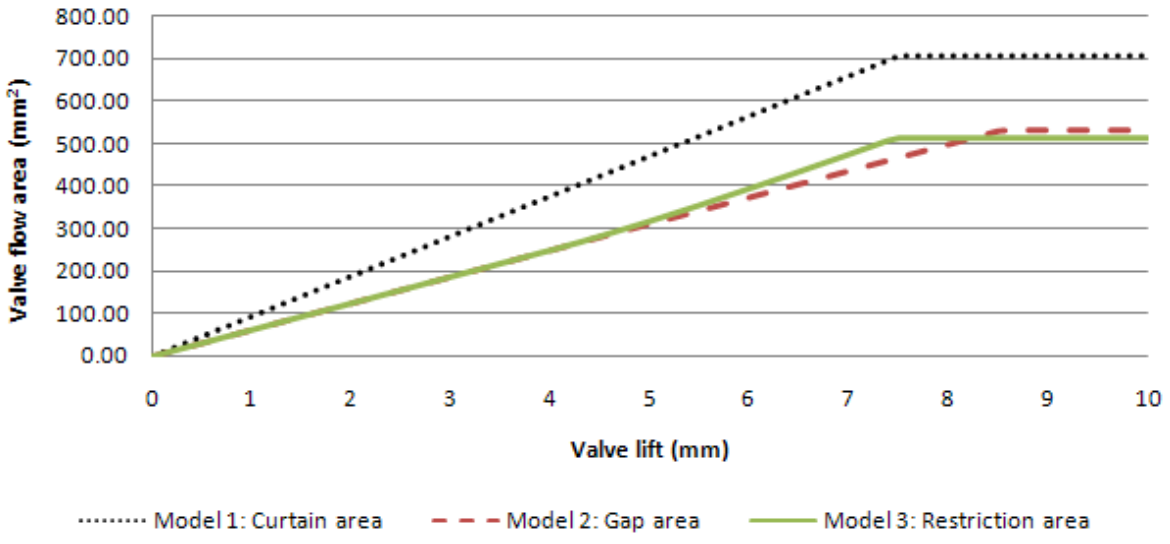

Figure 5.22: Valve flow area models comparison

Table 5.1: Model inputs comparison

Model	Amount of Inputs	Symbol of inputs
Model 1	2	D, L
Model 2	4	D, Di, L, θ
Model 3	5	D, d, Di, L, θ

The following picture (Figure 5.23) is a typical calculation of the valve flow area for the three different models through a valve lift event during one cycle.

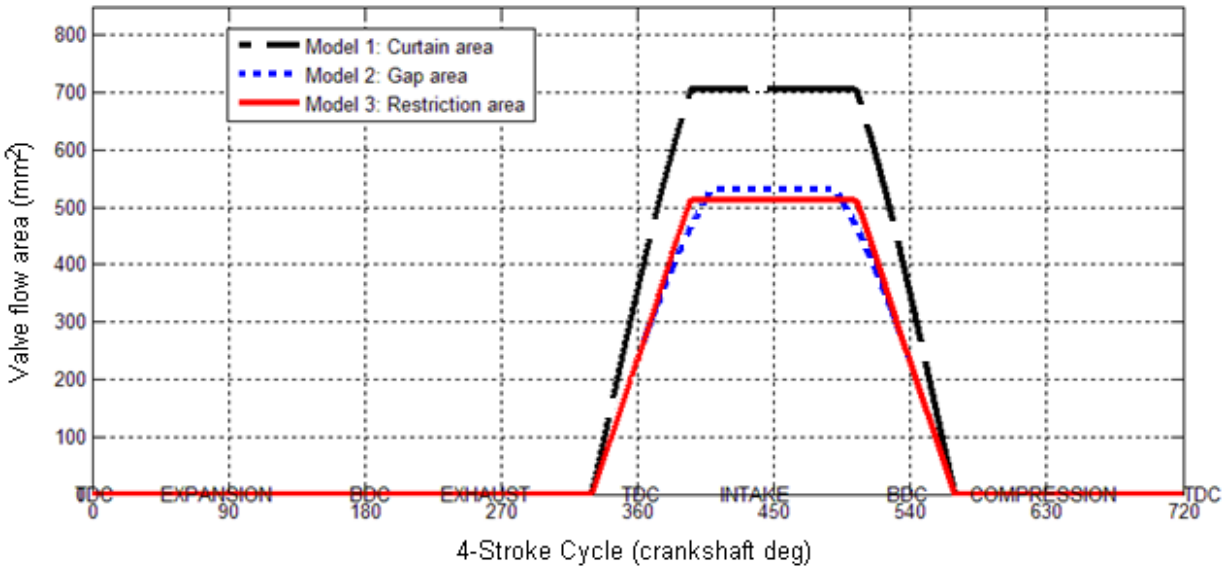

Figure 5.23: Valve flow area models comparison (one typical complete cycle)

CHAPTER 6: Throttle kinematics

The throttle controls the power output control of the engine by restricting the air flow into the intake manifold. It is important to accurately evaluate the throttle opening area as a function of throttle angle as they are inputs to most engine models or engine mapping procedures. The throttle type commonly used is the butterfly valve which consists of a rotating circular plate attached to a shaft inside the throttle bore (Figure 6.2).

The shaft size is usually sufficient to affect the air flow thus it is preferable to take it into account when evaluating the flow area. Another interesting point is that the throttle plate has a bigger diameter on its vertical axis to prevent locking inside the throttle bore at closed throttle [17]. The maximum effective flow area is obtained as soon as the throttle height has the same value as the shaft diameter.

Two throttle area models were found in the literature of which one of them is inaccurate and the second does not describe continuously the whole throttle range with one equation.

Model 1 [17]:

$$\frac{4A_{th}}{\pi D^2} = \left(1 - \frac{\cos\psi}{\cos\psi_0}\right) + \frac{2}{\pi}\left[\frac{l}{\cos\psi}(\cos^2\psi - l^2\cos^2\psi_0)^{\frac{1}{2}} - \frac{\cos\psi}{\cos\psi_0}\sin^{-1}\left(\frac{l\cos\psi_0}{\cos\psi}\right) - l(1-l^2)^{\frac{1}{2}} + \sin^{-1} l\right]$$

D is throttle bore, l is the ratio of the shaft diameter d over the throttle bore D, ψ_0 and ψ are the closed throttle angle and throttle angle opening respectively.

Model 2 [13]:

$$A_{th} = \frac{dD}{2}\left[1-\left(\frac{d\cos\psi_0}{D\cos(\psi_0+\psi)}\right)^2\right]^{1/2} - \frac{dD}{2}\left[1-\left(\frac{d}{D}\right)^2\right]^{1/2} + \frac{D^2}{2}\sin^{-1}\left\{\left[1-\left(\frac{d}{D}\right)^2\right]^{1/2}\right\}$$
$$-\frac{D^2\cos(\psi_0+\psi)}{2\cos\psi_0}\sin^{-1}\left\{1-\left(\frac{d\cos\psi_0}{D\cos(\psi_0+\psi)}\right)^2\right\}$$

The first model (*Model 1*) is inaccurate from the beginning of the throttle opening while the second one is accurate until the point that the maximum effective flow area is reached. The effective flow area should be estimated until wide open throttle (WOT) which for this simulated throttle was 90 degrees as a 0 degree closed throttle angle was used. It can be seen though that both models fall to a zero value after that point (Figure 6.1).

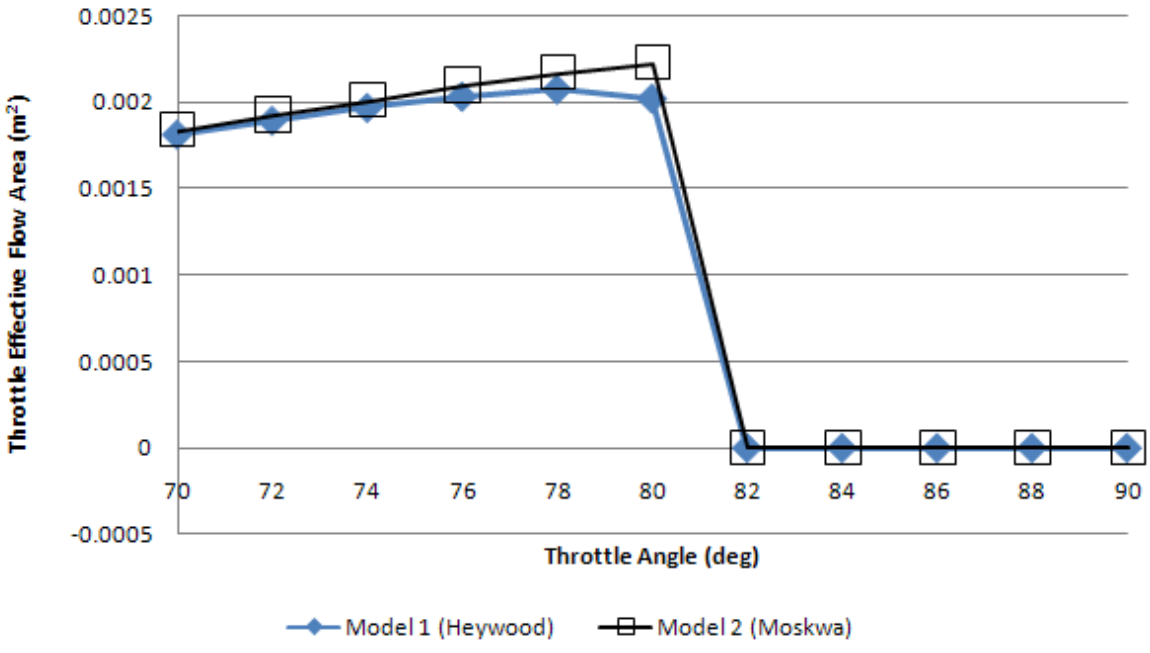

Figure 6.1: Throttle effective area models

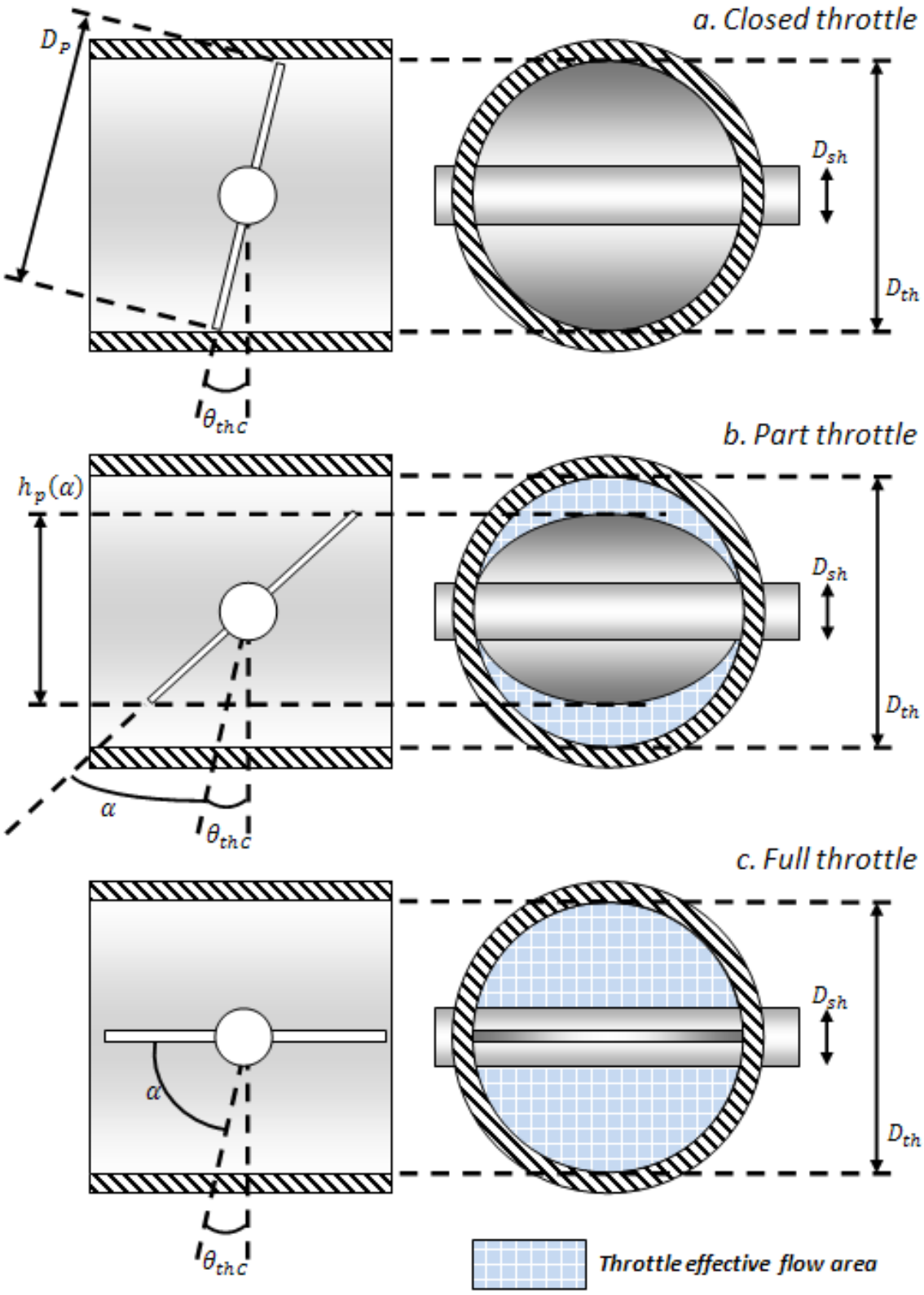

Figure 6.2: Throttle (butterfly type)

6.1 Maximum flow area

This section assumes that only a shaft is present inside the throttle bore, it is also the same effective flow area that occurs at wide open throttle. This effective flow area is evaluated as two circular segments (Figure 6.3).

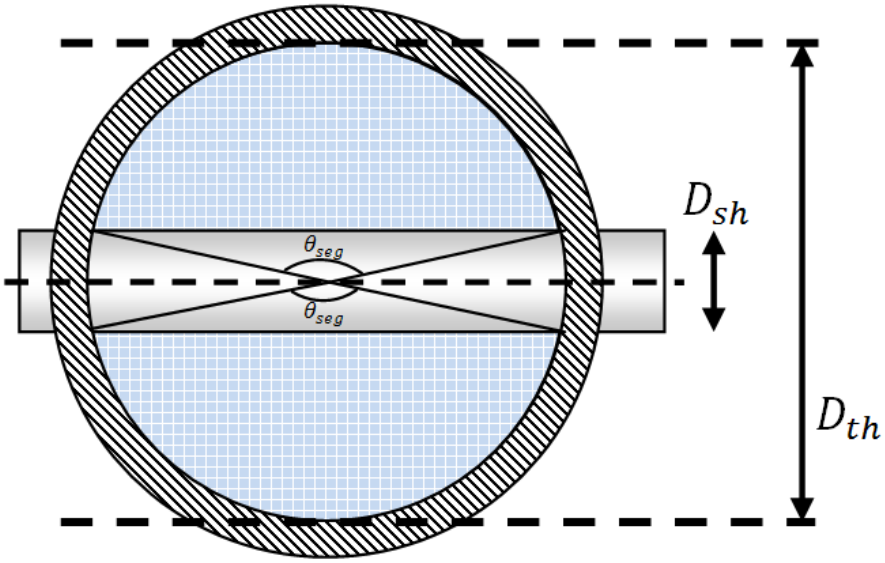

Figure 6.3: Maximum flow area

The maximum throttle flow area A_{th}^{max} is given by the area of both circular segments which is given by:

$$A_{th}^{max} = \frac{{D_{th}}^2}{4} 2\theta_{seg} - \frac{1}{2} D_{th} D_{sh} \sin(\theta_{seg}) \quad \text{(Eq. 6.1)}$$

$$\theta_{seg} = \cos^{-1} \frac{D_{sh}}{D_{th}} \quad \text{(Eq. 6.2)}$$

D_{sh} is the throttle shaft diameter and D_{th} is the throttle bore diameter.

6.2 Closed plate angle

One of the parameters needed for the throttle area model is the angle of the throttle plate when closed. It is usually easier to measure the plate diameter of the large axis on throttles ($\mathrm{D_p}$ in Figure 6.2-a.) than the actual closed angle (θ_{thC}) which is given by:

$$\theta_{thC} = \cos^{-1}\frac{D_{th}}{D_p} \tag{Eq. 6.3}$$

6.3 Throttle area

The throttle flow area is modelled as an elliptic area which has one of its sides varying with the throttle angle (Figure 6.2-b). Thus, the plate height $h_p(\alpha)$ is a function of throttle angle α and the throttle plate diameter D_p:

$$h_p(\alpha) = D_p \cos(\theta_{thC} + \alpha) \tag{Eq. 6.4}$$

The elliptic throttle plate area A_{th}^{plate} excluding the area covered by the shaft is given by:

$$A_{th}^{plate}(\alpha) = \frac{h_p(\alpha) D_{th}}{4} 2\theta_{seg}^{plate} - \frac{1}{2} D_{th} D_{sh} \sin\left(\theta_{seg}^{plate}\right) \tag{Eq. 6.5}$$

$$\theta_{seg}^{plate} = \cos^{-1}\frac{D_{sh}}{h_p(\alpha)} \in \mathbb{R} \tag{Eq. 6.6}$$

The real part of θ_{seg}^{plate} has to be evaluated due to the fact that once the throttle plate reaches the maximum effective flow area, the output is a complex number of which the real part is zero. If a complex invert cosine function is not available, then the function is going to return an error. On that case, the following functions should be used.

The above equation (Eq. 6.6) results in:

$$\alpha \leq \cos^{-1}\frac{D_{sh}}{D_p} - \theta_{thC} \longrightarrow \theta_{seg}^{plate} = \cos^{-1}\frac{D_{sh}}{h_p(\alpha)} \quad \text{(Eq. 6.7)}$$

$$\alpha > \cos^{-1}\frac{D_{sh}}{D_p} - \theta_{thC} \longrightarrow \theta_{seg}^{plate} = 0 \quad \text{(Eq. 6.8)}$$

SIMULINK automatically outputs a zero value when an error is occurred, thus eliminating the need of equations (Eq. 6.7) and (Eq. 6.8). Finally, the effective opened throttle area A_{th} is:

$$A_{th} = A_{th}^{max} - A_{th}^{plate}(\alpha) \quad \text{(Eq. 6.9)}$$

The throttle area rate of change $\frac{dA_{th}}{dt}$ may find use for transient throttle control or mapping. For this reason it was evaluated and the result is given below:

$$\frac{dA_{th}}{dt}(\alpha, \omega_\alpha) = \omega_\alpha \, C_{th}(\alpha) \quad \text{(Eq. 6.10)}$$

ω_α is the throttle angular speed (rad/sec) and $C_{th}(\alpha) \in \mathbb{R}$.

$$C_{th}(\alpha) = \frac{D_{sh} D_{th} \sin(\theta_{thC} + \alpha)}{2\cos(\theta_{thC} + \alpha)\sqrt{1 - \frac{{D_{sh}}^2 \cos(\theta_{thC})^2}{{D_{th}}^2 \cos(\theta_{thC} + \alpha)^2}}} + \frac{{D_{th}}^2 \sin(\theta_{thC} + \alpha)\cos^{-1}\left[\frac{D_{sh}\cos(\theta_{thC})}{D_{th}\cos(\theta_{thC} + \alpha)}\right]}{2\cos(\theta_{thC})} - \frac{{D_{sh}}^3 \cos(\theta_{thC})^2 \sin(\theta_{thC} + \alpha)}{2D_{th}\cos(\theta_{thC} + \alpha)^3\sqrt{1 - \frac{{D_{sh}}^2 \cos(\theta_{thC})^2}{{D_{th}}^2 \cos(\theta_{thC} + \alpha)^2}}} \quad \text{(Eq. 6.11)}$$

A 3D throttle body has been made in the I-DEAS 3D CAD software from which the throttle effective flow area at different angles (Figure 6.5) was found to be exactly equal to the model output (Figure 6.4).

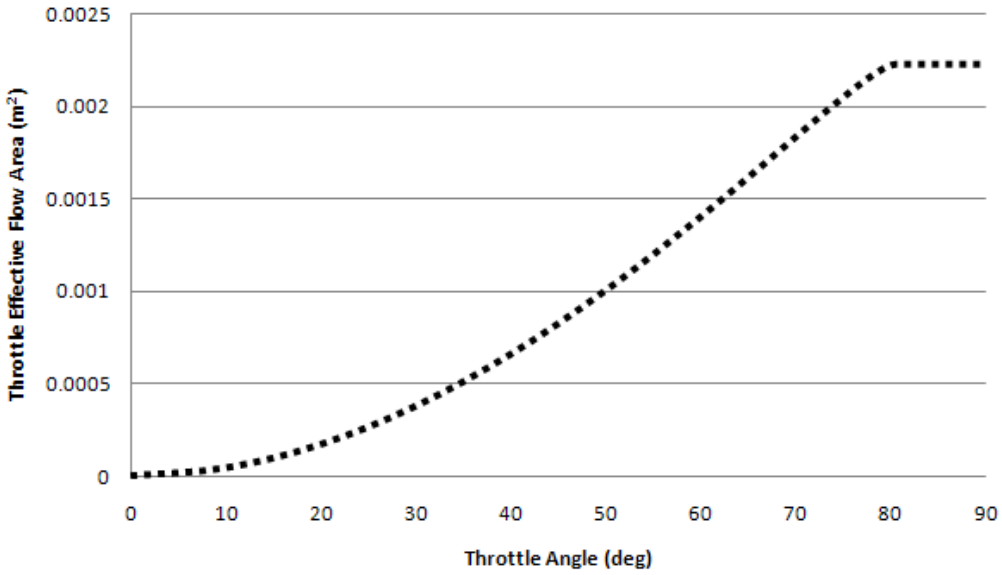

Figure 6.4: Throttle effective flow area

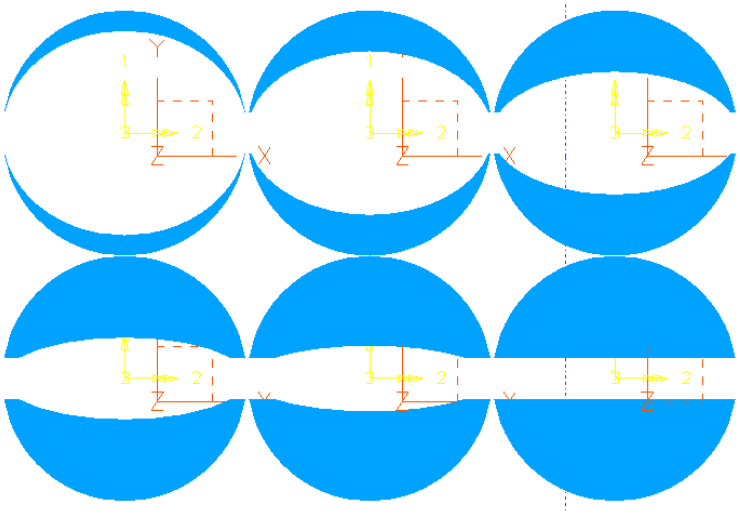

Figure 6.5: Throttle area model validation

6.4 Parameters effect

In order to study the effect of each input parameter, three sets of inputs were chosen (Table 6.1). The first set is going to be the "zero reference" for comparison, the second has an increased shaft diameter compared to the zero reference throttle, while the third has an increase in closed angle.

Table 6.1: Throttle model inputs

	Zero reference	***Increased shaft diameter***	***Increased closed angle***	***Symbols***	***Units***
Throttle bore	0.06	0.06	0.06	D_{th}	*m*
Shaft diameter	0.01	0.02	0.01	D_{sh}	*m*
Closed angle	0	0	15	θ_{thC}	*deg*

An increase in shaft diameter reduces the maximum effective flow area of the throttle body with minimal effects on the part throttle region. In addition, the throttle angle at which the maximum effective flow area is reached at a smaller plate opening angle (Figure 6.6).

On the other hand, an increase in closed throttle angle tends to increase the response of the throttle area at small openings. This can be seen in (Figure 6.7) as the initial value of the rate of change at the closed throttle is not zero anymore, while the peak value is almost unchanged.

The full range effect on the throttle area and rate of change can be seen in (Figure 6.6) and (Figure 6.7) respectively. The throttle's area rate of change was evaluated using (Eq. 6.10 and Eq. 6.11) using a throttle opening speed of 1rad/sec.

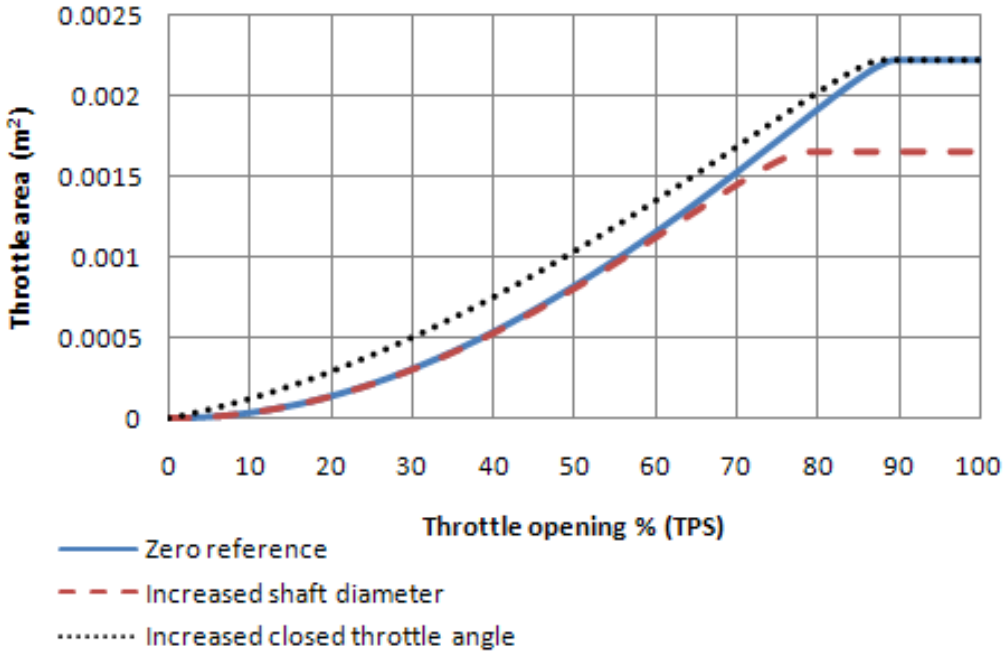

Figure 6.6: Input parameters effect on throttle area

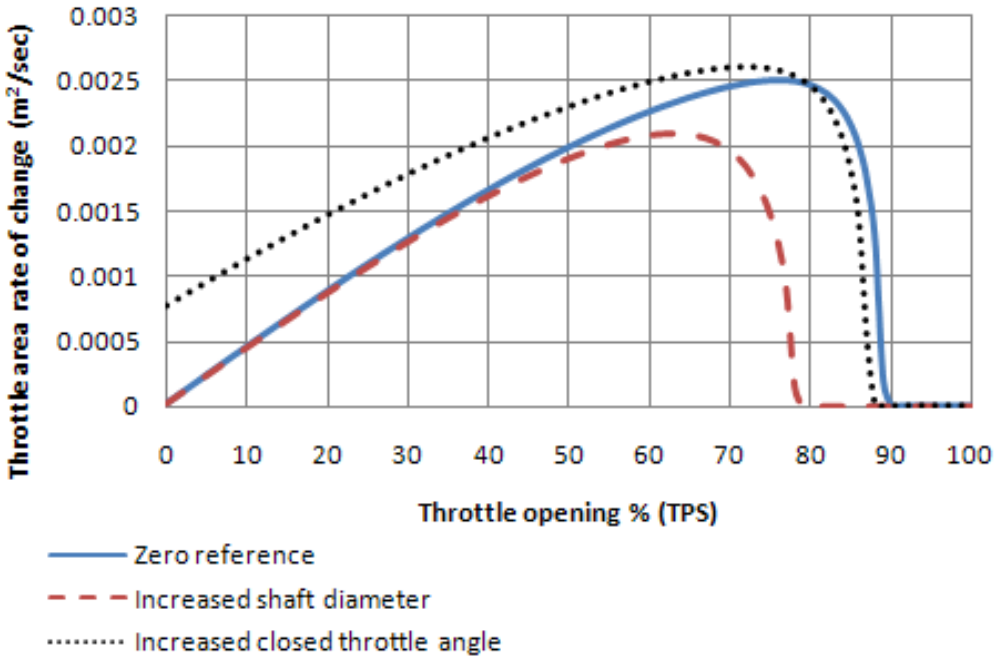

Figure 6.7: Input parameters effect on throttle area rate of change

6.5 Approximation

The throttle area equations are frequently used in RT or embedded systems in order to evaluate the mass air flow entering the inlet manifold. The high fidelity model presented above can be quite demanding in terms of calculations for real-time applications. A simpler model has been formulated which has an error within 1-3% for common throttle parameters but requires noticeably less calculations (Figure 6.8).

Throttle area:

$$A_{th} = \frac{\pi D_{th}}{4}\left[D_{th} - D_p \cos(\theta_{thC} + \alpha)\right] \quad \text{(Eq. 6.12)}$$

$$limit\ A_{th} to\ A_{th}^{max} \ \text{(Eq. 6.1)} \quad \text{(Eq. 6.13)}$$

The throttle area rate of change is again given by:

$$\frac{dA_{th}}{dt}(\alpha, \omega_\alpha) = \omega_\alpha\ C_{th}(\alpha)$$

Part throttle: $\alpha \leq \cos^{-1}\frac{D_{sh}}{D_p} - \theta_{thC}$

$$C_{th}(\alpha) = \frac{\pi D_{th} D_p \sin(\theta_{thC} + \alpha)}{4} \quad \text{(Eq. 6.14)}$$

Maximum effective area: $\alpha > \cos^{-1}\frac{D_{sh}}{D_p} - \theta_{thC}$

$$C_{th}(\alpha) = 0 \quad \text{(Eq. 6.15)}$$

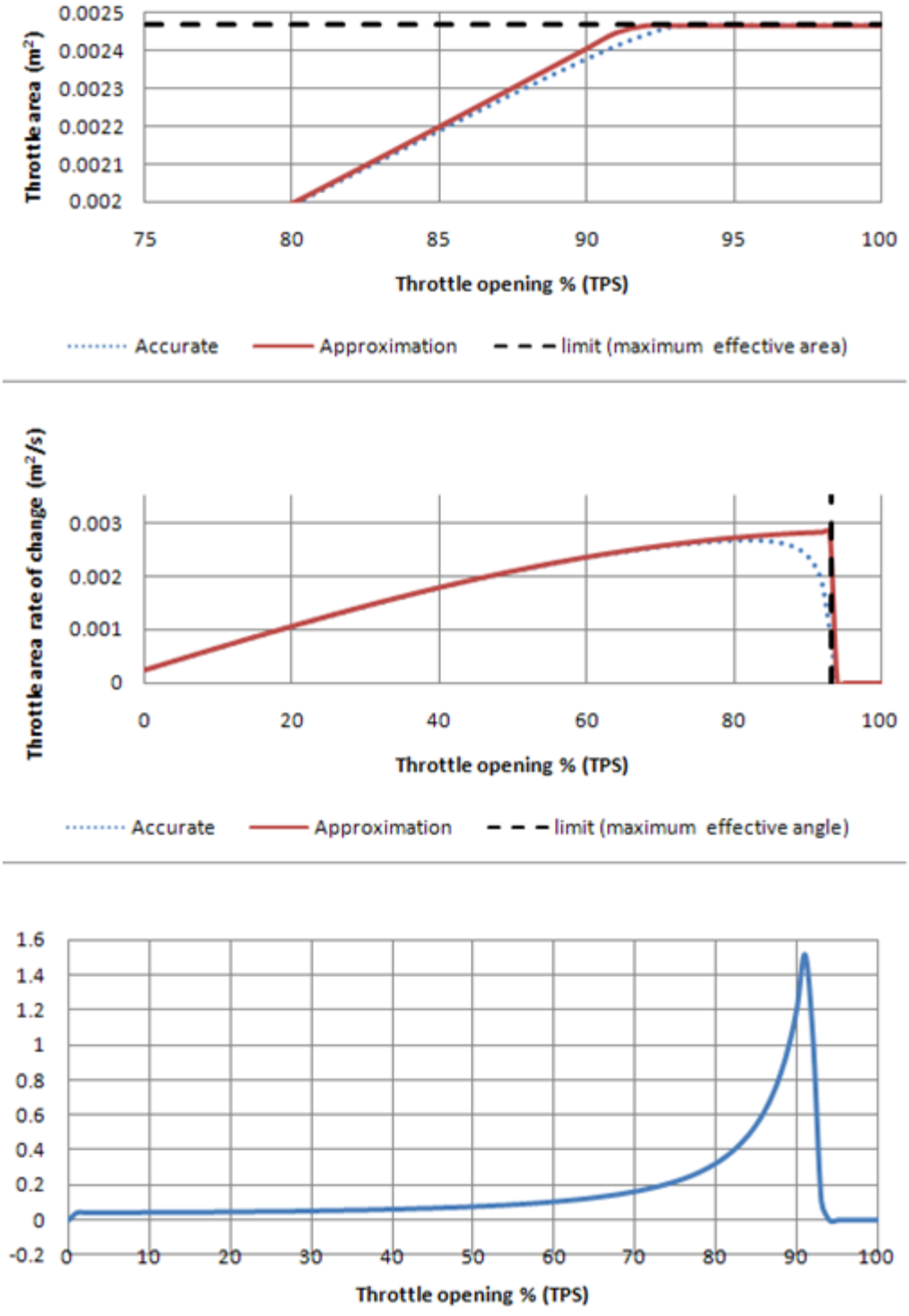

Figure 6.8: Approximation model results

6.6 Implementation

The equations described above can be used to evaluate the function of throttle area and its rate of change either using the accurate or approximation model set of equations. An interesting point is that the functions required $A_{th}(\alpha)$[12] and $C_{th}(\alpha)$[13] are constant for a given throttle, thus they can be used to initialise and use look-up tables for their evaluation making the model execution faster (Figure 6.9).

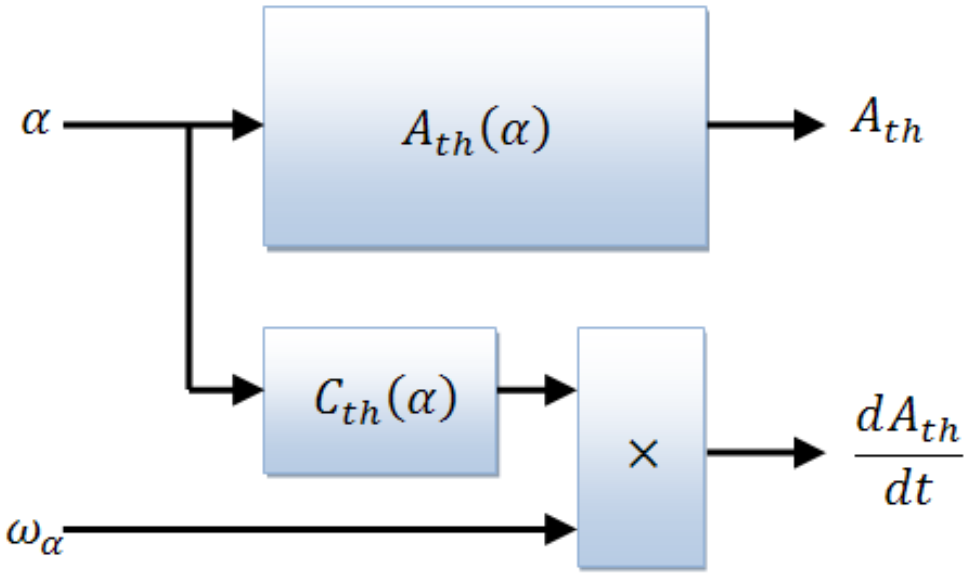

Figure 6.9: Throttle model structure (functions or look-up tables)

[12] Eq. 6.9 for accurate or Eq. 6.12 and 6.13 for approximation model
[13] Eq. 6.11 for accurate or Eq. 6.14 and 6.15 for approximation model

CHAPTER 7: Engine inertia

The 4-stroke engine has an intake and exhaust stroke that actually depends on their respective camshaft lobes. There is no need at this point to describe the valve opening mechanism, but just to note the fact that the camshafts have to rotate exactly at half the speed of the crankshaft. A relative rotation between crankshaft and camshafts should not exist, except of the condition that a variable valve system is present that operates by camshaft phasing.

The camshaft driving system principal function is to transfer a timed rotation to the camshafts. Other components can acquire a motion off this system as it can be used as a link to the crankshaft torque. The main driving systems used are: belt-pulleys, chain-sprockets or gear driven with the last one being probably the rarest encountered. A typical timing system is shown in (Figure 7.1).

The timing mechanism has an inertia which affects the engine acceleration and is going to be treated as rigid. This means that the entire mechanism inertia is going to always affect the engine's acceleration. In contrary to a *"flexible"* system which its inertia would not directly affect the acceleration due to the components stiffness and relative movements.

Before modelling the actual system, the modelling concept of obtaining the effective inertia of a simple gear mechanism is going to be described for clarification, before it is used to model the camshaft driving mechanism's inertia.

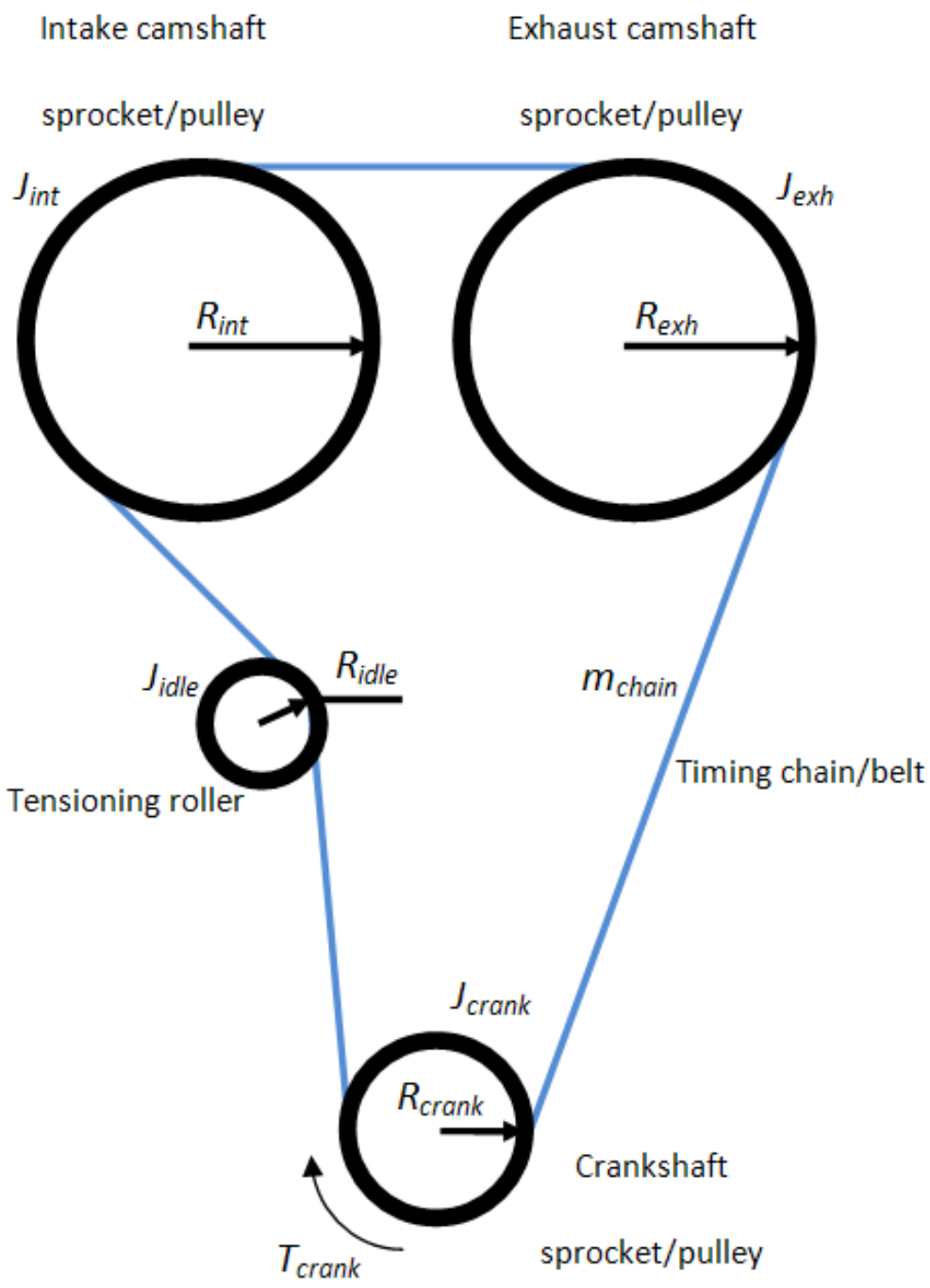

Figure 7.1: Camshaft driving mechanism

7.1 Relative inertia concept

The idea of this concept can be used on components that have a constant speed ratio and no relative movement between them. Assuming a gear system which is composed of two gears with no possible backlash as shown in (Figure 7.2):

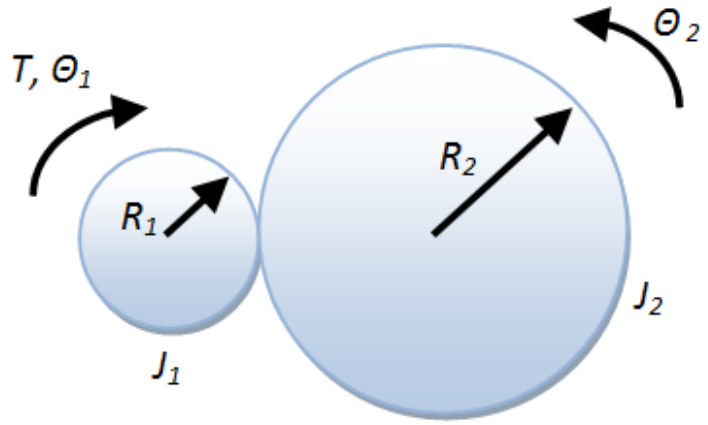

Figure 7.2: Gear system

The torque T is accelerating both gears of inertia J_1 and J_2. The equation of the above system can be described as:

$$\frac{d^2\theta_1}{dt^2}J_1 = T - \frac{d^2\theta_2}{dt^2}J_2 \qquad \text{(Eq. 7.1)}$$

As the assumption is that there is no relative movement between the two gears, the following expression can be used:

$$\frac{d^2\theta_1}{dt^2} = \frac{R_1}{R_2}\frac{d^2\theta_2}{dt^2} \qquad \text{(Eq. 7.2)}$$

Thus (Eq. 7.2 into Eq. 7.1) gives:

$$\frac{d^2\theta_1}{dt^2}\left(J_1 + \frac{R_2}{R_1}J_2\right) = T \qquad \text{(Eq. 7.3)}$$

θ is the rotation angle (rad), J is the component's inertia (kg m^2) and R is the gear contact radius (m).

This method translates the inertias of all system components onto one rotational acceleration used as reference. This simplifies the solution as only one unknown exists in the equation.

7.2 Mathematical model

The inertia of the camshaft driving system can be simplified using the relative inertia method described on the previous section assuming that the chain tension is high enough to neglect the relative movement of the components attached to it. A typical camshaft driving system's inertia can be evaluated as shown below using the diagram of (Figure 7.1).

Solving the entire mechanism of Figure 7.1 leads to:

$$T_{crank} = \frac{d^2\theta_{crank}}{dt^2}\left(J_{crank} + \frac{R_{idle}}{R_{crank}}J_{idle} + \frac{R_{int}}{R_{crank}}J_{int} + \frac{R_{exh}}{R_{crank}}J_{exh} + m_{chain}R_{crank}^2\right) \qquad \text{(Eq. 7.4)}$$

As the camshafts always rotate half the speed of the crankshaft:

$$\frac{R_{int}}{R_{crank}} = \frac{R_{exh}}{R_{crank}} = 2 \qquad \text{(Eq. 7.5)}$$

Thus equation (Eq. 7.4) can be summarised as:

$$T_{crank} = \frac{d^2\theta_{crank}}{dt^2}\left[J_{crank} + 2(J_{int} + J_{exh}) + \frac{R_{idle}}{R_{crank}}J_{idle} + m_{chain}R_{crank}^2\right] \qquad \text{(Eq. 7.6)}$$

Every engine has a different arrangement but the inertia can be evaluated with the same method. A fuel pump, water pump or even an intake compressor might be driven by the crankshaft, those can be added in the equation as the idle gear component described above.

In addition, the secondary belt driving accessories such as alternator, power steering pump or air conditioning can be modelled with the same method if it is assumed that there is no belt slip on their pulleys.

Generalising the equation for the effective engine inertia J_{eff} :

$$J_{eff} = J_{crank} + 2(J_{int} + J_{exh}) + m_{chain/belt}\,R_{crank}{}^2 + \frac{1}{R_{crank}}(R_1J_1 + .. + R_NJ_N) \qquad \text{(Eq. 7.7)}$$

7.3 Experimental measurement formulation

A simple experimental procedure has been derived to measure the inertia of the engine. This method requires only a speed measurement during two transient accelerations. The experimental measurements as well as the calculations required are demonstrated on a typical simulation below.

The concept is to add a known inertia I_a to the unknown engine inertia I_e and accelerate them through the same torque. Then, a formula can be derived which will evaluate the unknown engine inertia. The two different configurations can be seen in Figure 7.3.

The equations describing the system (Figure 7.3) are:

a) $\alpha_e I_e = T_e$ (Eq. 7.8)

b) $\alpha_a (I_e + I_a) = T_a$ (Eq. 7.9)

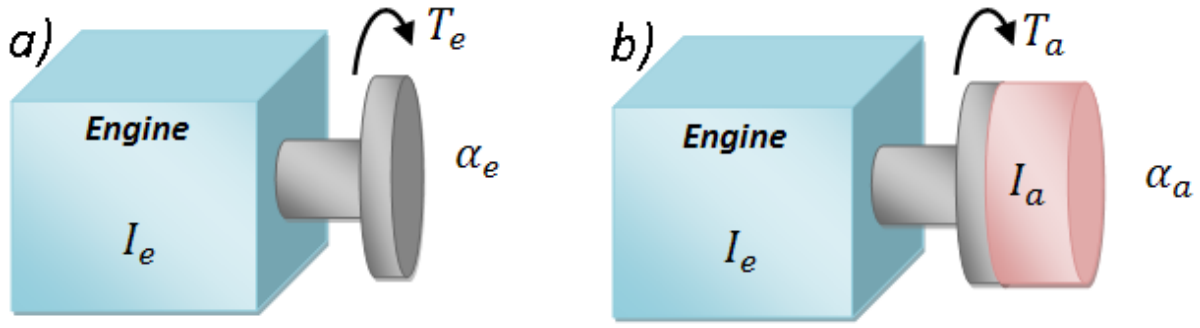

Figure 7.3: Experimental setup. a) engine inertia b) engine and added inertia

α_e and α_a are the engine accelerations (rad/sec^2) produced during the experimental setup a) and b) respectively. T_e and T_a are the engine torque output (Nm).

The next equation is based on the assumption that the engine torque output is independent of the engine acceleration. So, the torque output will be equal during both configurations (Figure 7.3) when the engine is at the same speed.

$$T_e^N = T_\alpha^N = T^N \quad \text{(Eq. 7.10)}$$

T^N: Engine torque output (Nm) at *N* speed

So, using equations (Eq. 7.8, Eq. 7.9 and Eq. 7.10):

$$\alpha_e^N I_e = \alpha_\alpha^N (I_e + I_\alpha) \quad \text{(Eq. 7.11)}$$

Which solving for the unknown engine inertia I_e:

$$I_e = \frac{\alpha_\alpha^N I_\alpha}{\alpha_e^N - \alpha_\alpha^N} \quad \text{(Eq. 7.12)}$$

7.4 Simulated experiment

The methodology is going to be demonstrated with a simulated experiment so that data can be obtained. The wide opened throttle engine's torque output is assumed to be a function of engine speed as shown in (Figure 7.4) in which the acceleration does not have a significant effect on a real engine. The engine and added inertias are going to be both assumed as they are needed for the simulation of the system.

The following unknown engine inertia I_e and known added inertia I_α are assumed for this example.

$$I_e = 0.3\ kgm^2 \qquad I_\alpha = 0.5\ kgm^2$$

The engine inertia is assumed in order to simulate the engine transients. The calculations should lead to a result equal to this engine inertia.

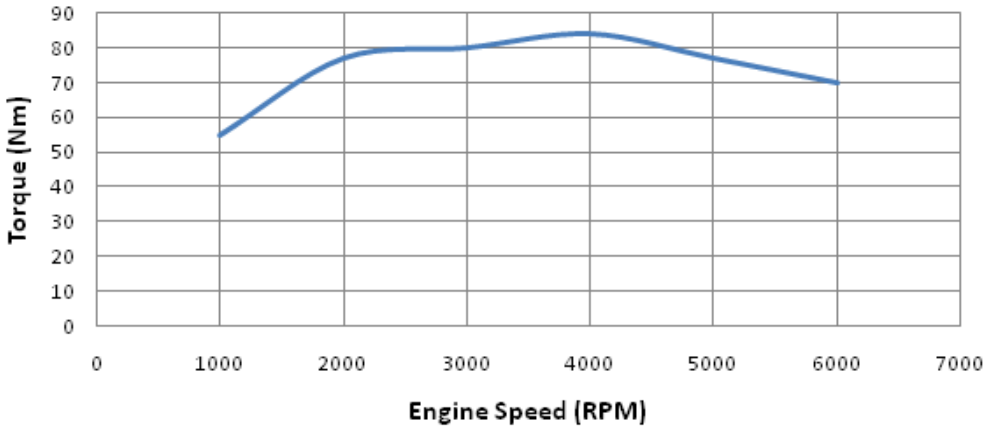

Figure 7.4: Assumed wide open throttle (WOT) torque output

Running a simulation for an engine speed from N=2000 to N=7000 rpm for both configurations, the speed and acceleration transients can be obtained (Figure 7.5).

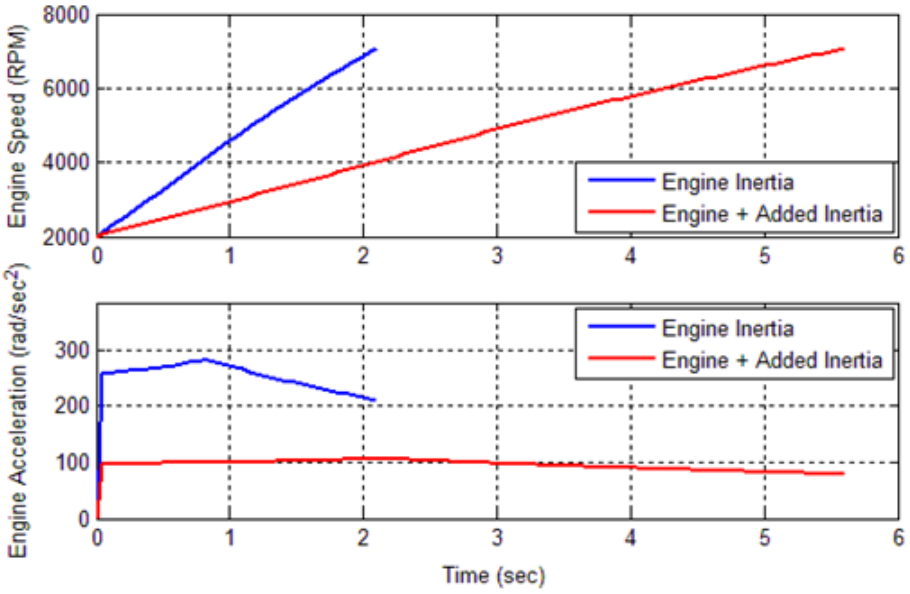

Figure 7.5: Speed and acceleration transients

The speed transient can be obtained just by data-logging the engine speed during a WOT acceleration from idle to the rev limiter. Then, the engine angular acceleration transient can be easily evaluated as:

$$\alpha = \frac{d\omega}{dt} \qquad \text{(Eq. 7.13)}$$

The next step is to change the X reference axis (Figure 7.5) from time to engine speed on the acceleration curves. These are actually the instantaneous engine angular accelerations at specific speeds. Doing so for the two test results produce the following points (Figure 7.6).

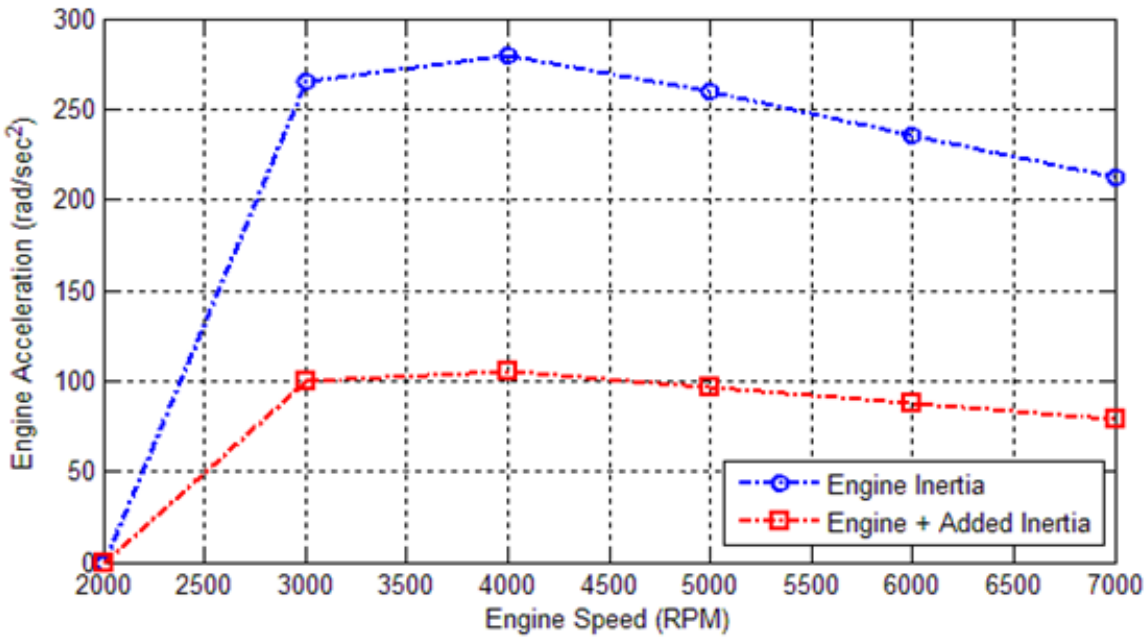

Figure 7.6: Instantaneous engine acceleration over the engine speed range

Now the unknown engine inertia can be evaluated using equation (Eq. 7.12) at each speed using the circular points for α_e and square points for α_α respectively from (Figure 7.6). The results can be seen in (Figure 7.7) which matches the assumed engine inertia used on the simulation.

If these calculations were made using experimental data there would be some deviations from the actual correct inertia value due to measurement errors and some deviations of the engine torque output because of different manifold dynamics. This is mainly the cause of the difference in engine acceleration. The conclusion is though that the smaller the added inertia is, the more accurate the results are going to be. In any case, the test should be repeated a couple of times and all the evaluated inertias should be averaged to obtain the final engine inertia.

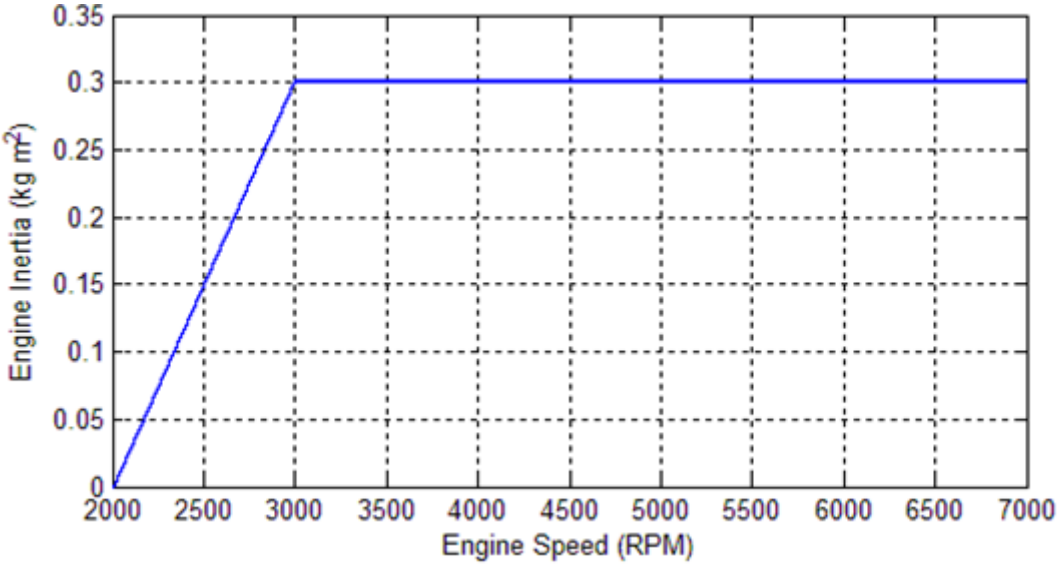

Figure 7.7: Engine inertia estimation (simulated)

An interesting point as well is that this methodology can be used to estimate an electric motor's or a component's inertia. The electric motor can take directly the place of the engine's described above. In case of a component, the motor's inertia should be known and the component's inertia would then be the unknown inertia used in the equations.

CHAPTER 8: Thermodynamic cycle simulation

A study of the engine thermodynamics has to be done In order to develop acceptable kinematic sub-models so that they can actually be usable for cycle-by-cycle engine simulations. The variables, parameters and calculation procedure will then be understood, so that the models have a correct working structure. The main objective at this point is going to be the formulation for evaluating the working mixture properties inside the cylinder. The thermodynamic cycle of an engine is usually represented on a P-V diagram. The area enclosed within the diagram is the work produced by that particular cylinder. A P-V diagram of an ideal Otto cycle is show in (Figure 8.1) which is the kind of data that can be obtained using an in-cylinder pressure sensor.

The four processes of the ideal Otto cycle are:

- Process 1-2 – Compression
- Process 2-3 – Heat addition
- Process 3-4 – Expansion
- Process 4-1 – Heat rejection

An isentropic compression of the assumed working mixture occurs between 1 and 2 as the piston moves from BDC to TDC. Heat is then added instantaneously at constant volume (Q_a) during the process 2 to 3 while the piston is assumed to be momentarily at rest at TDC. The result is a temperature and pressure increase during this process which pushes the piston back towards BDC resulting in an isentropic expansion. Once the piston reaches BDC, it is

assumed again that it is momentarily at rest while the heat (Q_r) is rejected. This cycle is also called Constant Volume Cycle due to the fact that when heat is added or rejected from the enclosed system (cylinder/combustion chamber); the piston is assumed momentarily at rest which means that there is no change in volume inside the cylinder.

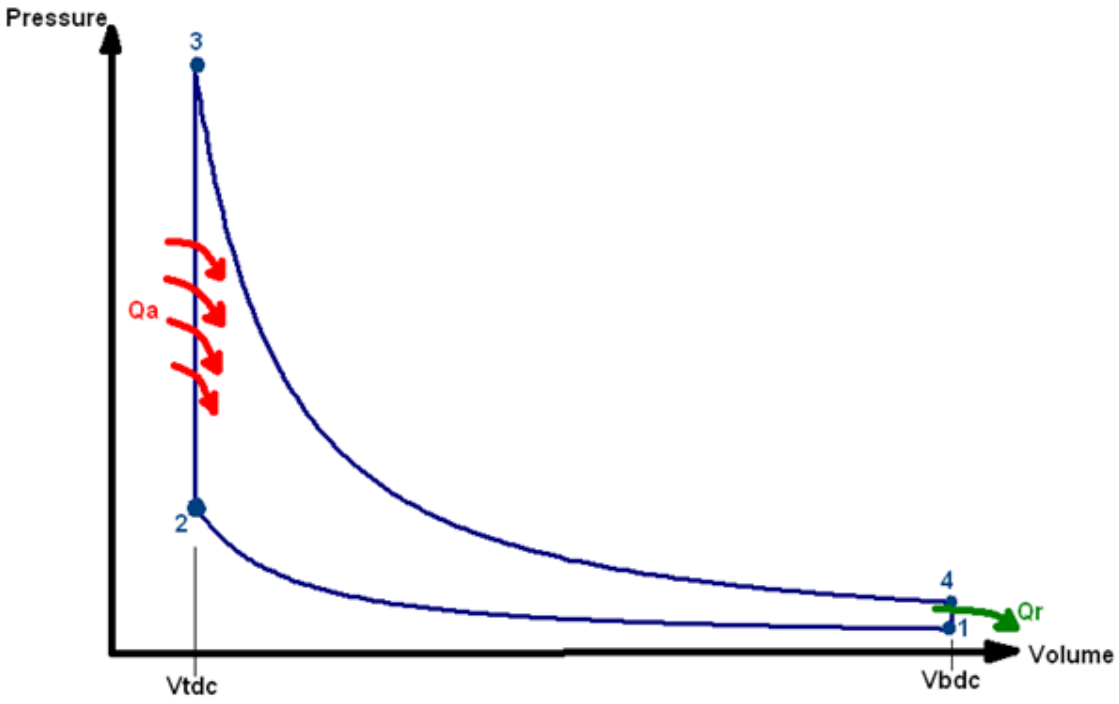

Figure 8.1: P-V diagram of the ideal Otto cycle

8.1 Compression ratio equivalence

The calculation of the pressure and temperature changes inside the cylinder during a small crankshaft angle increment requires the cylinder volume change during that step as it is going to be shown in the following equations.

Assuming that at *t=0* the cylinder volume is V_0 and at *t=1* is V_{new}, then the cylinder pressure P_{new} and temperature T_{new} are given by [17]:

$$P_{new} = P_0 \left(\frac{V_0}{V_{new}}\right)^k \quad \text{(Eq. 8.1)}$$

$$T_{new} = T_0 \left(\frac{V_0}{V_{new}}\right)^{k-1} \quad \text{(Eq. 8.2)}$$

k is the ratio of working mixture's specific heats for that step.

The term compression ratio equivalence is then the only kinematic variable that is needed for in-cylinder cyclic pressure and temperature calculation due to piston movement and is denoted as:

$$r_{equ} = \frac{V_0}{V_{new}} \quad \text{(Eq. 8.3)}$$

Although this term looks simple to calculate, it can be quite a challenge when trying to evaluate it in a flow type modelling software such as MATLAB Simulink. This is because both volume variables do not exist in memory at the same time step increment. In the contrary, line based programming provides the ability to access a variable any time by temporary memory storage.

The compression ratio equivalence has to be evaluated once the next cylinder volume calculation has been completed (Figure 8.2). This is possible by calculating the previous volume using the following equation.

$$V_0 = V_{new} - \frac{dV}{dt}dt \qquad \text{(Eq. 8.4)}$$

Thus, the compression ratio equivalence r_{equ} is given by dividing equation (Eq. 8.4) with V_{new} :

$$r_{equ} = 1 - \frac{\dot{V}}{V_{new}}dt \qquad \text{(Eq. 8.5)}$$

$\dot{V}$ is the cylinder volume rate of change during V_0 to V_{new} , and dt is the time step increment between V_0 to V_{new} .

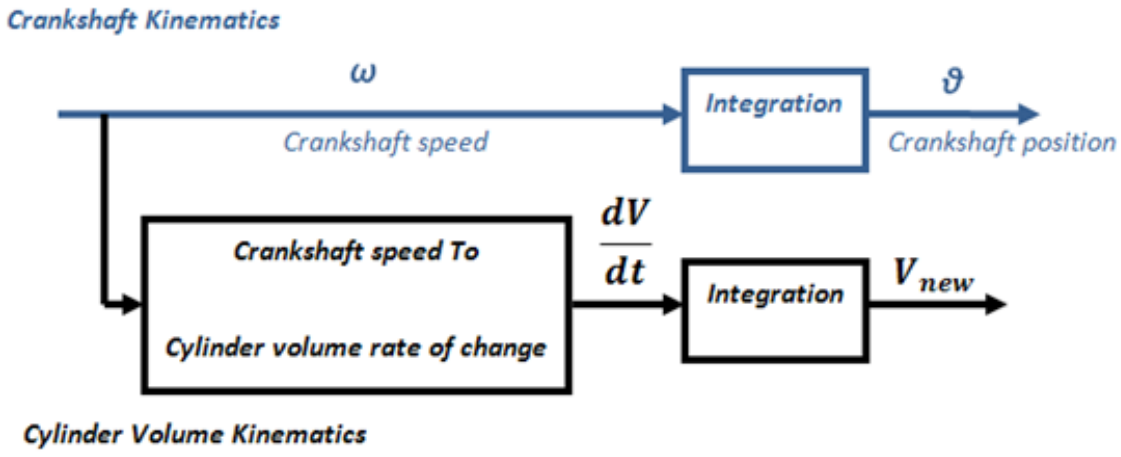

Figure 8.2: Compression ratio equivalence calculation

8.2 Specific heats

The specific heats of the working gas denote the amount of energy required to raise the temperature of its mass thus for example during compression, it is the variable defining the curvature on the P-V diagram. It is common to use a constant value when modelling as it

simplifies the calculations but as it is going to be shown can lead to totally different results depending generally on the temperature ranges inside the cylinder during the cycle.

The relations between the specific heats are given below (Figure 8.3):

$$C_p = C_v + R \quad \text{(Eq. 8.6)}$$

$$k = \frac{C_p}{C_v} = \frac{C_p}{C_p - R} \quad \text{(Eq. 8.7)}$$

C_p is the specific heat of constant pressure (kJ/kg K), C_v is the specific heat of constant volume (kJ/kg K) and R is the gas constant.

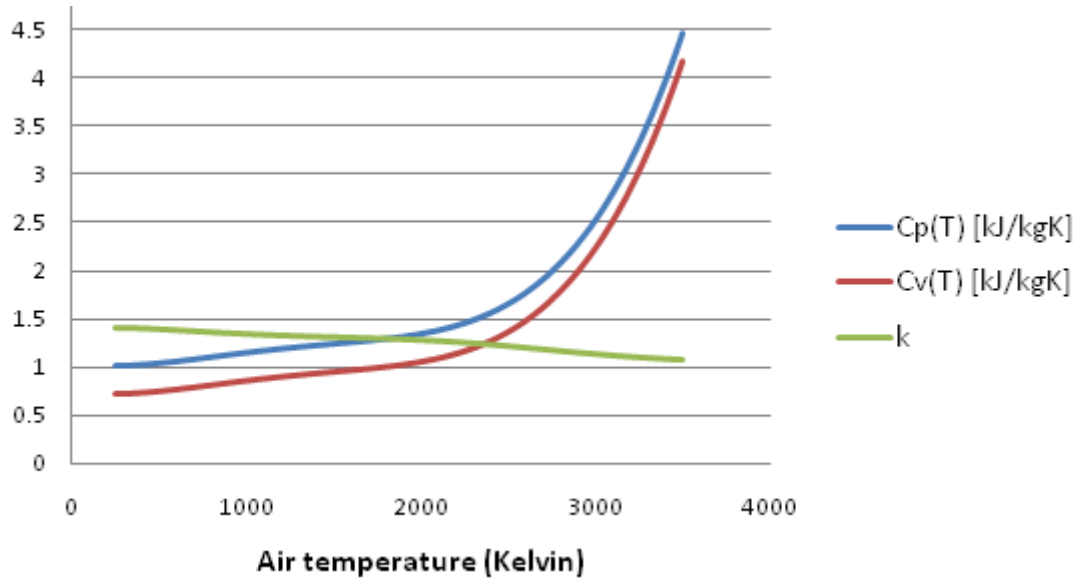

Figure 8.3: Specific heats of air

Particularly for air [86]:

$$C_p(T) = \sum_{N=0}^{4} [A(N)T^N] \quad \frac{kJ}{kg\ K} \quad \text{(Eq. 8.8)}$$

$$R_{air} = 0.28704 \quad \frac{kJ}{kg\ K} \qquad \text{(Eq. 8.9)}$$

Where:

T: Air temperature (Kelvin)

$A(0) = 0.103409E1$ $A(1) = -0.2848870E - 3$

$A(2) = 0.7816818E - 6$ $A(3) = -0.4970786E - 9$

$A(4) = 0.1077024E - 12$

The relation between the Kelvin temperature scale T_K and Centigrade T_C is:

$$T_K = T_C + 273.15 \qquad \text{(Eq. 8.10)}$$

8.3 Variable specific heats modelling

The ideal Otto cycle was simulated using constant values and the variable specific heat function for air (Eq. 8.8) in order to study the effect of variable specific heats on engine modelling.

It is noticeable that the results show a significant work output loss when using the variable specific heat function. This can be seen on the P-V diagrams (Figure 8.4). The simulations were repeated through a range of compression ratios in order to obtain the thermal efficiency effect which has shown as well to have a significant decrease (Figure 8.5). These results denote the importance to develop the model structure with the ability to use specific heats for simulations.

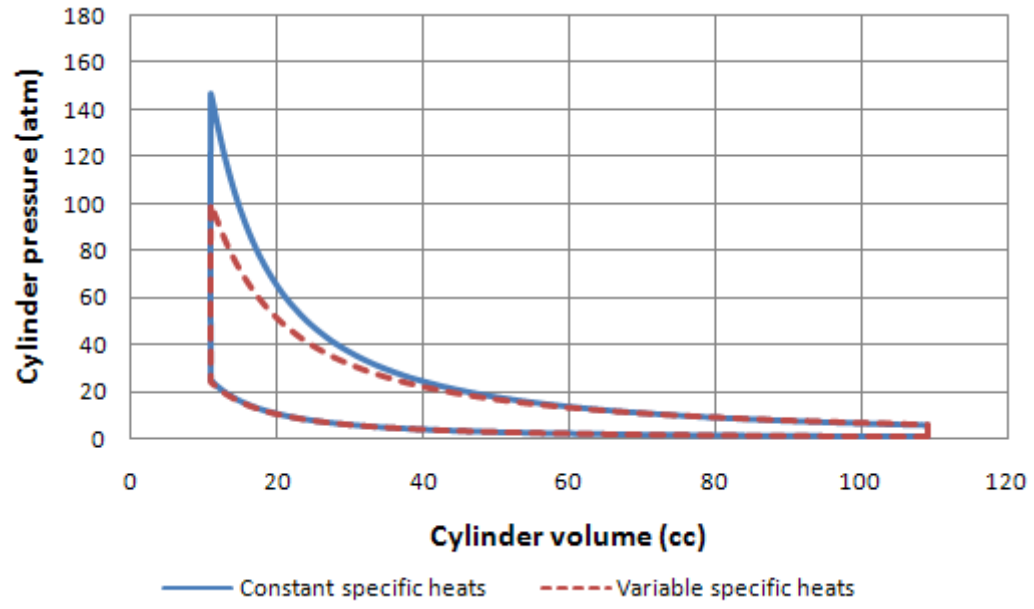

Figure 8.4: Ideal Otto cycle P-V diagram effect of variable specific heats

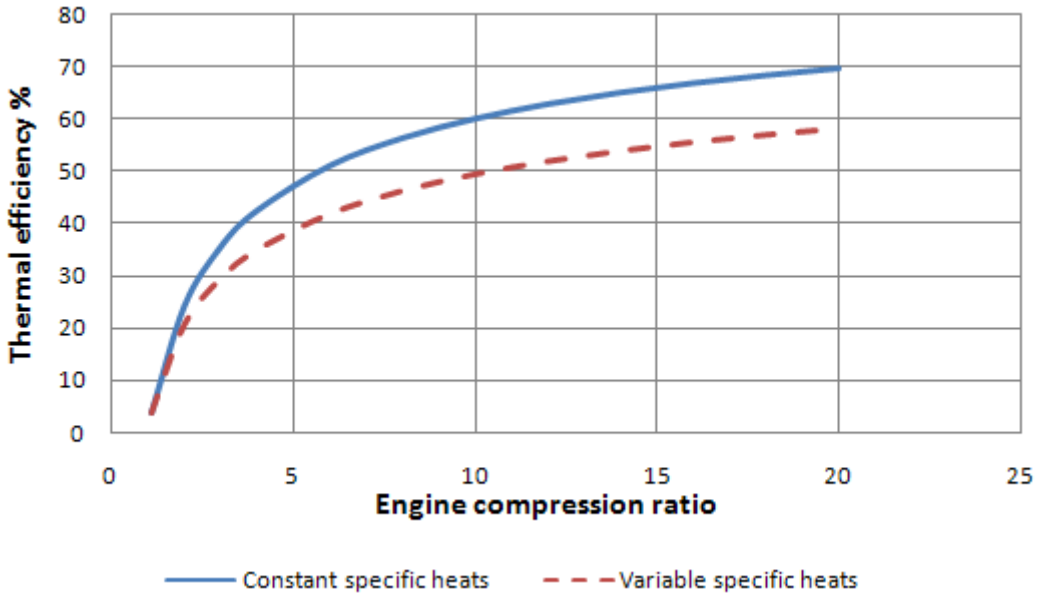

Figure 8.5: Ideal Otto cycle efficiency effect of variable specific heats

CHAPTER 9: SIES framework development

The development of the SIMULINK model structure mainly depends on the desired engine model application and on the structure of the model it has to connect to. The objective while developing the SIMULINK model was to achieve such a flexibility on its structure that it would allow the engine model to be used for any possible desired application such as a connection to a power train model, dynamometer model, and to be used as a dynamic virtual engine or as a static engine state model similar to manifold dynamic models used for control.

This flexibility can be achieved by modelling the engine crankshaft with the possibility of switching its outputs and inputs variables which would allow a greater range of model interconnection. This is due to the fact that power train models expect a torque output from the engine model, and the engine acceleration and speed is evaluated by the power train model. On the other hand, taking the case of a dynamometer model, the inputs to the engine model is just the torque of the dynamometer and its inertia; the engine acceleration and speed have to be evaluated by the engine model itself.

Another important issue to have in mind is to develop the structure without the usage of any “algebraic loop” which increases significantly the simulation time. The algebraic loop is basically the request of a parameter that has not been yet evaluated, or depends on the output of the calculation in which it is needed. This makes the solver iterate on that calculation until the error is below a threshold value slowing down the simulation speed.

9.1 Crankshaft dynamics

The crankshaft dynamics structure is the base of the cycle by cycle engine model and as it is the coupling component on a real engine (gear box, clutch or dynamometer), the modelling of the virtual coupling (connection to a gear box model, clutch model or dynamometer model) has to be developed within this structure.

The starting point of this model is the relation between torque *T*, inertia *J* and crankshaft acceleration α.

$$\frac{T}{J} = \propto \qquad \text{(Eq. 9.1)}$$

The two structures chosen which provide the flexibility to connect the engine model to any coupling type of model structure and application are the “virtual engine structure” and “engine sub-model structure” which are explained in the following.

9.1.1 Virtual engine structure

This structure has been named “virtual engine structure” due to the fact that it allows the engine model to run alone dynamically, thus meaning it evaluates its own instantaneous crankshaft acceleration, speed and position. This structure can be visualised by thinking of an engine which is not connected to any clutch, gearbox or shaft but has only the flywheel attached to the crankshaft.

This configuration implies that the coupling model evaluates its effective inertia and the torque applied on the engine, and feeds them to the engine model. The engine model uses

these variables to evaluate its brake torque output and then its crankshaft acceleration, speed and position (Figure 9.1). Even a complete vehicle system could use an engine model with this structure, but there would be a need to evaluate the complete vehicle's effect on the crankshaft as an inertia and effective torque.

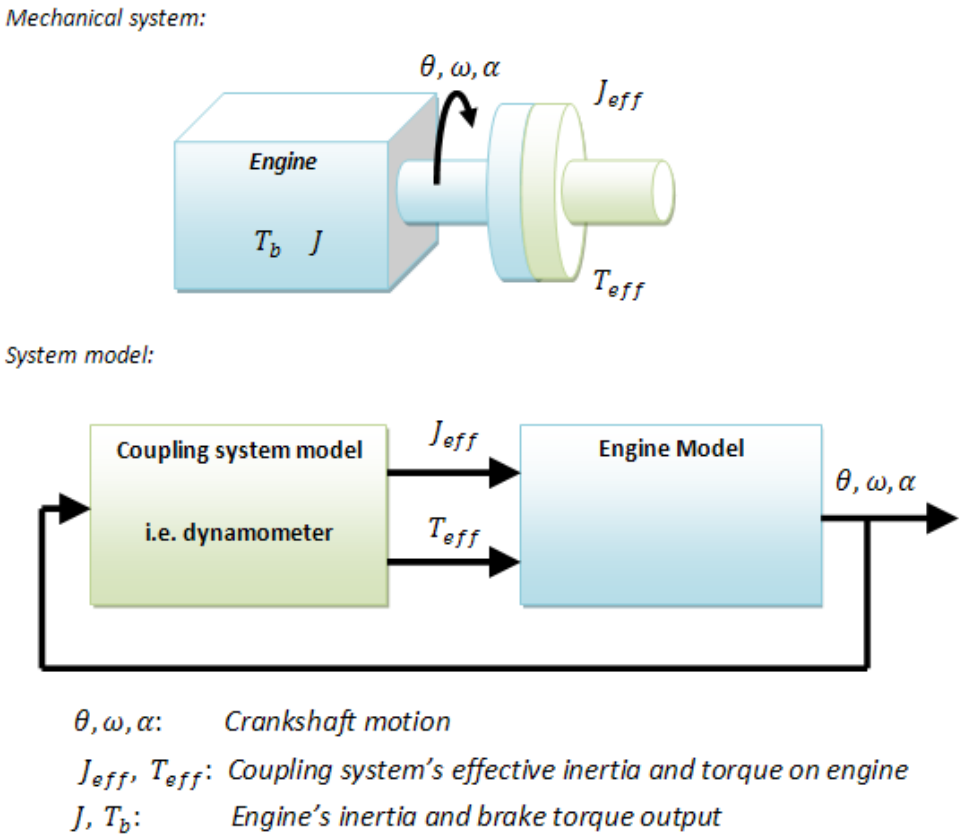

Figure 9.1: Virtual engine model structure

Another straightforward application is the connection to a clutch mechanism. The coupling effective torque on the crankshaft would be the dynamic friction or the stiction friction, respectively depending on the case that the clutch is slipping or not. The effective inertia on the other hand, would be the clutch component attached on the flywheel in case of clutch

slip, or the complete vehicle, clutch, gear box, wheels etc in the case that the clutch is locked and that there is no slip on the wheels.

9.1.2 Engine sub-model structure

Sometimes, there is the need to run the engine model at a constant speed or its speed controlled by an input. This facilitates its connection to a powertrain model, or its usage in control applications. The powertrain model will have to evaluate the engine kinematics and thus allow the engine model to evaluate its instantaneous brake torque output. Due to the fact that the dynamics calculations are not evaluated by the engine model, this structure has been named *"engine sub-model structure"* (Figure 9.2).

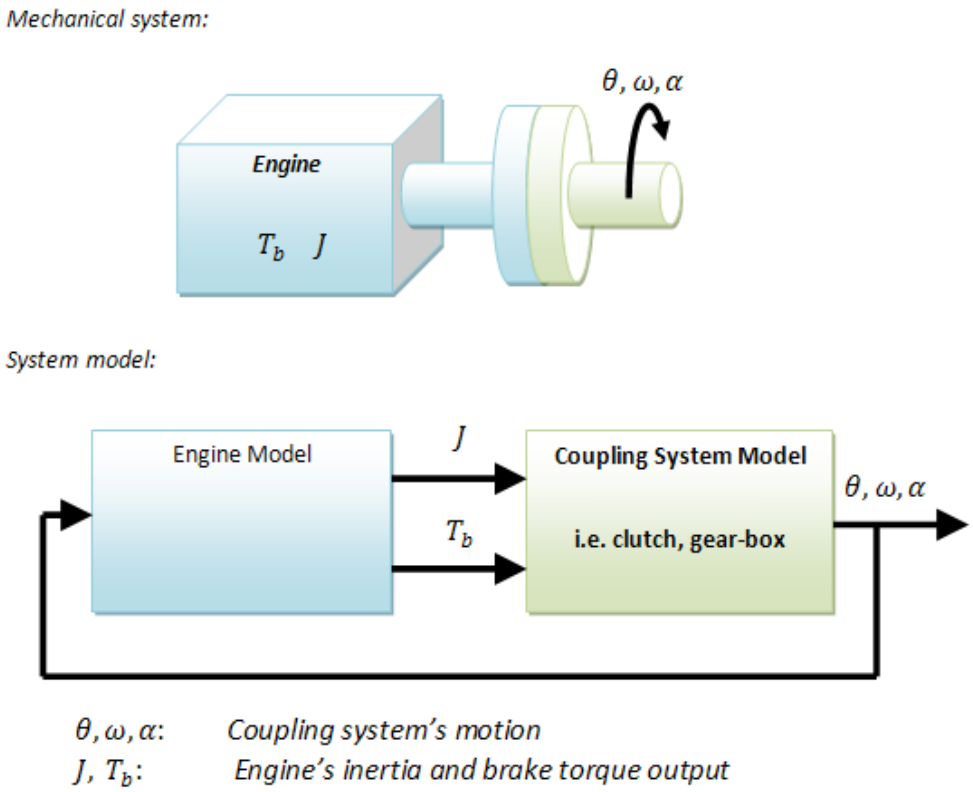

Figure 9.2: Virtual engine model structure

9.1.3 Dual model structure

The final decision was to develop the crankshaft dynamics for both structures described previously and develop a simple way to switch between the two structures parametrically during parameter input or simulation. The following picture shows the developed Engine Connection SIMULINK block diagram (Figure 9.3).

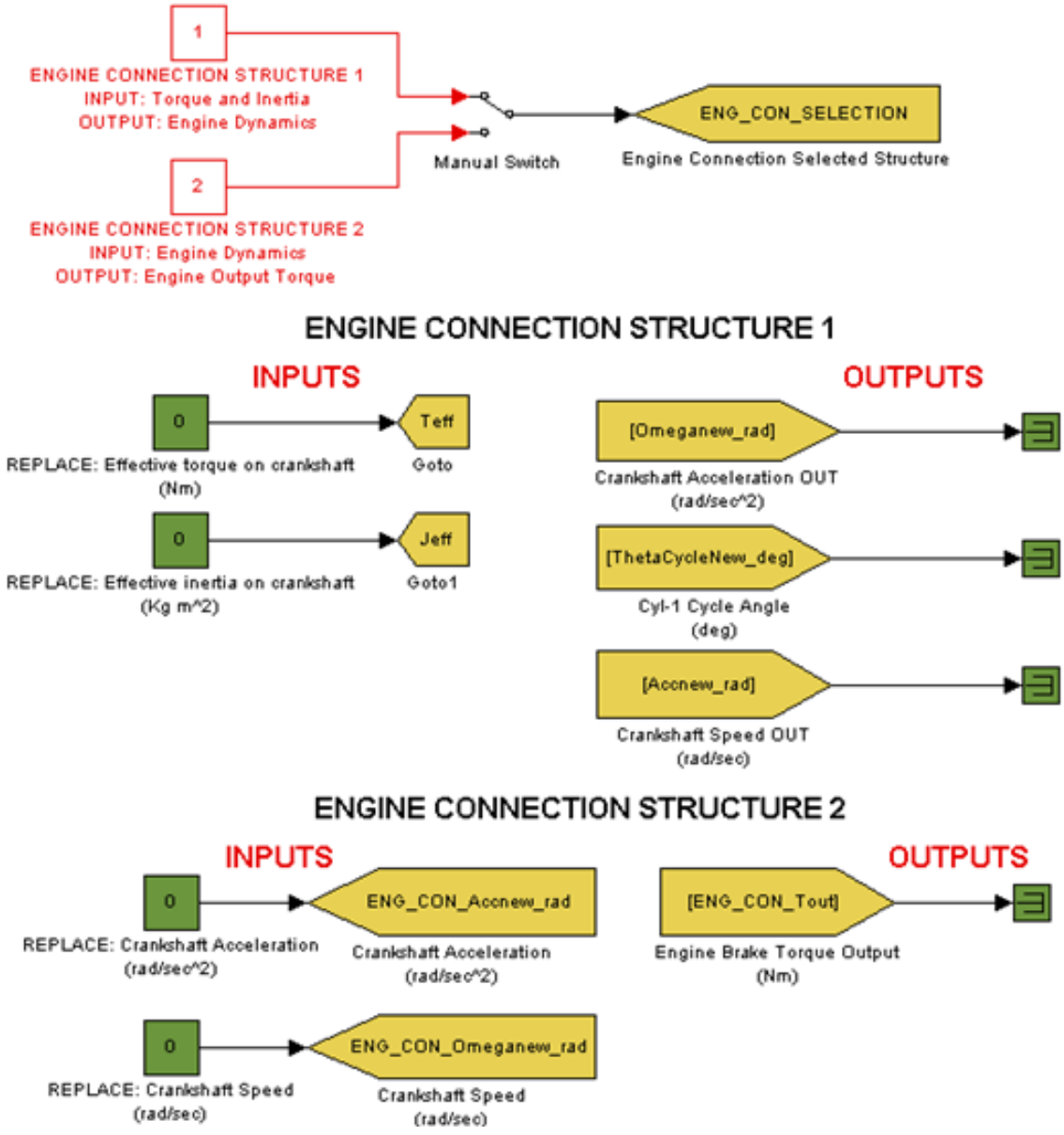

Figure 9.3: Engine Connection SIMULINK block diagram

The inputs and outputs connection notations are made with reference to the engine model. This block diagram is the place where to connect a coupling model to the engine model and where the variables between the two systems are interchanged. The higher level representation of this block can be seen in (Figure 9.4) as the *"Engine connection"* block.

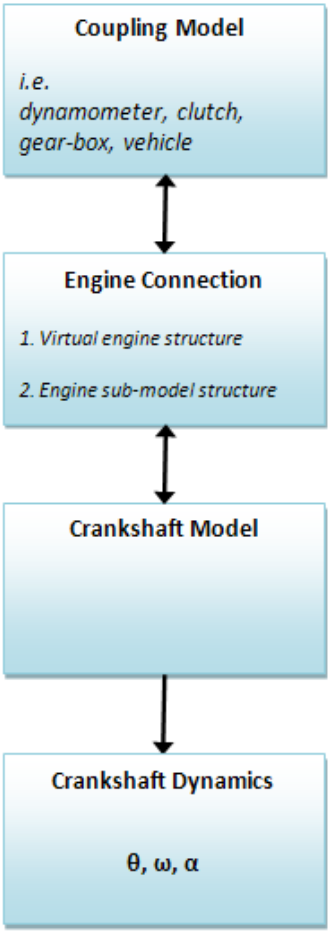

Figure 9.4: Engine model communication

Independent of the engine structure selected during simulation, the variables that are needed from the Engine Dynamics block to evaluate all engine parameters for the next time step are the crankshaft dynamics (α, ω, ϑ).

9.1.4 Dual structure engine dynamics

The engine dynamics block diagram is based on a simple dynamic system structure which consists of evaluating the acceleration from the torque and inertia. Then, the speed and position are calculated through a first and second integration as shown below (Figure 9.5).

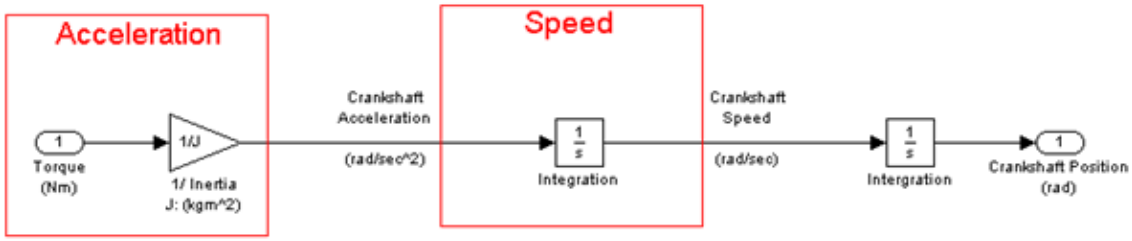

Figure 9.5: Engine dynamics base structure

The components in which the acceleration and speed are calculated on the base structure are replaced by dual option block diagrams so that the engine model can be connected to any coupling model.

The acceleration block diagram can be seen in (Figure 9.6) and the structure selection input is the connection (ENG_CON_SELECTION) which is received from the Engine Connection block diagram described previously.

The connection shown as “ENGINE BRAKE TORQUE OUTPUT” (Figure 9.6) will have to be connected to the cyclic brake torque engine output. This connection is mandatory for the “virtual engine structure” as it will evaluate along with the inertia, the cyclic acceleration and engine speed.

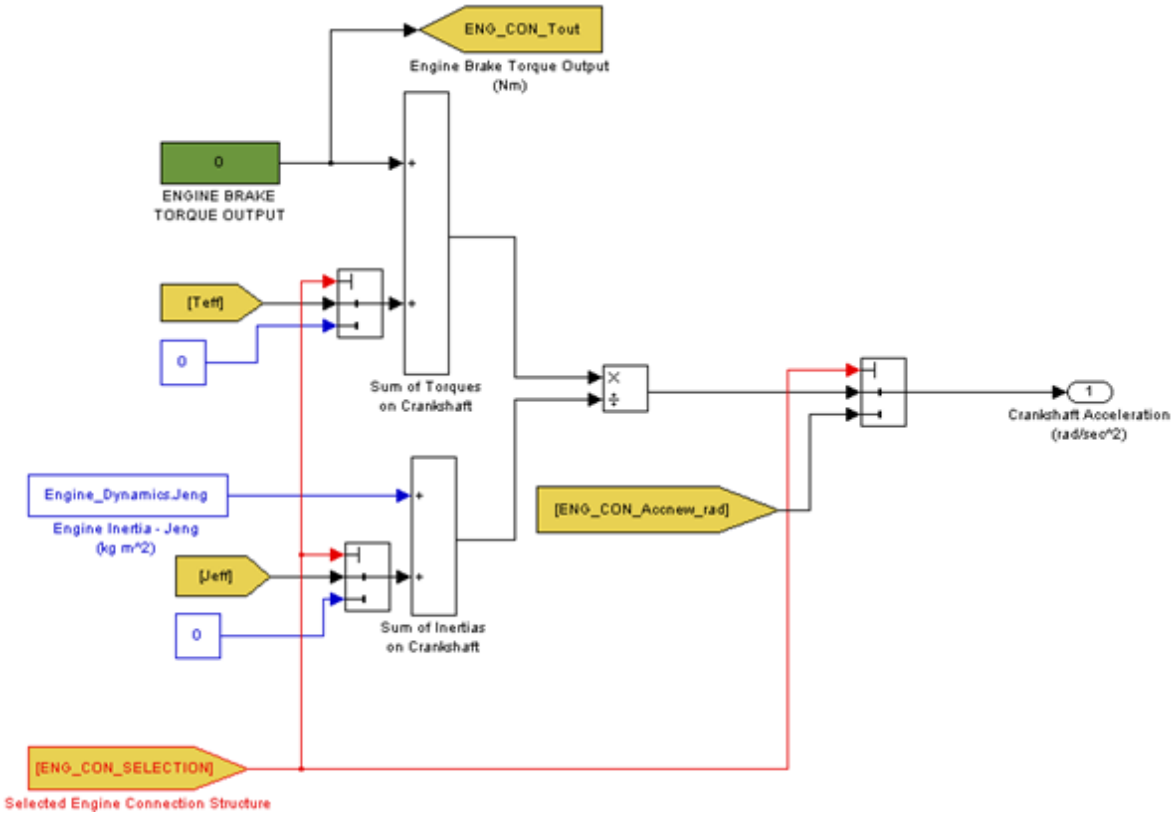

Figure 9.6: Engine dynamics (acceleration)

The speed evaluation block diagram is also replaced with a dual option structure. The selection input is the same connection as for the acceleration calculation. The engine speed is either evaluated through integration of acceleration (virtual engine structure) or the input given in the Engine Connection block diagram (ENG_CON_Omeganew_rad) is just passed through (Figure 9.7).

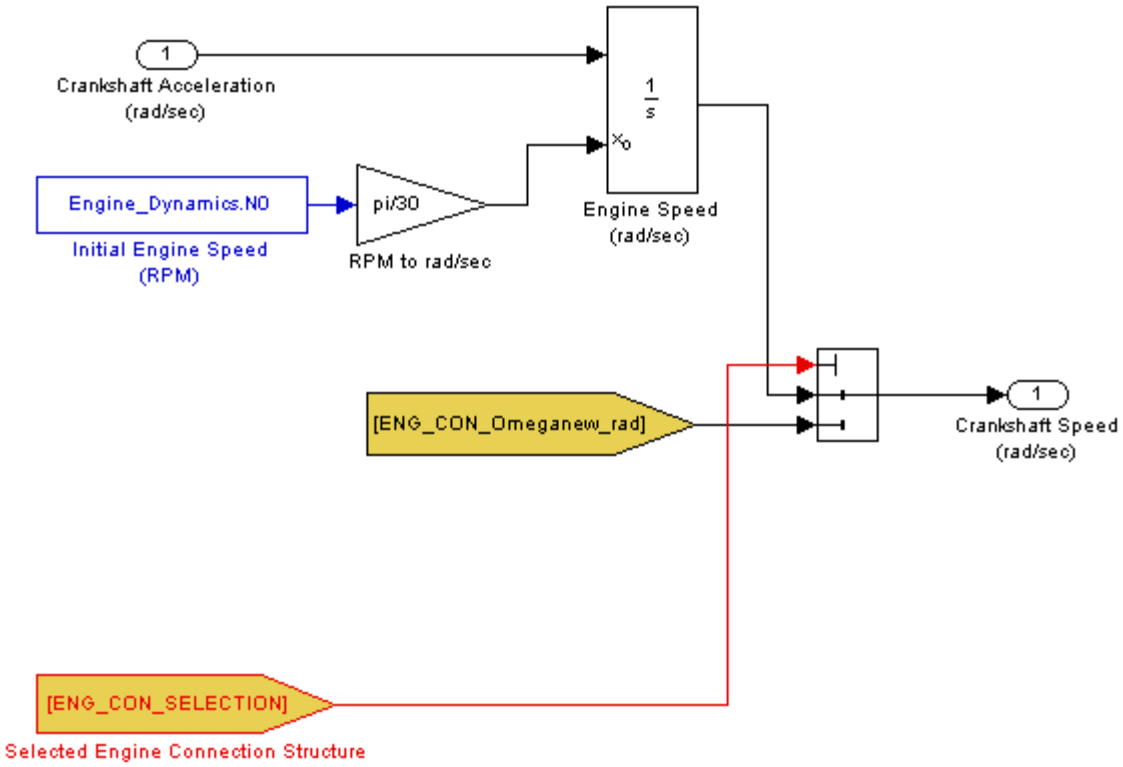

Figure 9.7: Engine dynamics (speed)

9.2 Cycle angle

The Engine Dynamics block diagram is able at this point to evaluate the crankshaft dynamics (acceleration, speed and position). A very useful conversion can be done at this point which is to convert the engine position angle to the equivalent cycle angle.

The engine position angle is a value that starts from zero and which keeps rising through until the simulation is stopped. It is the total rotation of the engine done through the simulation. This value is not a parameter that can be used directly for cycle thermodynamics or other calculations.

The cycle angle is going to be a value that tracks the actual cycle position of cylinder-1 with zero being TDC of cylinder-1 before the expansion stroke. The block diagram that converts the engine angle to the cycle angle can be seen in (Figure 9.8).

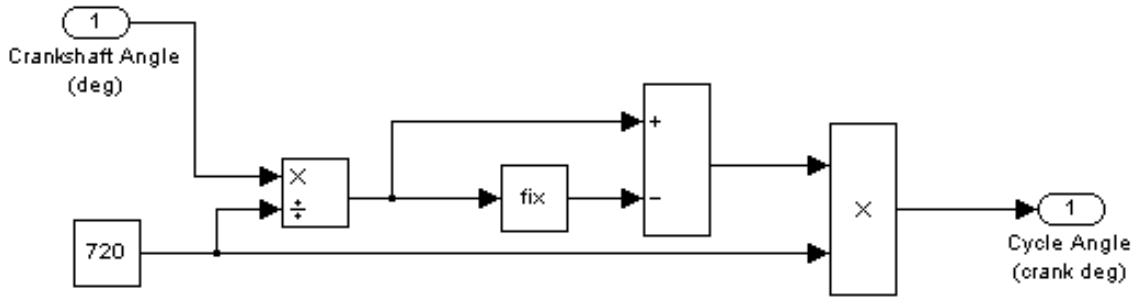

Figure 9.8: Cycle angle

The cycle angle output can be used for example to read a cyclic look-up table as it is going to be shown for the valve lift or used as a reference for every engine timings when an engine position reference is needed such as spark advance, injection timing, variable valve timing, etc.

The cycle angle function calculation result (Figure 9.9) is a sawtooth wave of half crankshaft speed frequency. A similar effect can be achieved by resetting the position integrator every time it reaches a value of 720 but that would mean losing the total engine rotation through the simulation which develops some problems when the cylinder phasings are later on calculated. Thus, this mathematical approach is preferable.

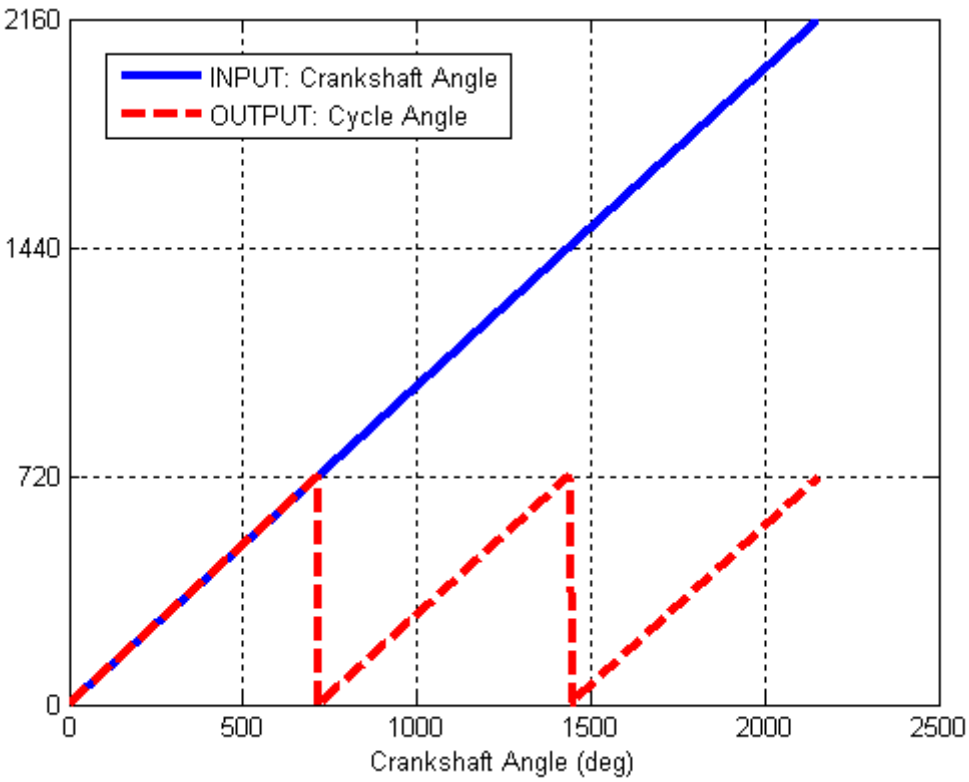

Figure 9.9: Cycle angle function

9.3 Crankshaft mechanism

As at this point the position angle in the cycle is known, the equations which evaluate the reciprocating engine variables can be applied (Figure 9.10). The cycle angle is the main input parameter in these equations, while the crankshaft speed and acceleration scale the output magnitudes of the rates of change.

The calculations done inside the “crank mechanism model” block diagram are the set of equations presented in “CHAPTER 4: Crankshaft mechanism”. The detailed block diagram is not presented as it consists of a large number of sub-blocks but have a simple input-output evaluation structure.

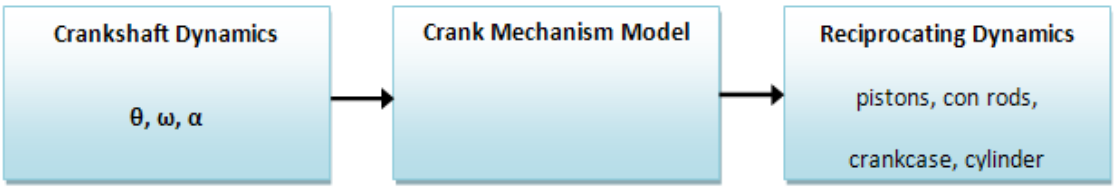

Figure 9.10: Crankshaft mechanism

On the other hand, the "crankcase kinematics" block diagram (Figure 9.11) is shown to illustrate the concept described previously in "8.1 Compression ratio equivalence". The same block is used inside the "crank mechanism kinematics" to obtain the individual cylinder compression ratio equivalences.

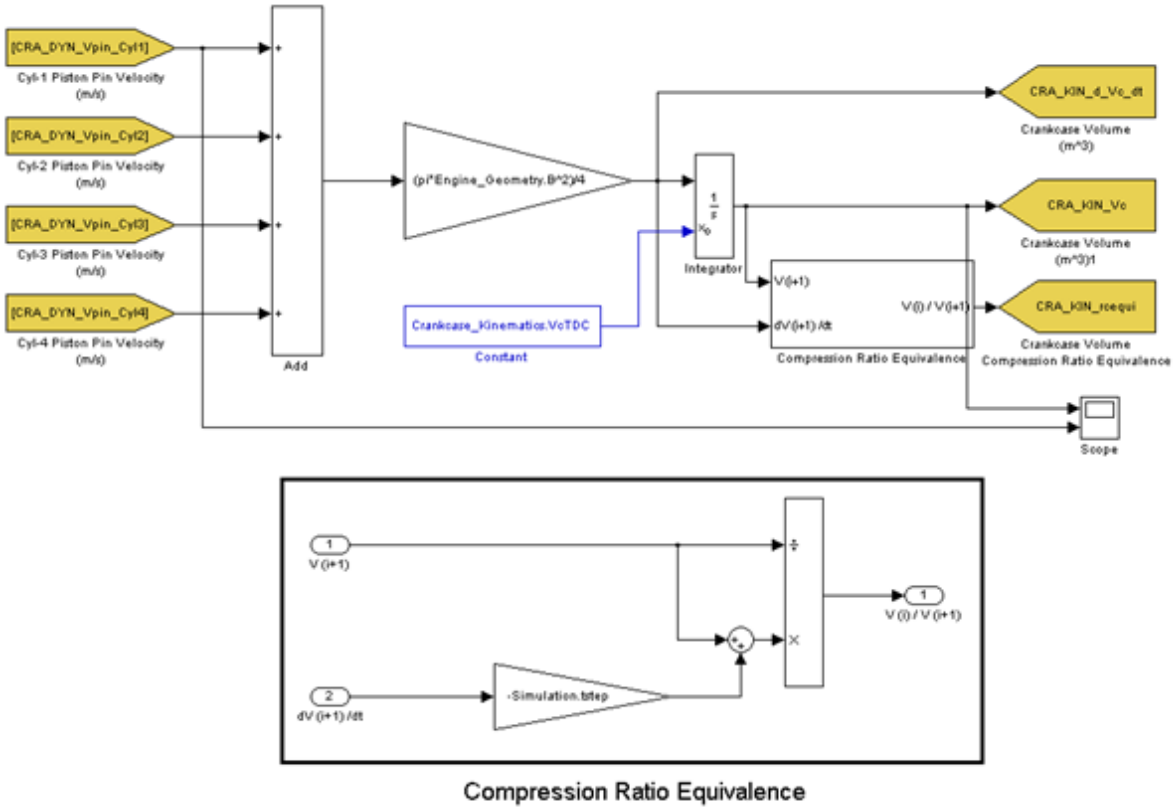

Figure 9.11: Crankcase kinematics

9.4 Variable valvetrain

In order to have an engine model which can cope with up-to date engines, it is necessary to have a valvetrain model which is capable of replicating different variable valve lift and timing strategies.

The variable valvetrain model consists of a "control" block diagram responsible for adjusting the camshaft phasings and rocker arm ratios as a function of a control input (i.e. engine speed) and a "valvetrain mechanism model" block which evaluates the valve flow area and valve kinematics as a function of crankshaft kinematics (Figure 9.12).

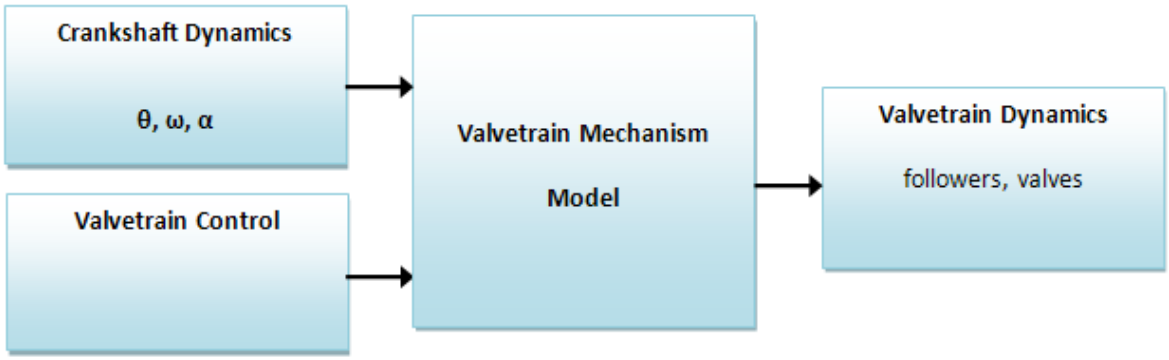

Figure 9.12: Valvetrain control and kinematics

9.4.1 Valvetrain control

The "valvetrain control" block diagram outputs the intake and exhaust camshaft phasing angle (variable timing control) as well as the intake and exhaust rocker arm ratios (variable lift control). The control data are 1-D look-up tables which by default use the engine speed as the control parameter (*Figure 9.13*). A simple structure like this was used at this point to develop the SIES framework as each engine uses different mechanical systems to adjust and

which makes it difficult to model a generic variable valvetrain system which can be applied to any engine. Thus, the look-up tables provide means to make the model generic.

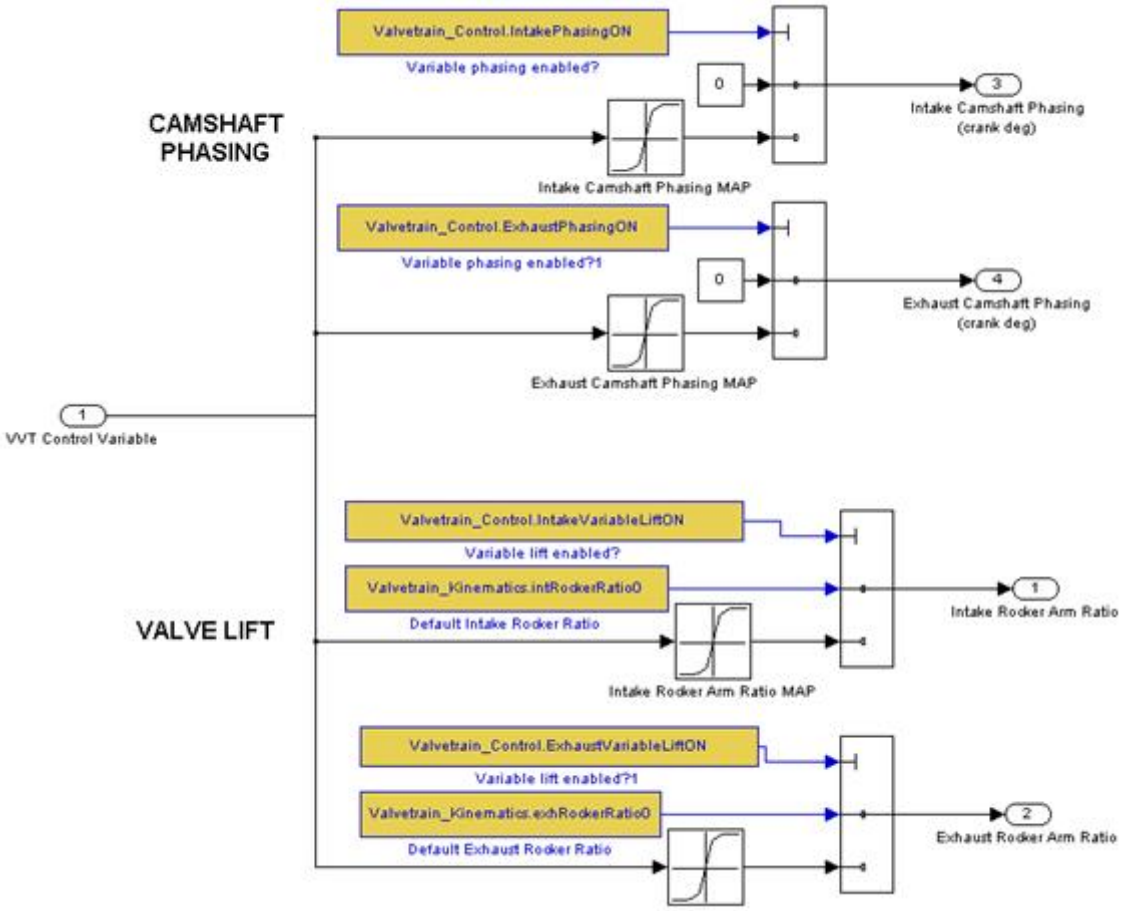

Figure 9.13: Variable valvetrain control

9.4.2 Valvetrain kinematics

The data file produced by the "Valve Timing" application (5.3 Valve timing) is loaded into 1-D look-up tables (intake and exhaust), and the relative follower lift can be retrieved for any cycle angle. Then, the relative rocker arm ratio is used to evaluate the valve lift for that moment (Figure 9.14). Finally, the valve flow area can be evaluated as it is a function of valve lift as presented in section "5.4 Valve flow area".

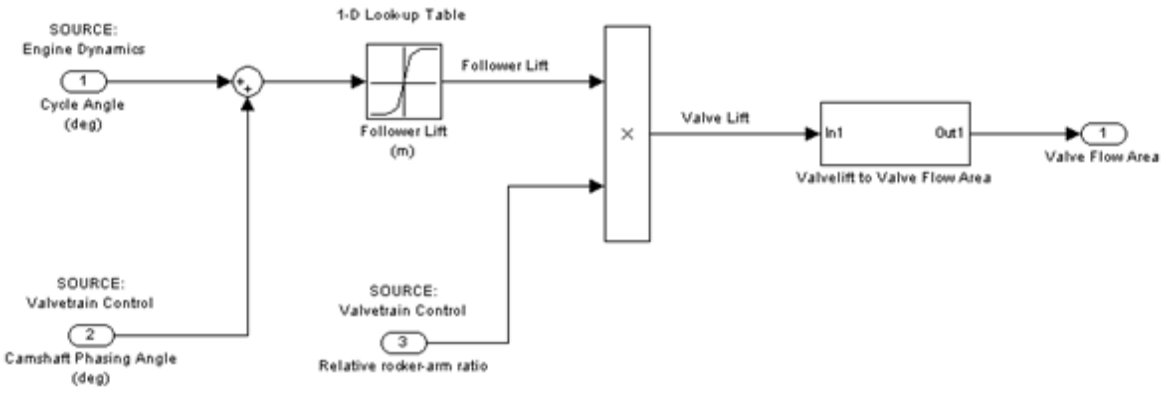

Figure 9.14: Variable valvetrain

9.5 Throttle

The throttle kinematics model is a separate system, independent of the engine dynamics meaning that there is no connection at the moment to the engine block diagrams described previously. The throttle plate receives its position in time from the “Throttle Control” block diagram and then the “Throttle body model” block evaluates the throttle effective flow area (Figure 9.15).

9.5.1 Throttle control

A set of throttle input selections have been placed inside the “Throttle Control” block diagram including a typical structure which will work for a throttle plate controller. The relative controller system has to be placed inside the “Throttle Plate Controller Dynamics” block and should evaluate the angular acceleration of the throttle plate (Figure 9.16) [87].

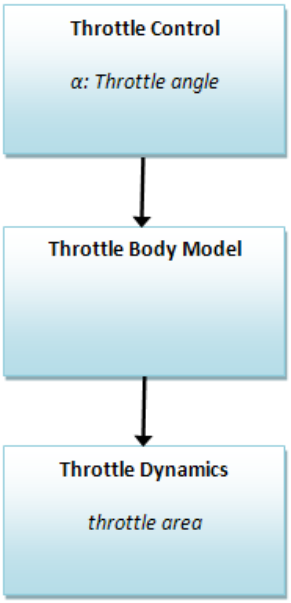

Figure 9.15: Throttle sub-model structure

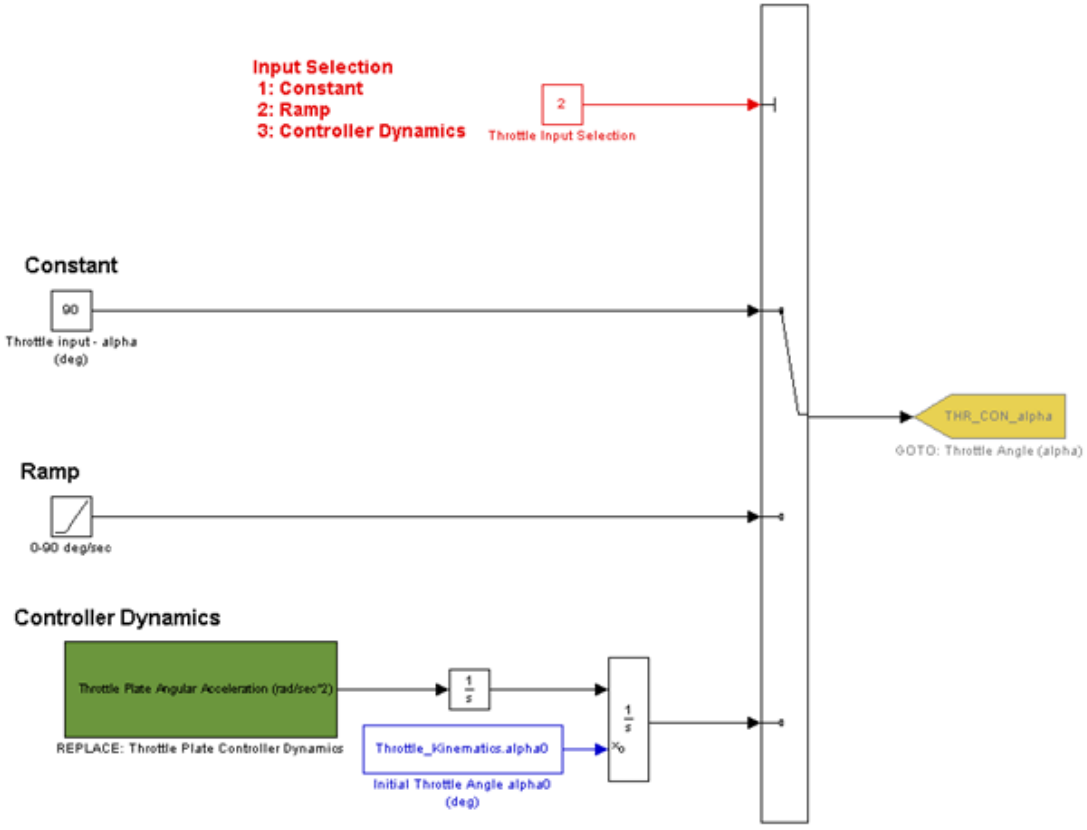

Figure 9.16: Throttle control

9.5.2 Throttle kinematics

The throttle effective flow area is evaluated for the throttle plate angle input “alpha” using the throttle effective flow area equations given in “CHAPTER 6: Throttle kinematics”. This output is passed to a “Goto” SIMULINK block which makes it retrievable from anywhere in the model. This type of connection facilitates the model structure development as every system is visualised as a separate sub-system.

9.6 SIES framework

The sub-systems presented on the previous sections have been connected together in a SIMULINK model to form the SIES Framework. The framework’s complete structure can be seen in Figure 9.17. It is a complete engine kinematics model which provides a robust base for cycle-by-cycle engine modelling. Due to the fact that the complexity of a cycle-by-cycle engine model arises mainly from its reciprocating motion and model structure, it is quite easy for example to develop a combustion pressure model using the already completed framework. The SIES Framework’s internal connections between sub-blocks are done using “Goto” and “From” SIMULINK model blocks to allow each module to be separate from the system. Thus, a module can be easily replaced, upgraded or used in another model. The SIES Framework modules (sub-models) are visible upon opening the model (Figure 9.18). There are two extra modules which have not been explained till now. Inside the “Shared Function Blocks” are placed developed function blocks and sub-systems such as unit conversion functions and engine specific calculations. This was done to increase the productivity and reduce the time of future further developments.

Due to the complexity of the system, it is preferable to have all the results accessible in one location which is the “Results” module.

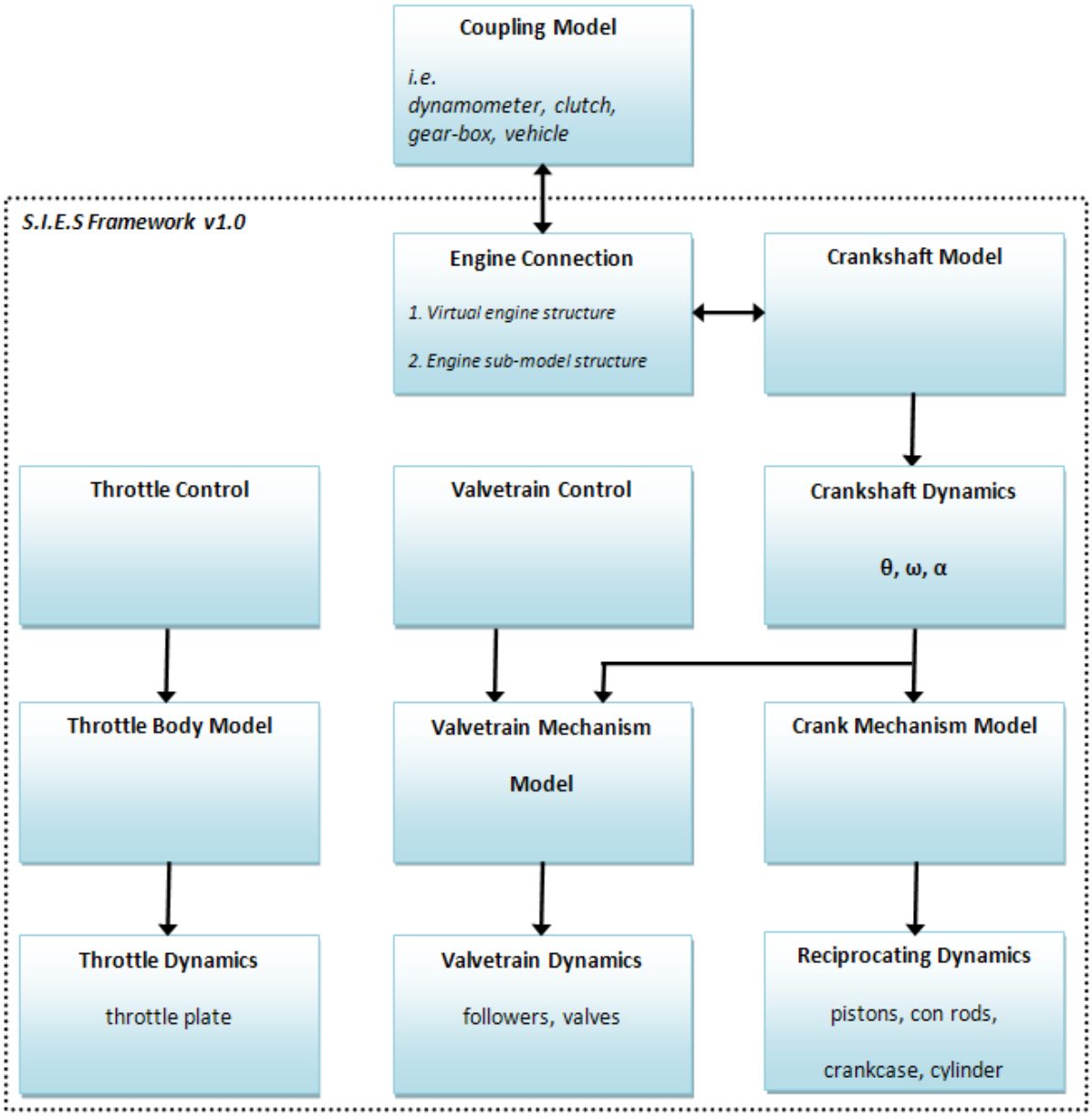

Figure 9.17: SIES framework structure

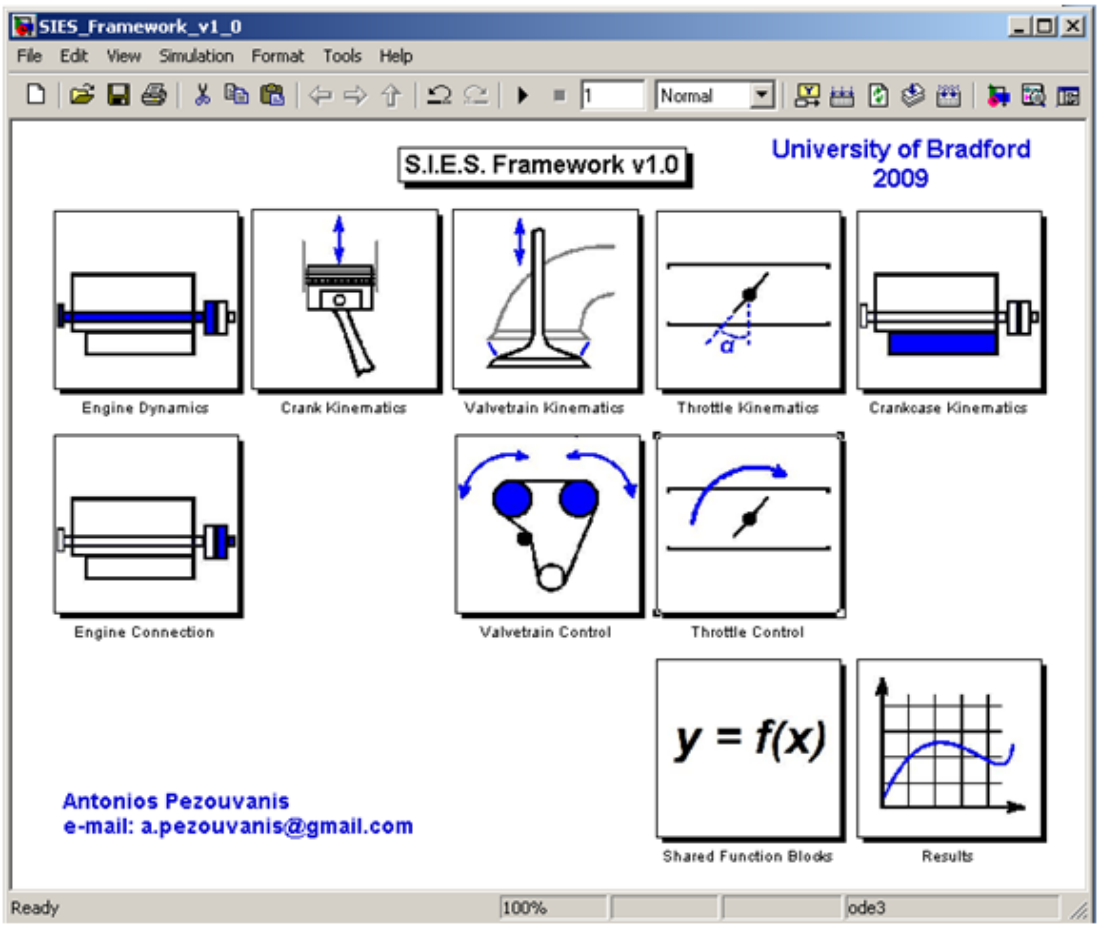

Figure 9.18: SIES framework (SIMULINK)

9.6.1 Results

The results of a constant speed simulation of a four cylinder engine can be seen in the following figures. The input parameters used are listed in Appendix A. The first figure (Figure 9.19) shows the results of the piston kinematics given by equations (Eq. 4.8 - 4.13). Figure 9.20 is the crankcase volume as described in "4.9 Crankcase volume" and given by Eq. 4.35.

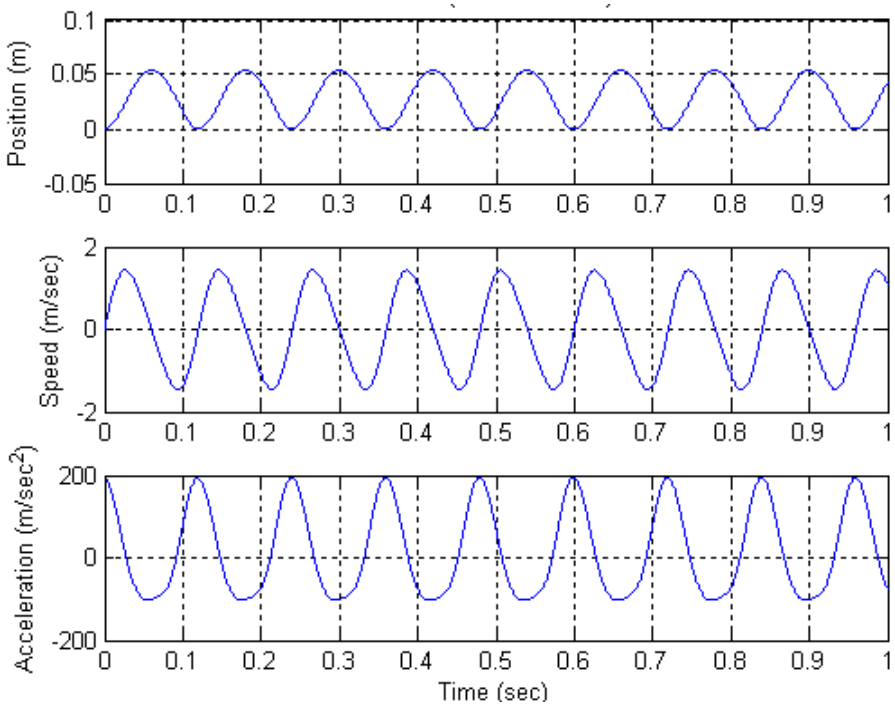

Figure 9.19: Piston kinematics (constant speed)

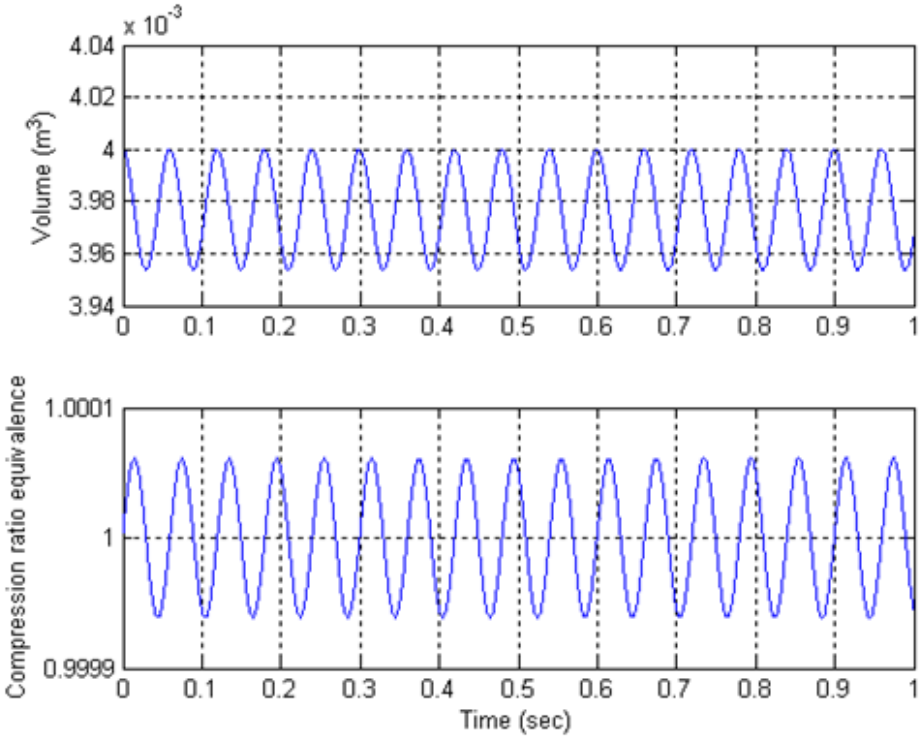

Figure 9.20: Crankcase volume (constant speed)

The following figure (Figure 9.21) displays the results of the first cylinder's kinematics. These are the results required to perform thermodynamic cyclic calculations. The cylinder area for example is required by heat transfer models.

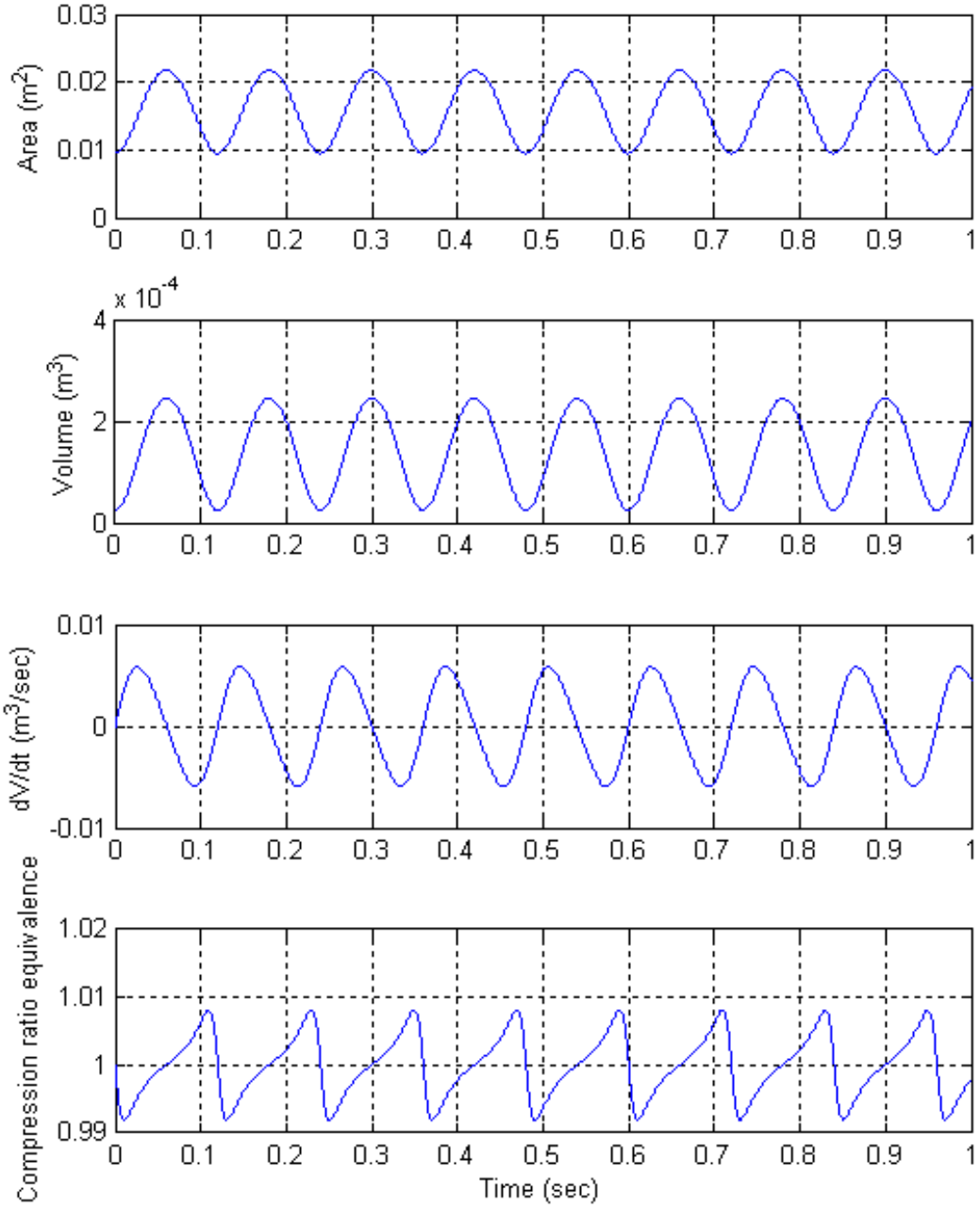

Figure 9.21: Cylinder - 1 kinematic results (constant speed)

The intake valve effective flow area has been evaluated for all four cylinders from which the total intake flow area is evaluated by adding the individual cylinders effective valve flow areas. This results in a waveform which describes the intake valve system geometry.

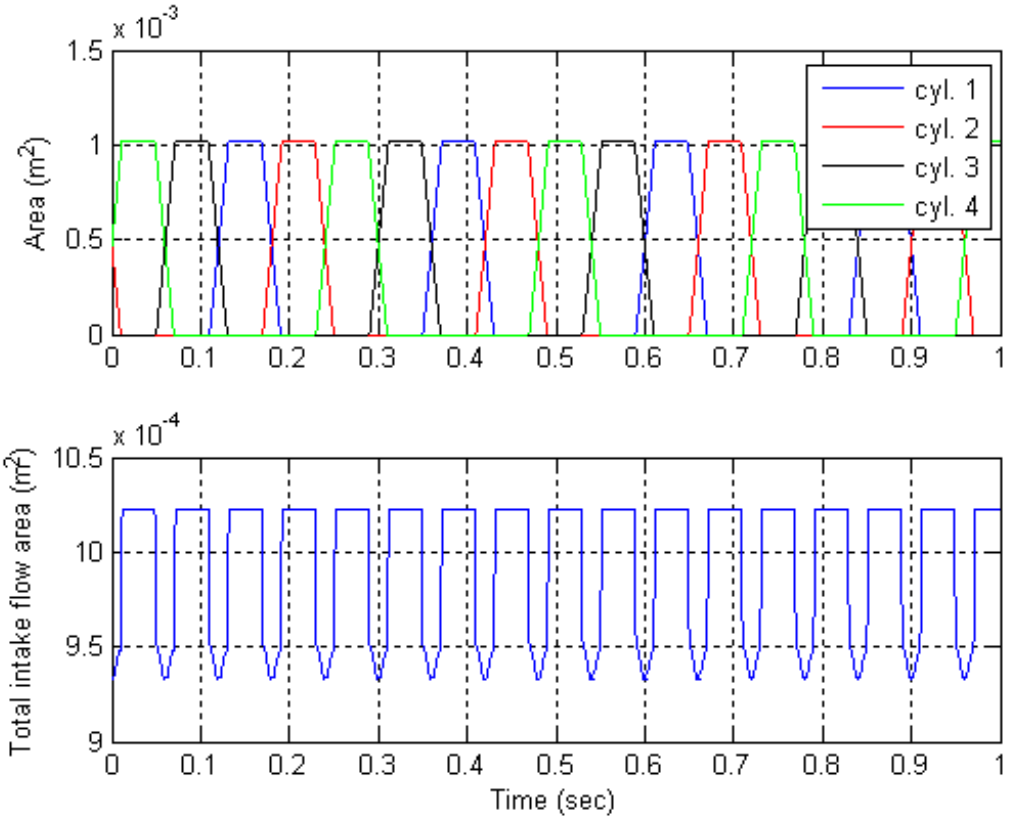

Figure 9.22: Intake results (constant speed)

A linear ramp angle input has been given to the throttle model so that its area function could be evaluated during the simulation (Figure 9.23) as it is not affected by the engine conditions (i.e. constant speed).

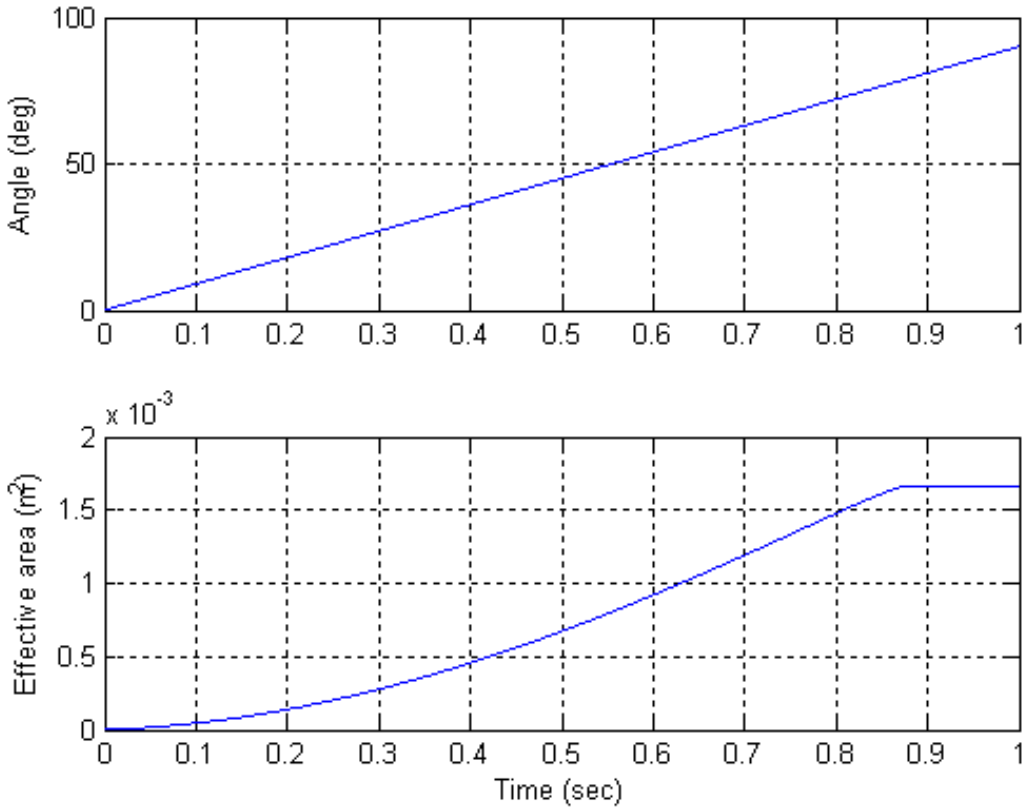

Figure 9.23: Throttle effective area results

A second simulation was done to show the dynamic capabilities of the developed engine model. This time, a constant engine torque output has been set to 100Nm which accelerates the engine at a constant rate. It can bee seen now that the results of the first cylinder's kinematics are waveforms having their frequency increase over the simulation time as the engine accelerates and those affected by engine speed (*dV/dt* and compression ratio equivalence in Figure 9.24) have also their peak to peak increased.

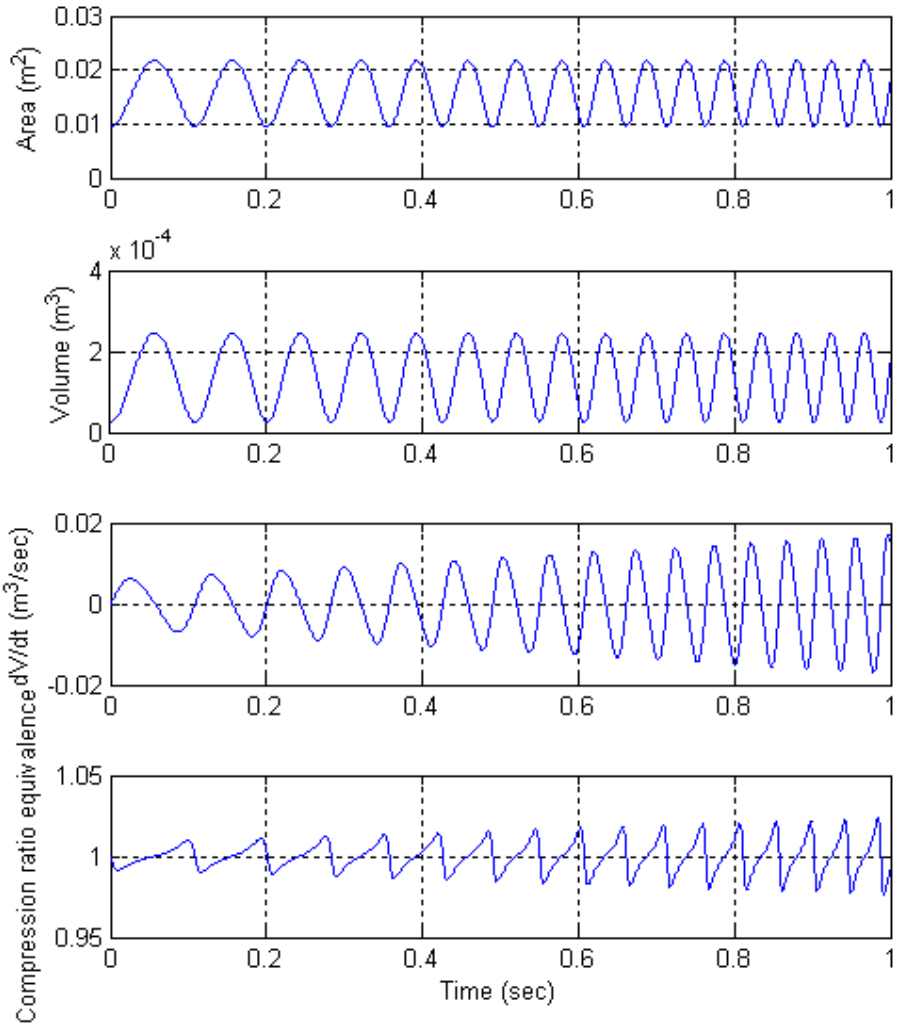

Figure 9.24: Cylinder - 1 kinematic results (during acceleration)

CHAPTER 10: EngMap framework development

An Engine Mapping framework (EngMap framework) has been developed alongside with the SIES framework to facilitate cycle-by-cycle custom engine mapping procedure development. The current EngMap framework version incorporates the models required for cycle-by-cycle engine flow mapping. It evaluates the throttle flow area, valve flow areas and piston kinematics.

The National Instruments LabVIEW software has been chosen to be the development platform as it provides an easy and fast way to read signals and develop “virtual instruments” as they are called. The sensory signals are sampled by a National Instruments hardware which selection depends on the signal type. Then, these signals can be made available as variable values in the LabVIEW software and used in calculations (Figure 10.1).

The LabVIEW applications that can be developed are limitless. They can be as simple as a voltage reading and plotting in real-time on the LabVIEW interface, custom data-logging or even complete engine mapping procedure (real-time depending on the hardware used).

A large range of hardware is available which are developed for the measurement of analogue and digital voltages, thermocouples, current, strain gauges, etc. On the other hand, output hardware is also available such as switches, analogue and digital voltage generators, which give the ability to control any desired actuator. The control algorithm can be developed in the LabVIEW software with its inputs provided by measurement hardware while the actuation done by output hardware.

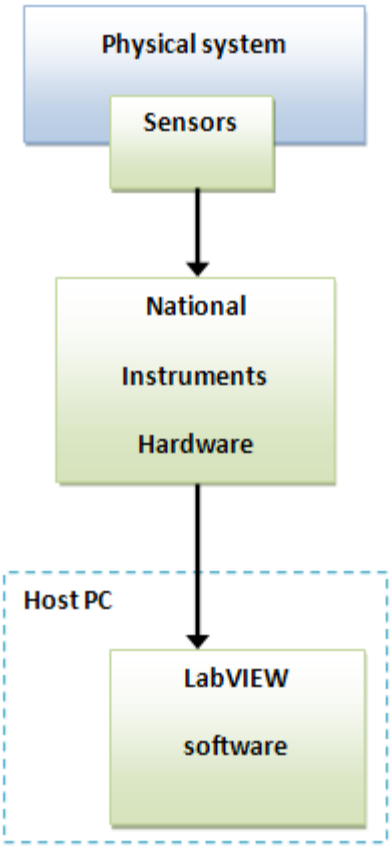

Figure 10.1: LabVIEW connection

The engine mapping hardware and sensors vary depending on the engine under consideration and test demands thus requiring a different EngMap framework structure. For this reason, the EngMap framework has been developed to be modular and different configurations are available to choose from.

In order to evaluate the models required for cycle-by-cycle engine flow mapping, the throttle position and crankshaft dynamics have to be acquired from the engine so that the models can be evaluated within LabVIEW.

10.1 TPS signal

The Throttle Position Sensor (TPS) signal is usually an analogue voltage between 0 and 5 Volts which varies linearly with the throttle angle. Thus in order to obtain the engine's throttle angle within the software, this voltage has to be measured, calibrated and converted to throttle angle. The TPS sensor is usually given in a percentage value which represents the position within the throttle range. Thus a value of 0% for closed and 100% for WOT.

10.1.1 Throttle calibration

The throttle calibration is required due to the fact that the signal voltages at closed V_{TPS}^{0} and WOT throttle V_{TPS}^{WOT} are never 0 and 5V respectively. The first framework module was then to allow a quick and easy calibration of the TPS sensor by inputting the recorded TPS voltages for closed and WOT so that the TPS % could be evaluated from a TPS voltage V_{TPS}.

$$TPS = \frac{V_{TPS} - V_{TPS}^{0}}{V_{TPS}^{WOT} - V_{TPS}^{0}} 100 \qquad \text{(Eq. 10.1)}$$

The LabVIEW block diagram (Figure 10.2) has been developed base on (Eq. 10.1) but has in addition an option to round the percentage output of the throttle position to the nearest integer so that the fluctuations are filtered which can be caused by signal noises.

10.2 Throttle area

The throttle angle position a has to be evaluated using the TPS % value described in the previous section. Then, a throttle area model can be used to calculate the throttle effective flow area. The only additional parameter required is the closed throttle angle θ_{thC}.

$$a = \frac{TPS}{100}\left(\frac{\pi}{2} - \theta_{thC}\right) + \theta_{thC} \qquad \text{(Eq. 10.2)}$$

The throttle area evaluation within LabVIEW has a different structure than the one used in the SIES framework. It has been developed to run faster by "initialising" the throttle body model in which all throttle model constant terms are evaluated before the application execution (Figure 10.3). That is the reason why the block named "Evaluate throttle model constants" is placed outside the execution loop which makes it run only once at the beginning of the execution.

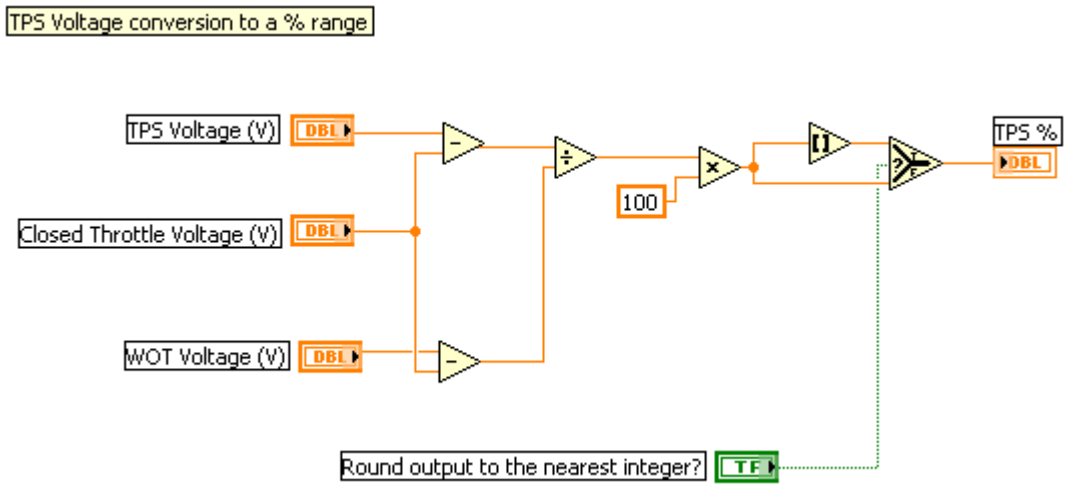

Figure 10.2: TPS calibration LabVIEW block diagram

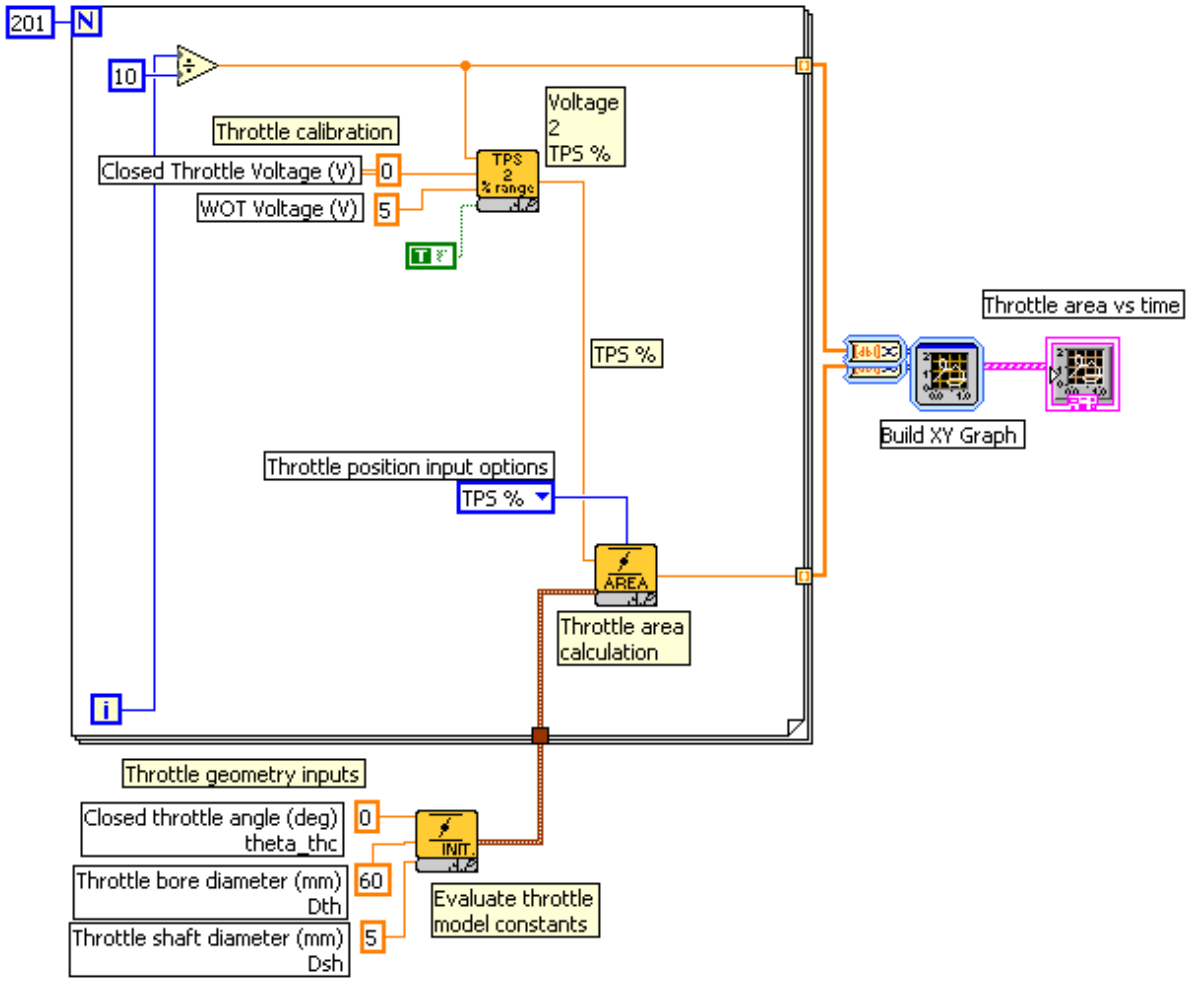

Figure 10.3: Throttle area block diagram (LabVIEW)

10.3 Reciprocating kinematics

The reciprocating kinematics of the piston pin motion have to be evaluated as they are the functions from which variables such as piston speed, acceleration and cylinder volume are calculated.

The LabVIEW block diagram is not presented for this section as it consists of simple input and output functions which relate the crankshaft position, speed and acceleration to the

piston pin kinematics. The interface of the LabVIEW block diagram can be seen in (Figure 10.4).

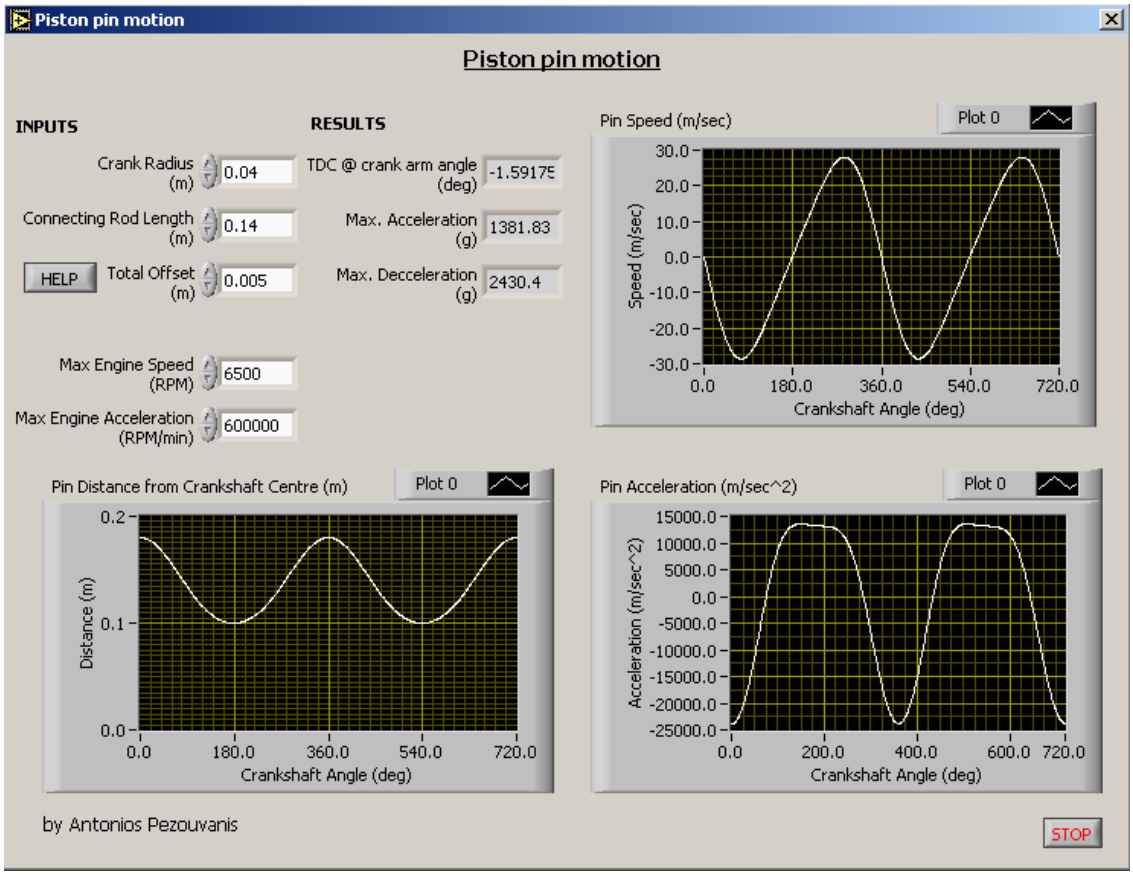

Figure 10.4: Piston pin motion (LabVIEW)

10.4 Valve flow area

The valve flow areas have to be calculated as well in LabVIEW for the engine mapping procedure. The valve flow areas can be evaluated through look-up tables in case that the engine does not have a VVT system. On the other hand, if a VVT system is present, then the complete valvetrain mechanism has to be modelled similarly to what has been done in the SIES framework. This case is going to be noted as the “crankshaft signal” model.

Another option is to measure the intake and exhaust valve lifts on the engine in real-time with the use of sensors. The model structure of this case has been named “valve lift signal” model which is also to be presented.

10.4.1 Crankshaft signal

The crankshaft signal model is using the crankshaft position cycle angle to evaluate all engine valve positions. This requires the evaluation of the intake and exhaust follower lift data as a function of crankshaft position (5.2.2 Contact solver). The camshaft phasing can then be applied by reading an offset flat follower lift value from the table. Then, the valve lift L is computed by multiplying the actual follower lift by the rocker arm ratio which is 1 for direct acting valvetrains (Figure 10.5 and Figure 10.6).

Once the valve lift at this point has been evaluated, the valve flow area can be calculated using one of the models presented in “5.4 Valve flow area”.

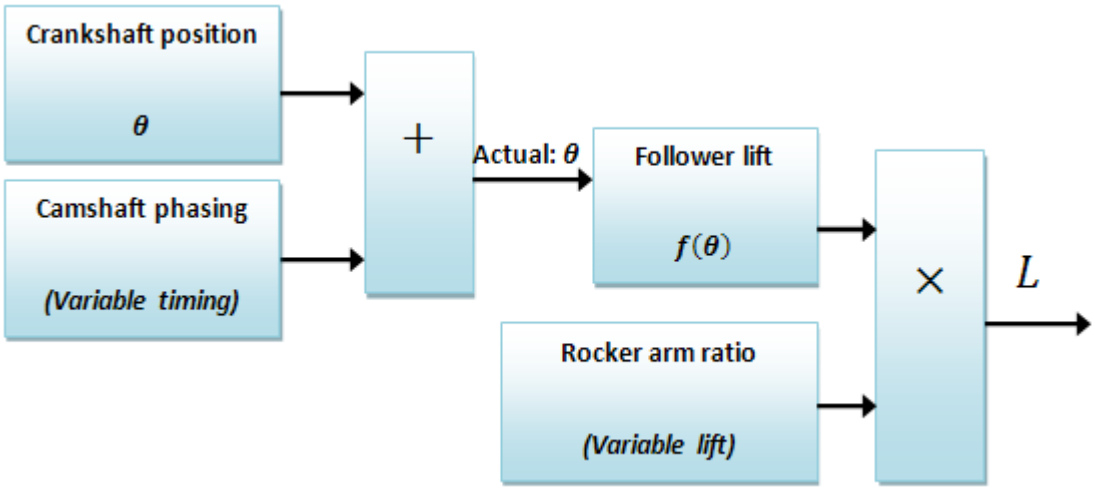

Figure 10.5: Crankshaft based VVT valve lift model

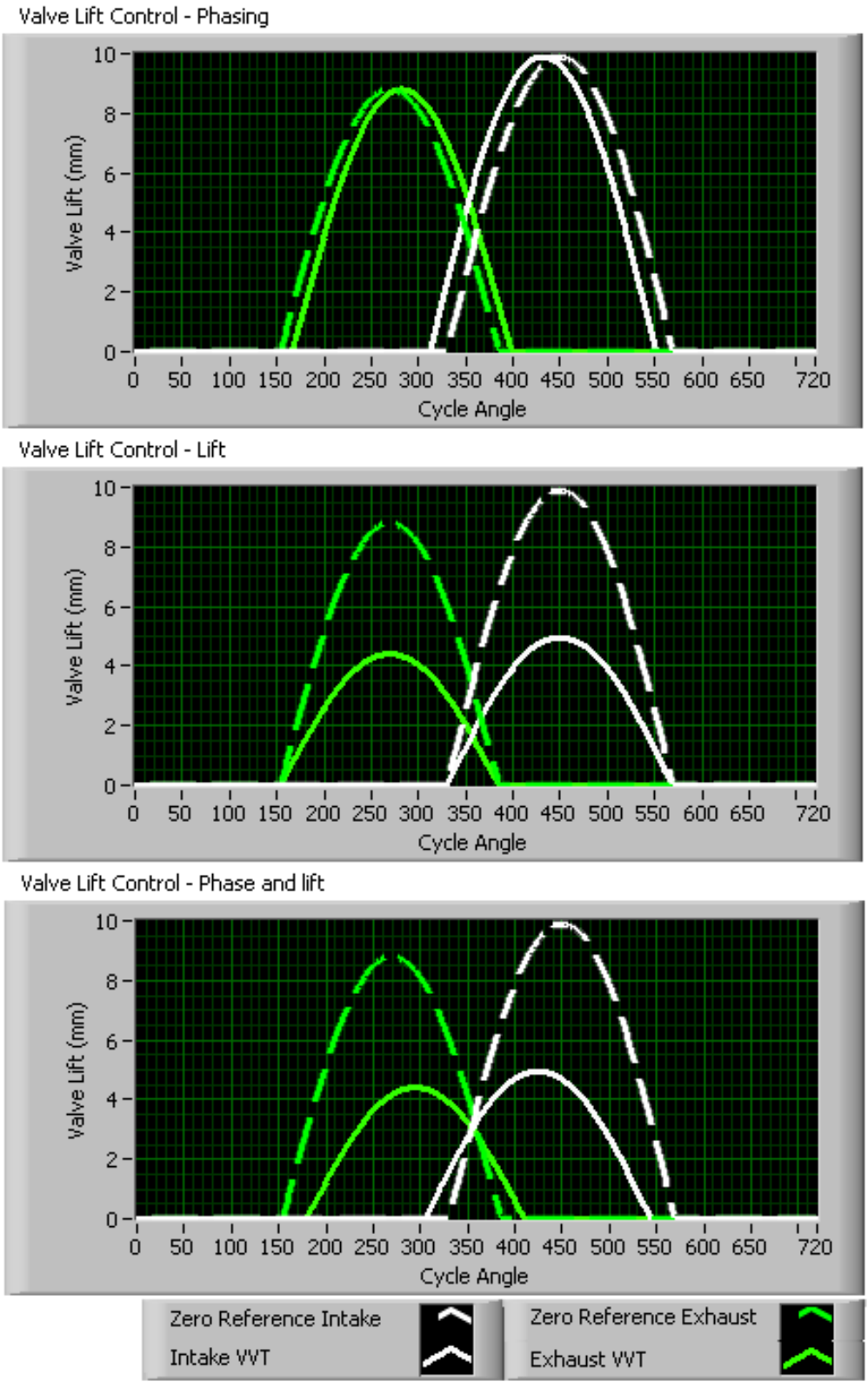

Figure 10.6: Variable valve phasing and lift

10.4.2 Valve lift signal

This structure is preferable if a valve lift sensor is available for direct measurement. This reduces the complexity and decrease significantly the valvetrain model calibration time. The valve lift sensor signal (i.e. voltage) is sampled by a "National Instruments" hardware and passed in the LabVIEW software where it is converted to a length unit (i.e. m). The valve lift sensor actually replaces the VVT valvetrain model (Figure 10.5) but still requires the valve flow area model (Figure 10.7). There is no need to install a sensor on every single valve as it can usually be assumed that all valves follow exactly the same motion during one cycle. Two sensors will then be sufficient, one installed on an intake and one on an exhaust valve. The remaining valve signals can be simulated by a phase shifting of the measured signal.

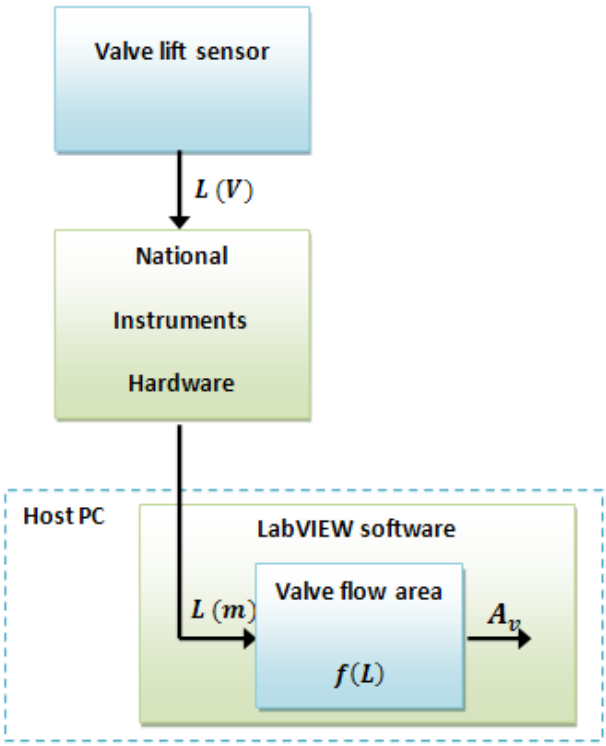

Figure 10.7: Valve lift signal based valve flow area

CHAPTER 11: Conclusions and future work

The main contributions of this thesis can be summarised below as:

- Literature review on engine modelling with emphasis on mean-value Vs cyclic models.
- Notation of the need to have unit-less parameterisation of models in engine mapping applications.
- High fidelity crank mechanism kinematic model taking into account the effect of piston pin offset and crankshaft acceleration while additional effects due to this mechanism movement are presented (i.e. crankcase volume).
- Valvetrain kinematic model with the ability to represent a fully variable valve lift and timing system.
- Modelling of the throttle body effective area as the ones found in the literature had errors. In addition, the evaluation of the throttle area rate of change has been done.
- Looking into modelling the complete engine and emphasising the need of to use variable specific heats on thermodynamic simulations.
- A rigid engine inertia model is presented.
- Development of the SIES framework capable of dynamic cycle-by-cycle simulations.
- Development of the EngMap framework in LabVIEW so that the mathematical models can be used alongside with real NI hardware for engine mapping.
- Proposition for a novel approach into flow model developments using the equations presented in this thesis.

The literature review clarified the main problem currently present in the engine modelling field which is the large amount of engine testing required to calibrate a mean-value model with engine data. It was as well noted that this data cannot be used on any other engine which creates the need of this process to be repeated on every single engine. It is believed that a cycle-by-cycle modelling and mapping approach will give insight to the engine processes and allow the development of engine flow models which will reduce the mapping time required or even make the mapping data reusable to an acceptable degree of accuracy on another engine. This could be achieved by using "key" engine variables in the mapping and simulation algorithms. Thus, the engine mapping data will not be specific to that particular engine, but to the particular processes. They could be applied to other engines due to the fact that they have other specific geometry data such as valve flow areas and cylinder dynamics. The mathematical models and structures required to obtain significant engine dependant data was presented in this work. They have been implemented in SIMULINK to form the base structure of a dynamic cycle-by-cycle model (SIES framework) and in LabVIEW for custom engine mapping application developments (EngMap framework). The cylinder volume and rate of volume change are "images" of a particular's engine crankshaft mechanism geometry. Their correct evaluation is mandatory and it was shown that the piston pin offset should not be neglected if present on the modelled engine. In addition, the crankshaft mechanism's components accelerations should be evaluated as well using the equations presented which take into account the piston pin offset as it may lead to inaccurate inertial forces.

The accurate evaluation of the effective areas on the flow path were shown which can be used on an engine simulation model or mapping application. The intake and exhaust engine flows were not modelled due to the unavailability of such models. The current modelling concept as described in the literature review, does not take into account the cylinder variable dynamics such as the rate of cylinder volume change. The cylinder flow in cycle by cycle models is modelled using (Eq. 1.2) which requires the pressure ratio between the cylinder pressure P_{cyl} and port pressure P_{port} as well as the effective valve flow area A_v (Figure 11.1 - b). It is understandable that the effects of engine speed and crankshaft mechanism geometry are not taken into account by the equation. The effect of the engine speed could be neglected only if the piston is not moving during the intake or exhaust process which is never the case on a working engine. A generic engine flow model should use the cylinder pressure P_{cyl}, port pressure P_{port}, effective valve flow area Av and the rate of cylinder volume change into the equations dV_{cyl}/dt as shown in (Figure 11.1 - a). The engine geometry variables of valve flow areas (Figure 11.2 - b) and cylinder volume rate of change (Figure 11.2 - a) could be used as single terms in order to develop a correct and generic cylinder flow model, or combined into a single term for intake and exhaust. The idea of this concept is to evaluate the effective cylinder volume rate of change that is affecting the intake and exhaust ports as they are important parameters defining for the overlap period.

The evaluation that follows is an example of how the data produced in this thesis can be used to develop a variable that defines the complete engine geometry into a single term for the intake and exhaust valves (Figure 11.2 - c).

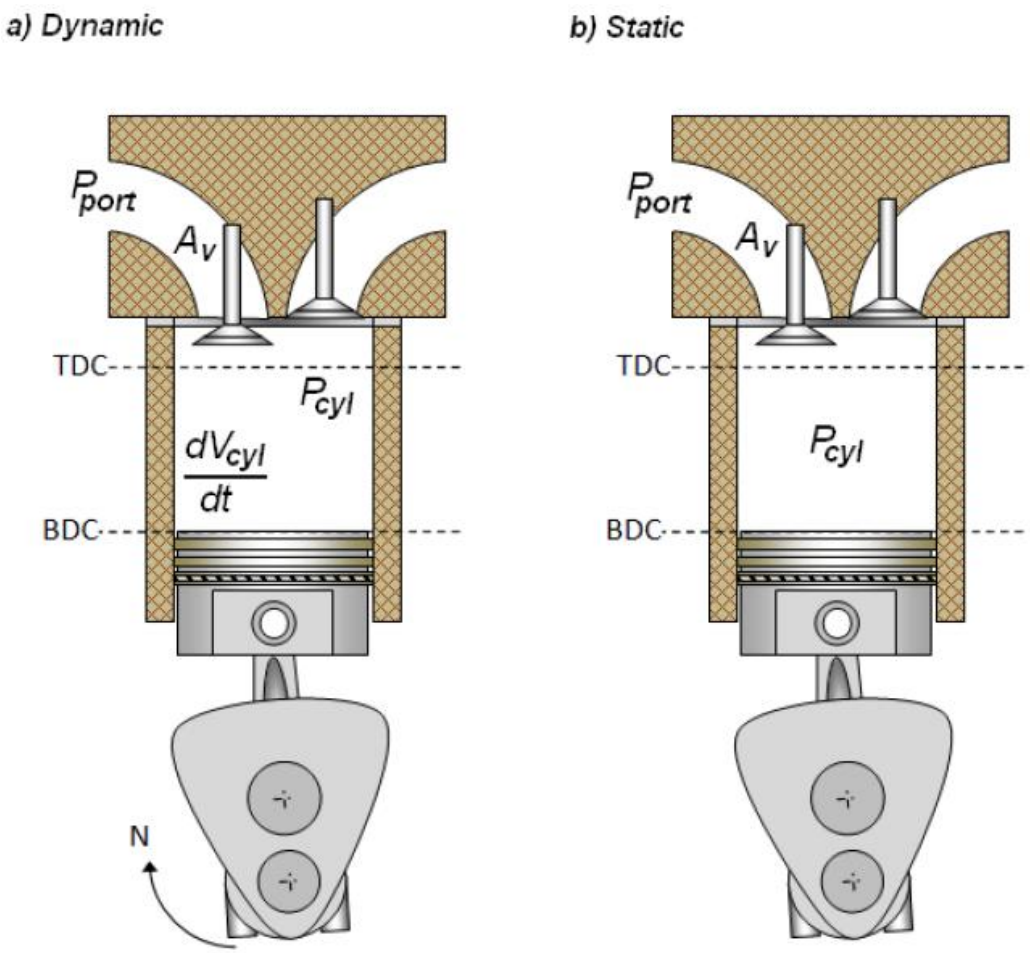

Figure 11.1: Engine cylinder flow modelling. a) dynamic. b) static

Intake effective volume rate of change:

$$\frac{dV_{int}}{dt} = \frac{dV_{cyl}}{dt}\frac{A_{int}}{A_{int} + A_{exh}} \quad \text{(Eq. 11.1)}$$

Exhaust effective volume rate of change:

$$\frac{dV_{exh}}{dt} = \frac{dV_{cyl}}{dt}\frac{A_{exh}}{A_{int} + A_{exh}} \quad \text{(Eq. 11.2)}$$

$\frac{dV_{int}}{dt}$ is the intake effective cylinder rate of volume change, $\frac{dV_{exh}}{dt}$ is the exhaust effective cylinder rate of volume change, $\frac{dV_{cyl}}{dt}$ is the cylinder volume rate of change, A_{int} is the intake valve opened area and A_{exh} is the exhaust valve opened area.

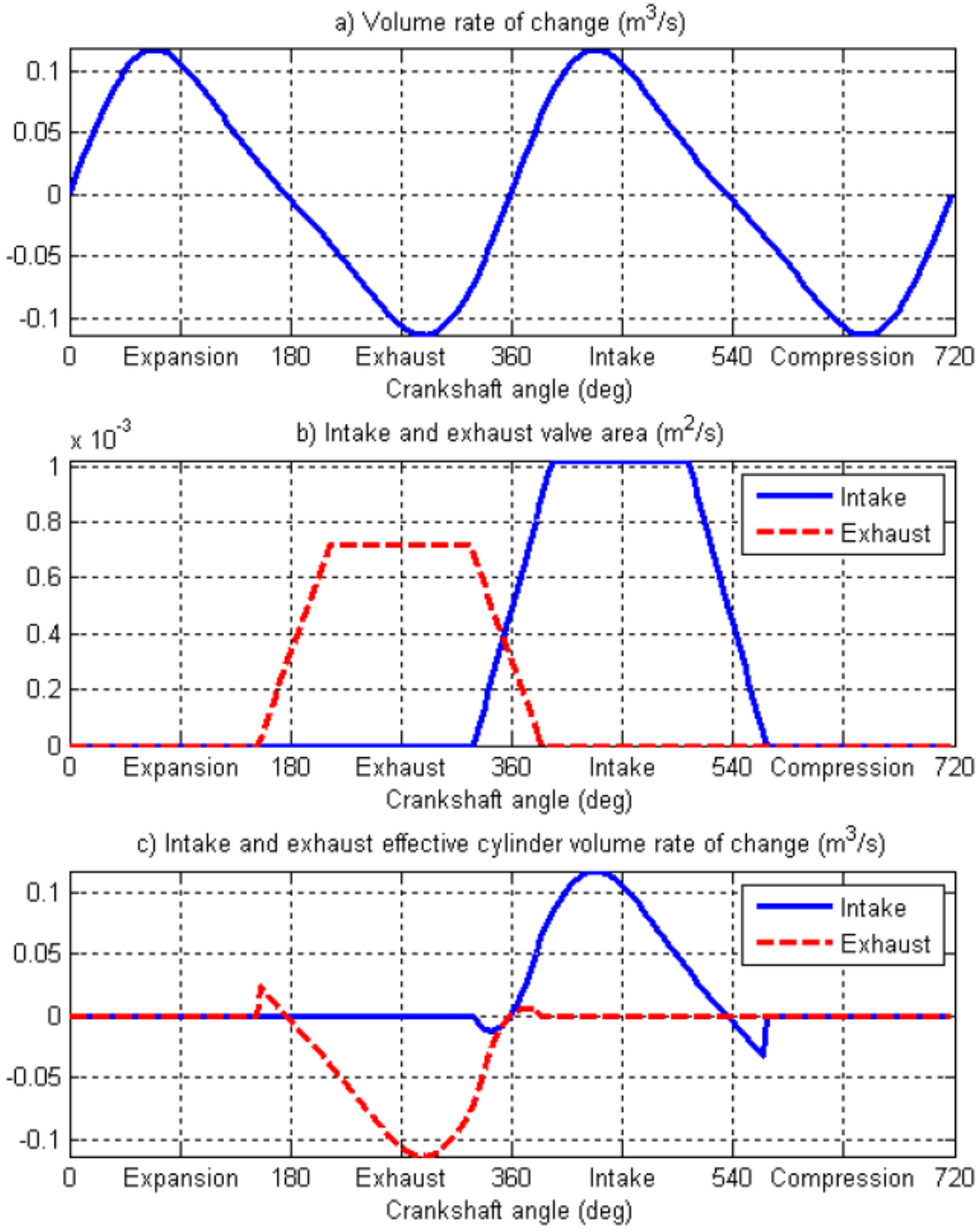

Figure 11.2: Cylinder-1 data for flow models

This data could be used to develop intake and exhaust cylinder flow models. This would imply a test rig consisting of one cylinder engine for which different pistons, valves, connecting rods and crankshaft sizes should be available in order to measure the effect of each component individually so that a correct model can be generated. Each engine components configuration will result in a particular intake and exhaust effective cylinder volume rate of change curve. The valve lift could either be measured on the engine though a valve lift sensor or from the crankshaft position using the valvetrain model presented. The engine should be motored using an electric motor so that high speeds could be achieved without the need of the combustion process. This will result in low temperature flow mapping allowing the use of cheaper mass air flow sensors. The next step would then be to validate the developed flow models under normal operating conditions (firing) of this one cylinder engine. Then, the models could be for example used on each individual cylinder of a 4-cylinder in order to derive the effect on the intake and exhaust manifolds on the cylinder flows. The four cylinder engine would basically represented by four identical phased cyclic cylinder flow models. This type of approach once accomplished, will give rise to cyclic engine mapping procedures which will result in a faster experimental mapping procedure which will be done just to derive the maps required for the virtual cycle-by-cycle engine model. Then, the engine model will be able to be used for virtual engine mapping which can be either to fit mean-value engine models or any other application.

The next version of the SIES framework is already in development which will have the crankshaft torque evaluated due to the engine rotation. This cyclic torque is the engine's inertial torque which is produced by the crankshaft mechanism, valvetrain system and engine frictions.

References

[1] E Hendricks and S. C Sorenson, SI engine controls and mean value engine modelling. SAE International, 1991. SAE: 910258

[2] R Leithgoeb, F Henzinger, A Fuerharpter, K Gschweitl, and A Zrim, Optimization of new advanced combustion systems using real-time combustion control. SAE International, 2003. SAE: 2003-01-1053

[3] J Lampinen, Cam shape optimisation by genetic algorithm.
Elsevier Science Ltd, 2003. Computer-Aided Design Volume 35, Issue 8, July 2003, Pages 727-737 Genetic Algorithms

[4] M Goyal, Glen Scharpf, and G Borman, Mathematical simulation of single cylinder intake and exhaust systems. SAE International, 1967. SAE: 670478

[5] M. J Arnold, M. J Tindal, and T. J Williams, Measurement of induction gas velocities in a reciprocating engine cylinder.
SAE International, 1972. SAE: 720115

[6] G. G Lucas and E. H James, A computer simulation of a spark ignition engine. SAE International, 1973. SAE: 730053

[7] W. J. D Annand and G. E Roe, Gas flow in the internal combustion engine: power, performance, emission control, and silencing. G. T. Foulis, 1974. ISBN-10: 0854291601

[8] Paul K Houpt and Han Ngee Tan, Identification of a thermodynamic model for spark ignited internal combustion engines.
IEEE, 1981. IEEE: 10.1109/CDC.1981.269500

[9] Richard D Rabbitt, Fundamentals of reciprocating engine airflow Part I: Valve discharge and combustion chamber effects.
SAE International, 1984. SAE: 840337

[10] W. F Powers, Internal combustion engine control system research at FORD.
IEEE, 1981. IEEE: 10.1109/CDC.1981.269499

[11] Jeffrey A Cook and Barry Powell, Modeling of an internal combustion engine for control analysis.
IEEE, 1988. IEEE: 10.1109/37.7726

[12] D. J Dobner, A mathematical engine model for development of dynamic engine control.
SAE International, 1980. SAE: 800054

[13] J. J Moskwa and J. K Hedrick, Automotive engine modeling for real time control application. IEEE, 1987. American Control Conference, 1987, Pages: 341 – 346.

[14] V Ganesan, Computer simulation of spark-ignition engine processes.
Universities Press, 1996. ISBN: 8173710155

[15] John L. Lumley, Engines An Introduction.
Cambridge University Press, 1999. ISBN-10: 0521644895

[16] Colin R Ferguson and Allan T. Kirkpatrick, Internal Combustion Engines - Applied Thermosciences, 2nd ed.

John Wiley & Sons, 2001. ISBN: 978-0-471-35617-2

[17] John B. Heywood, Internal Combustion Engine Fundamentals.

McGraw-Hill, 1998. ISBN 0-07-100499-8

[18] Gordon P. Blair, Design and Simulation of Four-stroke Engines.

Society of Automotive Engineers, 1999. ISBN 0-7680-0440-3

[19] Y. J Zhai and D. L Yu, Neural network model-based automotive engine air/fuel ratio control and robustness evaluation. Elsevier Ltd., 2008.

Engineering Applications of Artificial Intelligence Volume 22, Issue 2, March 2009, Pages 171-180

[20] K Atashkari, N Nariman-Zadeh, M Golcu, A Khalkhali, and A Jamali, Modelling and multi-objective optimization of a variable valve-timing spark-ignition engine using polynomial neural networks and evolutionary algorithms. Elsevier Ltd., 2006. Energy Conversion and Management Volume 48, Issue 3, March 2007, Pages 1029-1041

[21] S Leonhardt, H Gao, and V Kecman, Real-time supervision of diesel engine injection with RBF-based neural networks. IEEE, 1995. American Control Conference, 1995. Proceedings of the 1995, Pages 2128-2132 vol.3

[22] G De Nicolao, R Scattolini, and C Siviero, Modelling the volumetric efficiency of IC engines: Parametric, non-parametric and neural techniques. Elsevier Ltd., 1996. Control Engineering Practice Volume 4, Issue 10, October 1996, Pages 1405-1415

[23] Martin Müller, Estimation and Control of Turbocharged Engines. SAE International, 2008. SAE: 2008-01-1013

[24] Jeff L Kainz and James C Smith, Individual Cylinder Fuel Control With a Switching Oxygen Sensor. SAE International, 1999. SAE: 1999-01-0546

[25] Eilyan Y Bitar, Harold J Schock, and Antoni K. Oppenheim, Model for control of combustion in a piston engine. SAE International, 2006. SAE: 2006-01-0401

[26] Gustaf Olsson, Arthur I Cohen, and Harish S Rao, An approach to air-fuel ratio control for automobile engines using self-tuning regulators. IEEE, 1981. IEEE: 10.1109/CDC.1981.269475

[27] Robert W Weeks and John J Moskwa, Automotive engine modeling for real-time control using MATLAB/SIMULINK. SAE International, 1995. SAE: 950417

[28] R Pursifull and H Keener, Motorized Throttle Positioning Simulation Model. SAE International, 2003. SAE: 2003-01-0222

[29] Eldon G Leaphart, Steve E Muldoon, and Jill N Irlbeck, Application of Robust Engineering Methods to Improve ECU Software Testing. SAE International, 2006. SAE: 2006-01-1600

[30] C Hardie et al., Automated tuning of an engine management unit for an automotive engine. Professional Engineering, 2002. Proceedings of the Institution of Mechanical Engineers, Part D: Journal of Automobile Engineering, Volume 216, Number 10 / 2002, Pages 841-849

[31] P Strandth and R Egnell, Modeling SI-engines for hybrid vehicles. SAE International, 2001. SAE: 2001-01-0575

[32] J. J Moskwa and J. K Hedrick, Modeling and validation of automotive engines for control algorithm development. Journal of Dynamic Systems, Measurement, and Control, 1992. Volume 114, Issue 2

[33] Y Shen, J Bedford, and I. S Wichman, Thermodynamic modeling of direct injection methanol fueled engines. Elsevier Ltd., 2008. Applied Thermal Engineering Volume 29, Issues 11-12, August 2009, Pages 2379-2385

[34] Y Chamaillard, P Higelin, and A Charlet, A simple method for robust control design,application on a non-linear and delayed system: engine torque control. Elsevier Ltd., 2003. Control Engineering Practice Volume 12, Issue 4, April 2004, Pages 417-429

[35] L Mianzo and H Peng, Modeling and Control of a Variable Valve Timing Engine. AACC, 2000. Proceedings of the Institution of Mechanical Engineers, Part D: Journal of Automobile Engineering, Volume 218, Number 10 / 2004, Pages 1159-1171

[36] Francis T Connolly and Andrew E Yagle, Modeling and Identification of the combustion pressure process in internal combustion engines using speed fluctuations. IEEE, 1993. IEEE: 10.1109/MWSCAS.1993.343094

[37] J Francoa, M. A Franchekb, and K Grigoriadis, Real-time brake torque estimation for internal combustion engines. Elsevier Ltd., 2007. Mechanical Systems and Signal Processing Volume 22, Issue 2, February 2008, Pages 338-361

[38] Yahya H Zweiri and James F Whidborne, A mathematical transient model for the dynamics of a single-cylinder diesel engine. IEEE, 1998. International Conference on Simulation '98. Pages 145 – 151

[39] Elbert Hendricks et al., Modelling of the intake manifold filling dynamics. SAE International, 1996. SAE: 960037

[40] Elbert Hendricks and Spencer C Sorenson, Mean value modelling of spark ignition engines. SAE International, 1990. SAE: 900616

[41] P. F Puleston, G Monsees, and S. K Spurgeon, Air-fuel ratio and speed control for low emission vehicles based on sliding mode techniques. Professional Engineering Publishing, 2002. Proceedings of the Institution of Mechanical Engineers, Part I: Journal of Systems and Control Engineering, Volume 216, Number 2 / 2002, Pages 117-124

[42] Raymond C Turin and Hans P Geering, On-line identification of air-to-fuel ratio dynamics in a sequentially injected SI engine. SAE International, 1993. SAE: 930857

[43] Sten Gustavsson, Mattias Nyberg, and Lars Nielsen, Model based diagnosis for the air intake system of the SI-engine. SAE International, 1997. SAE: 970209

[44] L Glielmo, S Santini, and G Serra, Optimal Idle Speed Control with Induction-to-Power Finite Delay for SI Engines. Proceedings of the 7th Mediterranean Conference on Control and Automation (MED99), 1999.

[45] D. J Boam, I. C Finlay, and G. S Fairhead, The optimization of fuel enrichment patterns with throttle body injection. Mechanical engineering publications, 1988.

[46] P. R Crossley and J. A Cook, A non linear engine model for drivetrain system development. IEEE, 1991.

[47] B Saerens et al., Minimization of the fuel consumption of a gasoline engine using dynamic optimization. Elsevier Ltd., 2008. Applied Energy Volume 86, Issue 9, September 2009, Pages 1582-1588

[48] L Benvenuti, M. D Di Benedetto, C Rossi, and A Sangiovanni-Vincentelli, Injector Characteristics Estimation for Spark Ignition Engines. IEEE, 1998. Proceedings of the 37th IEEE Conference on Decision and Control, 1998, Volume 2, Pages 1546 – 1551

[49] F Zhaoa, M.-C Laia, and D. L Harringtonb, Automotive spark-ignited direct-injection gasoline engines. Elsevier Science Ltd, 1999. Progress in Energy and Combustion Science Volume 25, Issue 5, October 1999, Pages 437-562

[50] D. R Hamburg and J. E Hyland, A vaporized gasoline metering system for internal combustion engines. SAE International, 1976. SAE: 760288

[51] Qiang Hu, Sean F Wu, Ming-Chia Lai, Shari Stottler, and Ragu Raghupathi, Modeling of dynamic responses of injectors for an automotive fuel rail system. SAE International, 1999. SAE: 1999-01-0795

[52] Oliver Philipp, A Fuel Wall Wetting Model for Real-Time Applications. TESIS DYNAware GmbH http://www.dspace.de/ftp/papers/uc/philipp.pdf Last Accessed: 26 July 2009.

[53] Peter M Olin, A Mean-Value Model for Estimating Exhaust Manifold Pressure in Production Applications. SAE International, 2008. SAE: 2008-01-1004

[54] Per Andersson, Comparison of two Exhaust Manifold Pressure Estimation Methods. CCSSE, 2001.

[55] Jie Ma, Robert Allen, and Richard Bowen, Mathematical simulation of the transient performance of a petrol engine. SAE International, 1993. SAE: 930855

[56] M Sellnau, T Kunz, J Sinnamon, and J Burkhard, 2-step Variable Valve Actuation: System Optimization and Integration on an SI Engine. SAE International, 2006. SAE: 2006-01-0040

[57] P. S Kuo, Cylinder Pressure in a Spark-Ignition Engine: A Computational Model. Journal of Undergraduate Sciences Online, 1996.

[58] Paulina S Kuo, Cylinder Pressure in a spark-ignition engine: A computational Model. Journal of Undergraduate Sciences, 1996.

[59] J. R Serrano, F. J Arnau, P Piqueras, A Onorati, and G Montenegro, 1D gas dynamic modelling of mass conservation in engine duct systems with thermal contact discontinuities. Elsevier Ltd, 2008. Mathematical and Computer Modelling Volume 49, Issues 5-6, March 2009, Pages 1078-1088

[60] R. J Pearson and D. E Winterbone, The simulation of gas dynamics in engine manifolds using non-linear symmetric difference schemes. IMechE, 1997. Proceedings of the Institution of Mechanical Engineers, Part C: Journal of Mechanical Engineering Science, Volume 211, Number 8 / 1997, Pages 601-616

[61] D. E Winterbone and G. I Alexander, Efficiency of the manifolds of turbocharged engines. IMechE, 1985.

[62] P Oberg and L Eriksson, Modeling of the Gas Exchange Process in Variable Cam Timing Engines. Dept. of Electrical Engineering, Linkopings universitet, 2004.

[63] S Thompson and C Gong, Intake manifold modeling for the fuel metering control of spark ignited engines. ASME, 1997.
Journal of dynamic systems, measurement, and control, 1997, Volume 119, Pages 568-573

[64] L Le Moyne and F Maroteaux, Air-fuel flow modelling applied to the reduction of air-fuel ratio excursions during transients on port injected S.I. Engines.
SAE International, 1997. SAE: 970513

[65] L Guzzella and C Onder, Past, Present and Future of Automotive Control.: Swiss Federal Institute of Technology (ETH), Zurich, Switzerland, 2006.
Lecture Notes in Control and Information Sciences, Volume 329/2006, Pages 163-182

[66] A. A Malikopoulos, D. N Assanis, and P. Y Papalambros, A learning algorithm for optimal internal combustion engine calibration in real-time.
ASME, 2007. DETC2007-34718

[67] A. A Malikopoulos, D. N Assanis, and P. Y Papalambros, Optimal engine calibration for individual driving styles.
SAE International, 2008. SAE: 2008-01-1367

[68] A. A Malikopoulos, D. N Assanis, and P. Y Papalambros, Real-time, self learning optimization of diesel engine calibration. ASME, 2007. Journal of Engineering for Gas Turbines and Power, Volume 131, Issue 2

[69] N. P Fekete, U Nester, I Gruden, and J. D Powell, Model-based air-fuel ratio control of a lean multi-cylinder engine. SAE International, 1995. SAE: 950846

[70] Lino Guzzella, Models and model based control of IC-engines - A non linear approach. SAE International, 1995. SAE: 950844

[71] M. C Sellnau, F. A Matekunas, P. A Battiston, C Chang, and D. R Lancaster, Cylinder-Pressure-Based Engine Control Using Pressure-Ratio-Management and Low-Cost Non-Intrusive Cylinder Pressure Sensors.
SAE International, 2000. SAE: 2000-01-0932

[72] R.F Huang, H. S Yang, and C.-N Yeh, In-cylinder flows of a motored four-stroke engine with flat-crown and slightly concave-crown pistons. Elsevier Inc, 2008. Experimental Thermal and Fluid Science Volume 32, Issue 5, April 2008, Pages 1156-1167

[73] S.M Begg, M.P Hindle, T Cowell, and M.R Heikal, Low intake valve lift in a port fuel-injected engine. Elsevier Ltd., 2008. Energy Volume 34, Issue 12, December 2009, Pages 2042-2050

[74] M. J Throop and D. R Hamburg, Dynamic control of engine NOx emissions characterization and improvement of the transient response of an exhaust gas recirculation system. Proceedings of the American Control Conference, 1985.

[75] S Larsson and I Andersson, Self-optimising control of an SI-engine using a torque sensor. Elsevier Ltd., 2007. Control Engineering Practice Volume 16, Issue 5, May 2008, Pages 505-514

[76] A Chow and M. L Wyszynski, Thermodynamic modelling of complete engine systems - a review. Professional Engineering, 1999. Proceedings of the Institution of Mechanical Engineers, Part D: Journal of Automobile Engineering, Volume 213, Number 4 / 1999, Pages 403-415

[77] F. J Zeleznik and Bonnie J Mc Bride, Modeling the complete Otto cycle - Preliminary Version. SAE International, 1977. SAE: 770223

[78] J Benajes, J. R Serrano, S Molina, and R Novella, Potential of Atkinson cycle combined with EGR for pollutant control in a HD diesel engine. Elsevier Ltd., 2008. Energy Conversion and Management Volume 50, Issue 1, January 2009, Pages 174-183

[79] S. H Chan and J Zhu, Modelling of engine in-cylinder thermodynamics under high values of ignition retard. Elsevier SAS, 2001. International Journal of Thermal Sciences Volume 40, Issue 1, January 2001, Pages 94-103

[80] Heinz Heisler, Vehicle and Engine Technology, 2nd ed.: Butterworth - Heinemann, 1999. ISBN: 0768002370

[81] R Mikalsen and A. P Roskilly, Performance simulation of a spark ignited free-piston engine generator. Elsevier Ltd., 2007. Applied Thermal Engineering Volume 28, Issues 14-15, October 2008, Pages 1726-1733

[82] R Mikalsen and A. P Roskilly, Coupled dynamic–multidimensional modelling of free-piston engine combustion. Elsevier Ltd., 2008. Applied Energy Volume 86, Issue 1, January 2009, Pages 89-95

[83] R Mikalsen and A. P Roskilly, A computational study of free-piston diesel engine combustion. Elsevier Ltd, 2008. Applied Energy Volume 86, Issues 7-8, July-August 2009, Pages 1136-1143

[84] Piero Azzoni, Davide Moro, Fabrizio Ponti, and Nicolo Cavina, Model-based indicated torque estimation using non linear observers. IEEE, 1998.

[85] R. J Pierik and J. F Burkhard, Design and Development of a Mechanical Variable Valve Actuation System. SAE International, 2000. SAE: 2000-01-1221

[86] Thomas F Irvine and Peter E Liley, Steam and Gas Tables with Computer Equations. Academic Press Inc, 1984. ISBN-10: 0123740800

[87] Chang Yang, Model-Based Analysis and Tuning of Electronic Throttle Controllers. SAE International, 2004. SAE: 2004-01-0524

[88] Yushu Wang, Introduction to Engine Valvetrains. SAE International, 2007. ISBN: 978-0-7680-1079-4

[89] Richard Stone, Introduction to Internal Combustion Engines, 3rd ed. Palgrave, 1999. ISBN-10: 0333740130

[90] Robert W. Soutas-Little and Daniel J. Inman, Engineering Mechanics Dynamics. Prentice-Hall, 1999. ISBN 0-13-278409-2

[91] J. L. Meriam and L. G. Kraige, Engineering Mechanics Dynamics, 5th ed. John Wiley & Sons, 2003. ISBN 0-471-26606-X

[92] C. H. Onder L. Guzzella, Introduction to Modeling and Control of Internal Combustion Engine Systems. Springer, 2004. ISBN: 978-3-540-22274-3

[93] R. C. Hibbeler, Engineering Mechanics Dynamics, 9th ed. Prentice-Hall, 2001. ISBN 0-13-020004-2

Appendix

Appendix A: Simulation inputs

```
%   SIES Framework v1.0 Initialisation File
%   University of Bradford
%   2009
%
%   Antonios Pezouvanis
%   e-mail:    a.pezouvanis@gmail.com
%
%====================================

%General Simulation Parameters
Simulation.tstep=1e-4;          %Fixed Step Increment                (sec)

%Ambient Conditions
Ambient_Conditions.Patm=101325; %Atmospheric pressure                (Pa)
Ambient_Conditions.Tatm=20;     %Atmospheric temperature             (deg C)


%Engine Geometry Parameters
Engine_Geometry.K=0.027;         %Crank arm length                   (m)
Engine_Geometry.L=0.13;          %Connecting rod length              (m)
Engine_Geometry.Ot=-0.005;       %Crank mechanism total offset       (m)
Engine_Geometry.r=10;            %Compressio Ratio
Engine_Geometry.B=0.072;         %Cylinder bore                      (m)


%Multi-cylinder Variables
Engine_Geometry.zeta1=0;        %Cyl-1 Phase Angle           (deg crank)
Engine_Geometry.zeta2=540;      %Cyl-2 Phase Angle           (deg crank)
Engine_Geometry.zeta3=180;      %Cyl-3 Phase Angle           (deg crank)
Engine_Geometry.zeta4=360;      %Cyl-4 Phase Angle           (deg crank)


%Premilinary Calculations
Engine_Geometry.fiTDC=rad2deg(-
asin(Engine_Geometry.Ot/(Engine_Geometry.L+Engine_Geometry.K)));
 %Crank arm angle @ Cyl-1 TDC (deg)

%Sub-Model 1 Parameters:   Engine Dynamics

Engine_Dynamics.T0=0;           %Initial torque on crankshaft    (Nm)
Engine_Dynamics.Jeng=1;         %Engine inertia                  (kg m^2)
Engine_Dynamics.N0=500;         %Initial engine speed            (RPM)
Engine_Dynamics.Theta0=0;       %Initial crankshaft position     (deg)
(0 = Cyl-1 @ TDC)

 %Sub-Model 3 Parameters:   Valvetrain Kinematics
Valvetrain_Kinematics.valveareaModel=3;

Valvetrain_Kinematics.intNumVCyl=2;
Valvetrain_Kinematics.intD=30;
```

```
Valvetrain_Kinematics.intDi=26;
Valvetrain_Kinematics.intd=5;
Valvetrain_Kinematics.intthetaSeat=45;
Valvetrain_Kinematics.intRockerRatio0=1;

Valvetrain_Kinematics.exhNumVCyl=2;
Valvetrain_Kinematics.exhD=26;
Valvetrain_Kinematics.exhDi=22;
Valvetrain_Kinematics.exhd=5;
Valvetrain_Kinematics.exhthetaSeat=45;
Valvetrain_Kinematics.exhRockerRatio0=1;

 %Sub-Model 4 Parameters:   Throttle Kinematics
 Throttle_Kinematics.ThetaC=4;   %Closed throttle plate angle        (deg)
Throttle_Kinematics.Dth=0.050;  %Throttle bore diameter             (m)
Throttle_Kinematics.Dsh=0.006;  %Throttle shaft diameter            (m)
Throttle_Kinematics.alpha0=0;   %Initial throttle angle             (deg)
(0=Throttle closed)


%Sub-Model 5 Parameters:   Crankcase Kinematics

Crankcase_Kinematics.VcTDC=0.004;   %Crankcase Volume Cyl-1:TDC     (m^3)

%Sub-Model 8 Parameters:   Valvetrain Control
%CAMSHAFT PHASING
Valvetrain_Control.IntakePhasingON=0;   %Enable Intake Camshaft Phasing?
(0=off, 1=on)
Valvetrain_Control.ExhaustPhasingON=0;   %Enable Intake Camshaft Phasing?
(0=off, 1=on)

%Intake camshaft phasing map, Format=[crankshaft speed (RPM);phase angle
(crank deg)
Valvetrain_Control.IntakePhasingMap=[0 3000 3000.001 6000 6000.001 20000;0
0 0 0 -20 -20];

%Exhaust camshaft phasing map, Format=[crankshaft speed (RPM);phase angle
(crank deg)
Valvetrain_Control.ExhaustPhasingMap=[0 3000 3000.001 6000 6000.001 20000;0
0 0 0 10 10];

%CAMSHAFT LIFT
Valvetrain_Control.IntakeVariableLiftON=0;   %Enable Intake Camshaft
Phasing?   (0=off, 1=on)
Valvetrain_Control.ExhaustVariableLiftON=0;   %Enable Intake Camshaft
Phasing?  (0=off, 1=on)
    %Intake rocker arm ratio map, Format=[crankshaft speed (RPM);phase
angle    (crank deg)]
Valvetrain_Kinematics.intRockerRatioMap=[0 3000 3000.001 6000 6000.001
20000;0.5 0.5 0.7 0.7 1 1];
    %Exhaust camshaft phasing map, Format=[crankshaft speed (RPM);phase
angle   (crank deg)
Valvetrain_Kinematics.exhRockerRatioMap=[0   3000   3000.001   6000   6000.001

20000;0.5 0.5 0.7 0.7 1 1];
```